Terms and Conditions of Use of Digitised Theses from Trinity College Library Dublin

Copyright statement

All material supplied by Trinity College Library is protected by copyright (under the Copyright and Related Rights Act, 2000 as amended) and other relevant Intellectual Property Rights. By accessing and using a Digitised Thesis from Trinity College Library you acknowledge that all Intellectual Property Rights in any Works supplied are the sole and exclusive property of the copyright and/or other IPR holder. Specific copyright holders may not be explicitly identified. Use of materials from other sources within a thesis should not be construed as a claim over them.

A non-exclusive, non-transferable licence is hereby granted to those using or reproducing, in whole or in part, the material for valid purposes, providing the copyright owners are acknowledged using the normal conventions. Where specific permission to use material is required, this is identified and such permission must be sought from the copyright holder or agency cited.

Liability statement

By using a Digitised Thesis, I accept that Trinity College Dublin bears no legal responsibility for the accuracy, legality or comprehensiveness of materials contained within the thesis, and that Trinity College Dublin accepts no liability for indirect, consequential, or incidental, damages or losses arising from use of the thesis for whatever reason. Information located in a thesis may be subject to specific use constraints, details of which may not be explicitly described. It is the responsibility of potential and actual users to be aware of such constraints and to abide by them. By making use of material from a digitised thesis, you accept these copyright and disclaimer provisions. Where it is brought to the attention of Trinity College Library that there may be a breach of copyright or other restraint, it is the policy to withdraw or take down access to a thesis while the issue is being resolved.

Access Agreement

By using a Digitised Thesis from Trinity College Library you are bound by the following Terms & Conditions. Please read them carefully.

I have read and I understand the following statement: All material supplied via a Digitised Thesis from Trinity College Library is protected by copyright and other intellectual property rights, and duplication or sale of all or part of any of a thesis is not permitted, except that material may be duplicated by you for your research use or for educational purposes in electronic or print form providing the copyright owners are acknowledged using the normal conventions. You must obtain permission for any other use. Electronic or print copies may not be offered, whether for sale or otherwise to anyone. This copy has been supplied on the understanding that it is copyright material and that no quotation from the thesis may be published without proper acknowledgement.

Alanna Gannon B.A., B.A.I

An Investigation of Structure-Function Relations in Articular Cartilage during Skeletal Maturation

---

Trinity College Dublin, October 31st, 2013

A thesis submitted to the University of Dublin in partial fulfilment of the requirements for the degree of

Doctor in Philosophy

Supervisor: Dr. Daniel Kelly

Internal Examiner: Dr. Ciaran Simms

External Examiner: Dr. C.C. van Donkelaar (René)

Declaration

I declare that this thesis has not been submitted as an exercise for a degree at this or any other university and it is entirely my own work.

I agree to deposit this thesis in the University's open access institutional repository or allow the library to do so on my behalf, subject to Irish Copyright legislation and Trinity College Library conditions of use and acknowledgment.

"To seek, to strive, to find and not to yield"

Ulysses

Lord Tennyson

Summary

The over-riding objective of this thesis was to build upon our current understanding of the evolving nature of articular cartilage mechanics by elucidating how changes to structure and composition of the tissue during postnatal development and maturation impact the depth dependent compressive mechanical properties of the tissue.

The first objective of this thesis was to elucidate the role of the superficial region of articular cartilage in determining the dynamic properties of the tissue. It was hypothesised that removal of the superficial region will influence both the flow dependent and independent properties of articular cartilage, leading to a reduction in the dynamic modulus of the tissue. Compressive testing revealed that the superficial region is less stiff at equilibrium than the remainder of the tissue, however removal of this region from intact cores was found to significantly reduce the dynamic modulus of the remaining tissue, suggesting decreased fluid load support within the tissue during transient loading upon removal of the superficial region. Data fits to a biphasic model revealed a significantly lower permeability in the superficial region compared to the remainder of the tissue. It is postulated that the observed decrease in the dynamic moduli is due at least in part to the superficial region acting as a low permeability barrier, where its removal decreases the tissue's ability to maintain fluid load support. This result emphasises the impact that degeneration of the superficial region has on the functionality of the remaining tissue.

The second objective of this thesis was to explore how the equilibrium and dynamic compressive properties of articular cartilage change during postnatal development. In particular, to determine how changes to the superficial region of articular cartilage during skeletal development impact its functional properties. It was

hypothesised that a functional superficial region is not present in skeletally immature articular cartilage, and hence removal of this zone of the tissue would only negatively impact the dynamic modulus of the tissue with the attainment of skeletal maturity. The confined dynamic modulus significantly decreased in the mature tissue after removal of the superficial region, whilst no significant change was observed in the immature tissue. A similar trend result was seen in the unconfined dynamic tests. Biochemical analysis revealed a significant decrease ($P<0.0001$) in sGAG content with age, whilst collagen content significantly increased with age ($P<0.0001$) when normalised to percentage dry weight. A significant increase was also observed in fibril diameter with age ($P<0.0001$). Average fibril diameter in the superficial region of the tissue increased from 14.37 ± 7.28 nm in the four week old tissue significantly ($P<0.0001$) to 22.91 ± 11.41 nm in the one year old tissue, with a further significant increase ($P<0.0001$) to 75.91 ± 30.47 nm in the three year old tissue. From these results it is postulated that a functional superficial region is only present in mature tissue due to its high collagen fibril density, architectural organisation and low permeability, partially confirmed by Helium-Ion microscopy.

While surface-to-surface measurements provide information on the bulk properties of a tissue, they furnish only indirect insights to the internal behaviour of the tissue and its spatial heterogeneity. Understanding how compositional and architectural changes alter the depth dependent mechanical properties of articular cartilage during postnatal development is central to understanding how the tissue achieves its function. Therefore the final study of this thesis utilised digital image correlation to characterise the depth dependent mechanical properties of the tissue. The hypothesis of this study was that alterations to the collagen network that occur in developing articular cartilage with age correlate with dramatic changes to the depth dependent compressive properties of the tissue. An order of magnitude increase in the compressive properties of the deep zone of

articular cartilage (for low offset strains) was observed from birth to skeletally maturity. This occurred despite the fact that the sGAG content of articular cartilage was observed to decrease with skeletal maturity. It is postulated that this increase in cartilage stiffness with age is due to the change in alignment of the collagen network with skeletal maturation and an increase in the inherent stiffness of the collagen network; due to increases in the tissue collagen content and increases in the ratio of mature-immature collagen cross-links.

In conclusion, the results of this thesis demonstrate that the Benninghoff-type organisation of the collagen network of skeletally mature articular cartilage, as well as the inherent stiffness that this network attains due to increases in collagen content, fibril diameter and cross-linking with age, play a dominant role in determining the final compressive mechanical properties of the tissue.

Acknowledgements

This dissertation would not have been possible without the guidance and the help of several individuals who in one way or another contributed and extended their valuable assistance in the completion of this thesis. First and foremost, I would like to thank my supervisor, Daniel Kelly, who has supported me throughout my thesis with his patience and knowledge whilst allowing me the room to work in my own way. Your enthusiasm, positive and solution focussed attitude are qualities I have greatly appreciated and hope to attain and preserve throughout my own career. Next I would like to thank my internal examiner Dr. Ciaran Simms and my external examiner Dr. Rene van Donkelaar for the thought you put into preparing for my viva and the thorough and stimulating conversation that ensued. Your attention to detail paid my work and efforts the highest level of respect.

I would like to thank everybody in the lab, office and Trinity Centre for Bioengineering for the many laughs and the lasting friendships I have formed. Steve, Tat, Eoghan, Michael, Yurong, Oana, Grainne, Henrique, Andy, Simon, Adam, Alan, Masooma, Olivier, Amy, and of course Lu. Tag rugby leagues, sports days, sunny afternoons in the Pav and many coffee breaks are just some of the great times we've shared. Darren, Eamon and Tariq, knowing you were going through the same hard slog at the end made writing up a bearable and even fun experience, not to mention the four o'clock group. Thomas I'm not sure how to thank you. We went through our PhD's together and having your friendship helped me to complete mine. Your level head and sense of humour kept me going and our mutual appreciation for the bad laugh made it the more enjoyable an experience.

My friends - Eoin, Karl, Andy, Conor, Ellen, Karen, Ross, Conor, Eimear, Peadar, Sally, Blathnaid, Jayne, Sinead and Carina. I never would have guessed, walking into undergraduate engineering on my first day, that I would make such wonderful friends. Thank you for your continued support and friendship throughout my PhD.

My Family – Mom and Dad, you have been there every step of the way for me, not just during my PhD but my whole life. Your love and belief in me are what gave me the confidence and will to pursue my goals and your support and kindness are what gave me the ability to achieve them - right down to keeping me company during my many late nights in the lab! Carly and Arielle - there are no better friends than sisters, and there are no better sisters than you. Your love, humour and wisdom make everything special. They say a sister may be the keeper of one's identity, the only person with the keys to one's unfettered, more fundamental self. This is never truer than during my PhD when my basic self was more present than usual, however you bore it with kindness and laughter and endless love.

Michael you deserve much of the credit of this dissertation. You patiently supported me during the course of this entire journey and enriched my life by simply being in it. Throughout the toughest periods of this dissertation you were on hand to listen with care and love. You've rescued me off mountains, caught me countless times before I've fallen, driven me to the far corners of Ireland and England and smiled every step of the way! Everyone has their own angel and you are mine. I love you.

This study was funded by the Science Foundation Ireland (SFI) under the President of Ireland Young Researcher Award (PIYRA) 08/YI5/B1336 and IRCSET (G30345).

Table of Contents

List of Figures

List of Tables

Nomenclature

The nomenclature contains some abbreviations used throughout the thesis. It is not a full list of all abbreviations used – they will be explained in the text whenever used.

Articular-epiphyseal cartilage complex	AECC
Analysis of variance	ANOVA
Benninghoff	Benn
Calcium Chloride	$CaCl_2$
Deep zone	DZ
Extracellular matrix	ECM
Ethylenediaminetetraacetic acid	EDTA
Fixed charge density	FCD
Glycosaminoglycan	GAG
Helium ion microscopy	HIM
Hydrochloric acid	HCL
Hydroxylsylpyridinoline	HP
Isotropic	Iso
Magnesium chloride	$MgCl_2$
Middle zone	MZ
Polarised light microscopy	PLM
Proteoglycan	PG
Small leucine-rich proteoglycans	SLRPs
Superficial tangential zone	STZ
Superficial region	SR
Sulphated glycosaminoglycan	sGAG
Tissue engineering	TE
Weight per dry weight (%)	%d/w

Published Work

Gannon, A.R., Nagel, T., Kelly, D.J. The role of the superficial region in determining the dynamic properties of articular cartilage. Osteoarthritis and Cartilage 20 (2012) 1417-1425.

Conference Proceedings

Gannon, A.R., Bell, A., Avery, N., Kelly, D.J. The Changing Role of the Superficial Region in determining the Dynamic Compressive Properties of Articular Cartilage during Postnatal Development. In Orthopaedic Research Society ORS 2014 Annual Meeting. March 2014, New Orleans, Louisiana, USA.

Gannon, A.R., Bell, A., Avery, N., Nagel, T., Kelly, D.J. Changes to the Depth Dependent Compressive Mechanical Properties of Articular Cartilage from Birth to Skeletal Maturity are related to the Temporal Evolution of its Collagen Network. In Orthopaedic Research Society ORS 2014 Annual Meeting. March 2014, New Orleans, Louisiana, USA.

Gannon, A.R., Kelly, D.J. The changing depth dependent properties of articular cartilage during postnatal development. In American Society of Mechanical Engineers (Bioengineering Division) Summer Conference, June 2013, Sunriver, Oregon, USA.

Gannon, A.R., Kelly, D.J. The changing depth dependent properties of articular cartilage during postnatal development and maturation. In 19th Annual Conference of the Section of Bioengineering, Royal Academy of Medicine in Ireland, January 2013, Dublin, Ireland

Gannon, A.R., Kelly, D.J. The role of the superficial region in determining the dynamic properties of articular cartilage. In 18th Congress of European Society of Biomechanics, July 2012, Lisbon, Portugal

Gannon, A. R., Kelly, D. J. The Role of the Superficial Tangential Zone in Determining the Dynamic Properties of Articular Cartilage. In Orthopaedic Research Society 2012 Annual Meeting, February 4-7, 2012, San Francisco, California, USA

Gannon, A.R., Kelly, D.J. The role of the superficial tangential zone in determining the dynamic properties of articular cartilage. In 18th Annual Conference of the Section of Bioengineering, Royal Academy of Medicine in Ireland, January 2012, Belfast, UK

Gannon, A.R., Kelly, D.J. The Changing Depth Dependent Mechanical Properties of Articular Cartilage with Age and Topographical Location. In 17th Annual Conference of the Section of Bioengineering, Royal Academy of Medicine in Ireland, January 2011, Galway, Ireland

Gannon, A.R., Kelly, D.J. Spatial Variations in the Depth Dependent Properties of Porcine Osteochondral Tissue -Implications for Tissue Engineering. In 17th Congress of European Society of Biomechanics, July 2010, Edinburgh, UK

Gannon, A.R., Kelly, D.J. Spatial Variations in the Depth Dependent Properties of Porcine Osteochondral Tissue -Implications for Tissue Engineering. In 16th Annual Conference of the Section of Bioengineering, Royal Academy of Medicine in Ireland, January 2010, Dublin, Ireland

Gannon, A.R., Kelly, D.J. Strain Dependent Dynamic Properties of Porcine Articular Cartilage. In 15th Annual Conference of the Section of Bioengineering, Royal Academy of Medicine in Ireland, January 2009, Limerick, Ireland

Chapter 1 Introduction

1.1 Study Motivation

Articular cartilage is a thin layer of soft tissue that lines the articulating ends of all diarthrodial joints in the body (Mow and Guo, 2002). The main functions of this compliant, biphasic, viscoelastic tissue are to spread the very high loads that pass through our joints over a large area and to minimize the friction and wear associated with continual sliding and rolling movements of the opposing joint surfaces (Ateshian and Mow, 2005). These functional properties result from the unique properties of articular cartilage and synovial fluid. However articular cartilage has a poor capacity for repair due to its avascular nature and low cellularity. In addition, chondrocytes (the cell type in cartilage responsible for the turnover and maintenance of the tissue) have no significant migratory ability as they are embedded in the collagen matrix (Perera et al., 2012). Therefore, with the onset of diseases such as osteoarthritis, progressive degeneration of cartilage occurs, resulting in debilitating pain, stiffness and limitation in movement and activity.

Tissue engineering (TE) is the emerging discipline invoking strategies involving cells and/or bio regulatory factors, often in combination with polymeric materials to create a tissue *in vitro* (Butler et al., 2009). TE has the potential to revolutionise the next generation of implants to be more biologically interactive and long lasting. However, many challenges still remain, particularly for tissues that function within complex and demanding mechanical environments *in vivo*; such engineered tissues must be able to function within the context of physiological loading conditions once implanted (Butler et al., 2009). It is estimated that a human knee may experience one million cycles of loading per year (Mow et al., 1992). An essential prerequisite to tissue engineering truly

functional cartilage grafts is a detailed description of the nonlinear, flow dependent/flow independent viscoelastic and anisotropic behaviours of the native tissue. These details need to be correlated with the spatial and temporal variations in composition, structure, and function of articular cartilage (Mow and Guo, 2002).

During skeletal development and maturation, articular cartilage undergoes changes in its composition. In addition, significant structural adaptations occur within the collagen framework of the tissue as we age (Julkunen et al., 2009). The articular cartilage of the new-born appears homogeneous and in particular the collagen network does not show any zonal structure. In contrast, the collagen architecture within skeletally mature articular cartilage possesses an arcade like zonal structure; the parallel orientation of the collagen fibrils in the superficial tangential zone (STZ) arcade to a perpendicular orientation in the deep zone (DZ) of the tissue. This model of mature collagen architecture was first proposed by Benninghoff in 1925 based on an extensive study of several synovial joints by polarised light microscopy (PLM) (Benninghoff, 1925, Hwang et al., 1992). Surprisingly, despite the considerable time span from when this structure was first reported, relatively little is known about how the biomechanical properties of articular cartilage evolve during postnatal development and maturation (Brommer et al., 2005, Julkunen et al., 2009, Williamson et al., 2001). Understanding how the compositional and architectural changes that occur within the tissue during postnatal development alter the depth dependent mechanical properties of articular cartilage is central to understanding how the tissue achieves its function.

It has previously been demonstrated that the intrinsic material properties of articular cartilage vary through the depth of the tissue (Chen et al., 2001, Julkunen et al., 2009, Maroudas, 1976, Mow et al., 1980, Schinagl et al., 1997, Wang et al., 2002a), however, less is known about the depth dependent dynamic properties of the tissue and

how they depend on the tissue's composition and structural organisation. This is of critical importance, as in general, the loading mechanism of diarthrodial joints is cyclical and/or intermittent (Dillman, 1975). While the compressive modulus of the superficial region is lower than the rest of the tissue (Bevill et al., 2010, Glaser and Putz, 2002, Torzilli, 1993, Torzilli et al., 1983), it has been demonstrated that upon removal of this layer the tissue is more susceptible to damage from impact loading (Rolauffs et al., 2010). Elucidating the role of this region of the tissue in determining the dynamic properties of articular cartilage is critically important given that disruption to the superficial zone is often associated with the initiation and/or progression of osteoarthritis.

1.2 Hypothesis of Thesis

The over-riding objective of this thesis was to build upon our current understanding of the evolving nature of articular cartilage mechanics by elucidating how changes to structure and composition of the tissue during postnatal development and maturation impact the depth dependent compressive mechanical properties of the tissue. Changes to the structure and composition of articular cartilage during postnatal development and maturation will be evaluated using a unique combination of histological, biochemical and imaging techniques. The mechanical properties of articular cartilage will be determined using a combination of bulk testing and microscopic testing combined with digital image correlation. The hypotheses of the thesis are as follows:

The first hypothesis of this thesis is that removal of the superficial region will influence the flow dependent properties of articular cartilage, leading to a reduction in the dynamic modulus of the remaining tissue.

The second hypothesis is that a functional superficial region is not present in skeletally immature articular cartilage, and hence removal of this zone of the tissue would only negatively impact the dynamic modulus of the tissue with the attainment of skeletal maturity.

The third and final hypothesis of this thesis is that alterations to the collagen network that occur in developing articular cartilage with age correlate with dramatic changes to the depth dependent compressive properties of the tissue.

Chapter 2 Literature Review

2.1 Structure and Composition of Articular Cartilage

Articular cartilage is a multiphasic material consisting of two major phases; a solid phase consisting of a hypo-cellular porous extracellular matrix (ECM) (20-35% wet weight) and a fluid phase composed of water (65-80% wet weight) (van Turnhout et al., 2010a) which contains many mobile cations (Na^+, Ca^{2+} and K^+, << 1% by wet weight) (Lipshitz et al., 1976). The extracellular matrix is composed predominantly of a densely woven, strong collagen (mainly Type II) fibrillar network (15-22% by wet weight) enmeshed with charged proteoglycan aggregates (PG, 4-7% by wet weight) and chondrocytes (Lu and Mow, 2008). Proteoglycan (PG), known as an aggrecan, forms the second major structural component of articular cartilage. These are large complex molecules consisting of a core protein and one or more glycosaminoglycan (GAG) chains, with at least one negatively charged group i.e. carboxyl and/or sulphate (Mow and Guo, 2002). Aggrecan constitutes as much as 80% to 90% of proteoglycans in articular cartilage and its presence is considered the hallmark of chondrogenesis (Mow and Huiskes, 2005). Collagen on average, constitutes nearly two thirds of the dry tissue weight of adult articular cartilage (Eyre, 2002); it assembles to form small fibrils and larger fibres with an exquisite architectural arrangement and with dimensions that vary through the depth of the cartilage layer (Mow and Guo, 2002). Chondrocytes; the sparsely distributed cells in articular cartilage, account for less than 10% of the tissue volume (Muir, 1980) and manufacture, secrete, and maintain the organic component of the extracellular matrix (Mow and Huiskes, 2005).

For an understanding of cartilage swelling, the dissolved electrolytes within the interstitial fluid must be considered as a third phase, in addition to the fluid phase and the negatively charged solid phase (Gu et al., 1997, Gu et al., 1998, Mow and Huiskes, 2005).

Indeed, each phase of the tissue contributes significantly to its known mechanical and physiochemical properties. Whilst collagens (Eyre, 1980) and proteoglycans (Watanabe et al., 1998) provide the quantitatively major component of the organic ECM, quantitatively minor components include hyaluronan, link protein, the smaller proteoglycans versican, biglycan, decorin, fibromodulin, perlican, fibronectin, thrombospondins and cartilage matrix protein (Hardingham, 1979, Roughley and Lee, 1994). Whilst not major components in terms of absolute mass of the solid phase, some of them may approach the molar concentrations of collagen and aggrecan and serve important biological relating functions (Mow and Huiskes, 2005).

2.1.1 Interstitial water

Water is the most copious component of articular cartilage, occupying up to approximately 80% of its wet weight (Lipshitz et al., 1976). The fluid contains many mobile cations which influence the mechanical behaviour of the cartilage (Gu et al., 1993). This fluid component is also essential to the health of the tissue, in that it facilitates the diffusion of gases, nutrients e.g. glucose, and waste products between chondrocytes and the surrounding nutrient rich synovial fluid (Torzilli et al., 1983, O'Hara et al., 1990, Honner and Thompson, 1971). In native tissue it appears that a portion of this water; approximately 30%, resides within the intrafibrillar space of collagen and therefore is not available for transport under mechanical loading and is believed to be excluded from the proteoglycans (Maroudas and Bannon, 1981). The proteoglycan molecules, because of their larger size, are excluded from this intra-fibrillar space (Schinagl et al., 1997). This exclusion effectively raises the density of the fixed charges within the tissue thus raising the interstitial osmotic pressure. Hence, the effective fixed charge density is higher than if computed from total tissue water content (Buschmann and Grodzinsky, 1995, Maroudas and Bannon, 1981).

Theoretical and experimental studies have demonstrated during confined compression creep and stress relaxation that the interstitial fluid of cartilage pressurises considerably under loading, potentially supporting up to 90% of the applied load for several hundred seconds after loading (Soltz and Ateshian, 1998, Soltz and Ateshian, 2000). In addition, about 70% of the water may be removed from the tissue under loading. This movement is crucial for cartilage behaviour and joint lubrication (Ateshian et al., 1997). It has been demonstrated that interstitial fluid load support plays a dominant role in regulating the frictional response of cartilage, with the understanding being that the friction coefficient remains low as long as the interstitial fluid load support is high (Ateshian, 2009). As the collagen content and thereby the intra-fibrillar water content, is depth dependent, the influence of intra and extra-fibrillar water is also depth dependent, resulting in an extra dependency in the swelling pressures (Maroudas and Bannon, 1981, Mow and Guo, 2002, Wilson et al., 2007).

2.1.2 Collagen

The collagenous proteins form the largest part of the non-aqueous extracellular matrix. Collagen is a rod-shaped molecule with a high degree of structural organization. It is defined by the presence of right-handed triple helical collagenous domain formed by three polypeptide chains (Eyre, 2002). In articular cartilage, small diameter fibrils of 10 to 25 nm composed of type II tropocollagen molecules are formed in the pericellular region and larger diameter fibrils of up to 300 nm diameter are found in the territorial and inter-territorial matrix (Broom and Marra, 1986). The main function is the provision of stable tissue scaffolding and a reinforcing and restraining meshwork for cells. The collagens of adult articular cartilage are principally type II (95%), type XI (3 %) and type IX (1% - although it is present at a much higher concentration in foetal tissues) (Gardner, 1992, Mendler et al., 1989). The collagens can be categorised into different classes according

to their normal, preferred molecular and supramolecular organisation. Collagens type II and XI comprise the 300 nm triple helical, fibril forming collagens whilst type IX is of the class that are arranged as short helices. Collagen IX molecules can decorate fibril surfaces, particularly those thin fibrils in the pericellular basket (Hagg et al., 1998, Mendler et al., 1989). It is believed that collagen XI initially forms a head-to-tail self-cross-linked filament that becomes integrated and cross-linked laterally onto or within the body of collagen II fibrils (Eyre, 2002). Cross-linking studies have identified at least seven sites of cross-linking within the collagen IX molecule where covalent bonds form with either collagen II molecules or with other IX molecules (Eyre et al., 2006, Zhu et al., 1996), see Figure 2.1. This interaction may help to form and stabilize the collagen fibril meshwork and appears to have an important role in stabilizing the three dimensional organization of the of the collagen network (Mow and Huiskes, 2005, Zhu et al., 1996, Broom and Silyn-Roberts, 1990) and thus contributes to the ability of collagen to resist the swelling pressure of the proteoglycans and the tensile stresses developed within the tissue when it is loaded in situ (Maroudas, 1976). Thus the primary mechanical functions of collagen fibrils in cartilage are twofold. First, its structure provides tensile stiffness and strength to the tissue (Julkunen et al., 2008b). Second, the collagen network also functions to restrain the swelling pressure of the embedded proteoglycans, which provide compressive stiffness (Mow and Guo, 2002, Mow and Huiskes, 2005).

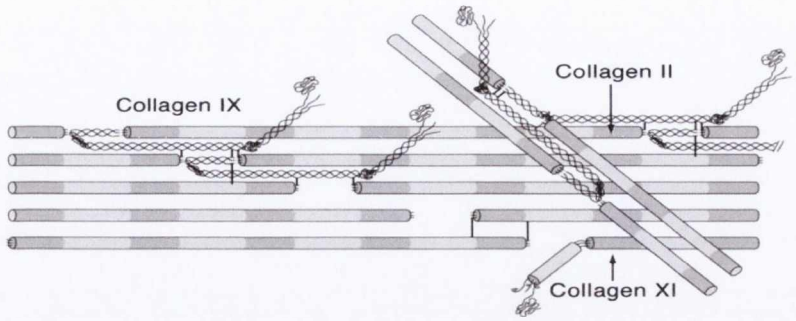

Figure 2.1. The collagen II/IX/XI heterofibril. An interaction model between surface collagen IX molecules and the collagen II polymer that can accommodate all known IX-to-IX and IX-to-II crosslinks and potential interfibrillar cross-links. Adapted from (Eyre et al., 2006).

2.1.3 Proteoglycans

Aggrecan is the main PG molecule found in articular cartilage. It is composed of a single protein core to which numerous negatively charged glycosaminoglycan (GAG) side chains are attached, see Figure 2.2. Most aggrecan molecules are further bound to a single hyaluronan chain of approximately 5×10^5 Da to form large PG aggregates (Hardingham, 1981, Muir, 1983). The large size and complex structure of the PG aggregates immobilise and restrain the molecule within the intrafibrillar space, thus forming the solid matrix of articular cartilage (Mow and Guo, 2002). The dimeric units of these GAGs are usually chondroitin sulphate (CS) and keratin sulphate (KS). At normal physiological conditions, each dimeric unit of CS has two negative charge groups (SO_3^- and COO^-), and each dimeric unit of KS has one negative charge group (SO_3^-) (Mow et al., 1998). Because these charges are held by the PG's enmeshed within the solid matrix, the total number of electrical charges, typically normalised by the volume of interstitial fluid, is called the fixed charge density (FCD) (Ateshian, 2009). As these negative charges cannot freely flow out of the tissue, the interstitial fluid must contain an excess of cations, relative to the external bathing solution, in order to maintain electro neutrality within the tissue (Ateshian and Hung, 2006). The net effect is that the osmolarity of ions inside the tissue

is greater than outside producing an osmotic pressure within the interstitial fluid (Ateshian, 2009, Brommer et al., 2005, Ateshian and Hung, 2006). This is known as the Donnan osmotic fluid pressure (Maroudas and Bannon, 1981, Frank et al., 1990, Donnan, 1995) and increases with increasing FCD. In addition, the FCD increases with compressive strain, as the charges get closer together. The total FCD in cartilage ranges from 0.05 to 0.3 mEq/g wet weight of the tissue (Maroudas et al., 1969, Mow and Huiskes, 2005). The rate of change of osmotic pressure with compressive strain may be construed as an osmotic modulus; hence, the proteoglycans of cartilage contribute to the tissue's compressive properties (Ateshian et al., 2004). Swelling pressure is reported to vary from 0.02MPa to 0.2MPa (Maroudas 1979) which, is consequently, reported to induce an initial tensile state of stress, known as pre-stress. These small associated swelling strains are consistent with the high tensile stiffness of the solid matrix (Chahine et al. 2004; Maroudas 1979).

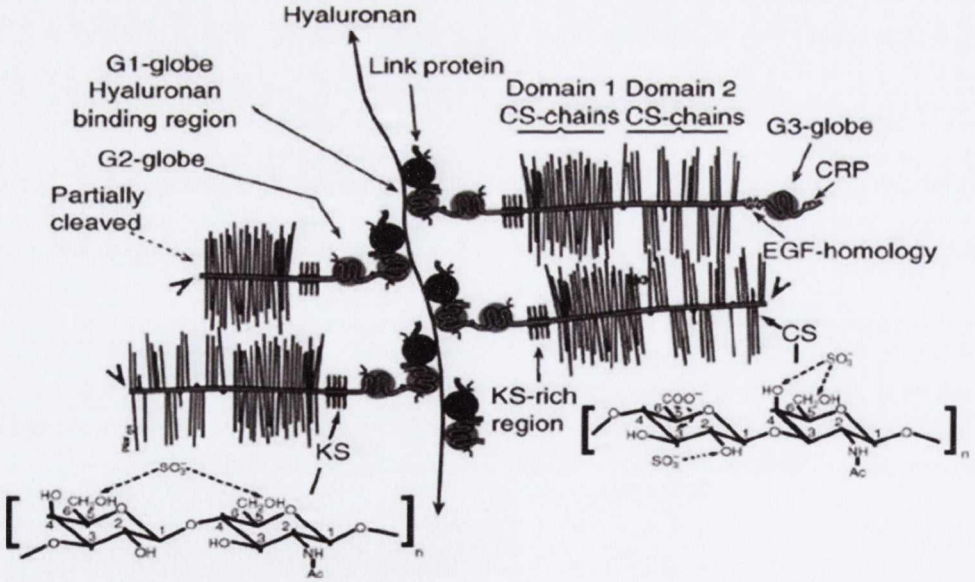

Figure 2.2. Schematic depiction of an aggrecan and its location on a PG aggregate. An aggrecan is composed of glycosaminoglycan chains (keratin sulfate and chondroitin sulfate) bound covalently to a core protein molecule (Lu and Mow, 2008).

2.1.4 Collagen-proteoglycan interactions

The swelling pressure exerted by the FCD serves to inflate the collagen network, Figure 2.3, and thus contributes to the shear stiffness to the ECM by holding the collagen network in place and allowing the collagen to be deformed (Zhu et al., 1993, Mow and Huiskes, 2005, Cohen et al., 1998). *In vitro*, viscometric studies of purified proteoglycan solutions at high concentrations have provided a means of determining physical interactions amongst proteoglycans (Hardingham et al., 1987, Zhu et al., 1996). Proteoglycans, in high concentrations, are able to interact with each other to form networks with significant mechanical strength and energy storage capability (Zhu et al., 1996, Schmidt et al., 1990, Zhu et al., 1993). Adding type II collagen and/or link protein seems to increase the interaction sites and strength (Zhu et al., 1996, Zhu et al., 1991, Mow and Huiskes, 2005) suggesting that these two proteins can also interact with the proteoglycan network and contribute significantly to the compressive stiffness of the tissue. The proteoglycan networks and the proteoglycan-collagen networks formed *in vitro* are capable of storing elastic energy, but their shear stiffness of ~10 Pa is less than 10^{-5} times that of normal articular cartilage (Mow and Huiskes, 2005). Therefore other factors such as collagen cross-linking and interactions with type IX collagen must have strong influences on the compressive and shear properties of articular cartilage (Schmidt et al., 1990, Zhu et al., 1993). The other aspect of interaction of PG and collagen lies in the fact that some small leucine-rich proteoglycans (SLRPs), including decorin and fibromodulin, can interact with and regulate collagen fibrillogenesis (Scott, 1988). Through these interactions, fibril assembly and diameter can be influenced (Scott, 1988, Mow and Huiskes, 2005).

Extraction of PGs from native articular cartilage has been used to provide further insight into the functional role of the collagen matrix alone. Canal Guterl et al. 2010 observed curling in mature articular cartilage after it had been excised from bone, indicative of residual stresses in the tissue. These residual stresses are generally attributed to the presence of proteoglycan molecules, which give rise to a swelling pressure in the tissue's interstitial fluid. However, though the reduction in PG content was not complete (~90.4%), the persistence of curling in digested samples is evidence that there are residual stresses in the collagen matrix not attributable to the osmotic pressure of the interstitial fluid (Broom, 1984, Schmidt et al., 1990, Narmoneva et al., 1999).

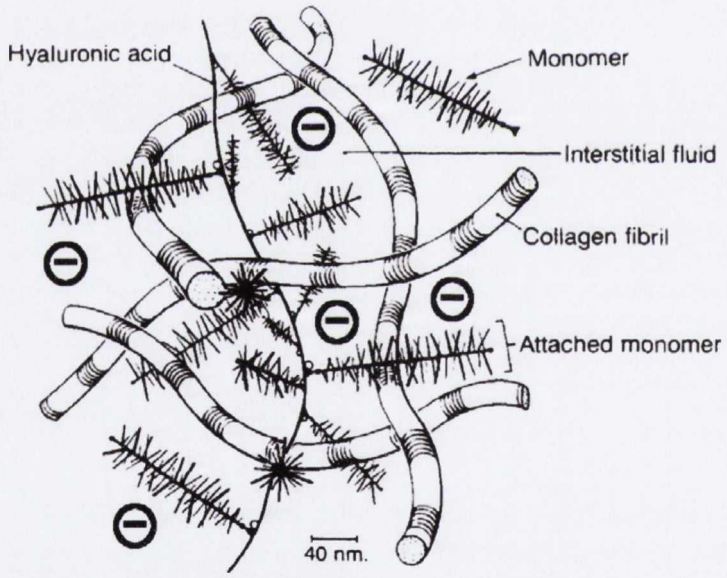

Figure 2.3. The PGs are entangled with the collagen network which counteracts the swelling pressure originating from the negatively charged GAGs. Adapted from (Mow et al., 1992).

2.1.5 Chondrocytes

The chondrocyte and its pericellular matrix seem to act as a structural and functional unit, see Figure 2.4. In skeletally mature cartilage, the ECM contributes the vast majority of the tissue volume, while the cells only occupy <10% of the total volume. The ECM affectively shields the ensconced chondrocytes from the high stresses and strains generated by joint loading, while not completely isolating the cells from the mechanical environment (Guilak et al., 1995). They are responsible for the synthesis, modification, assembly, and organisation of the ECM and for maintenance of homeostasis in the tissue (Klein et al., 2007). Chondrocytes interact with the ECM through cell surface receptors such as integrin's, annexin V, and CD44 (Mow and Huiskes, 2005). Through these interactions, chondrocytes can sense the changes in the ECM, such as the deformation caused by mechanical loading, or the composition changes caused by the degradation and depletion of the matrix molecules (Chahine et al., 2007). Chondrocytes are metabolically active and can adapt to these changes to a limited extent (Mow and Huiskes, 2005, Guilak et al., 1999).

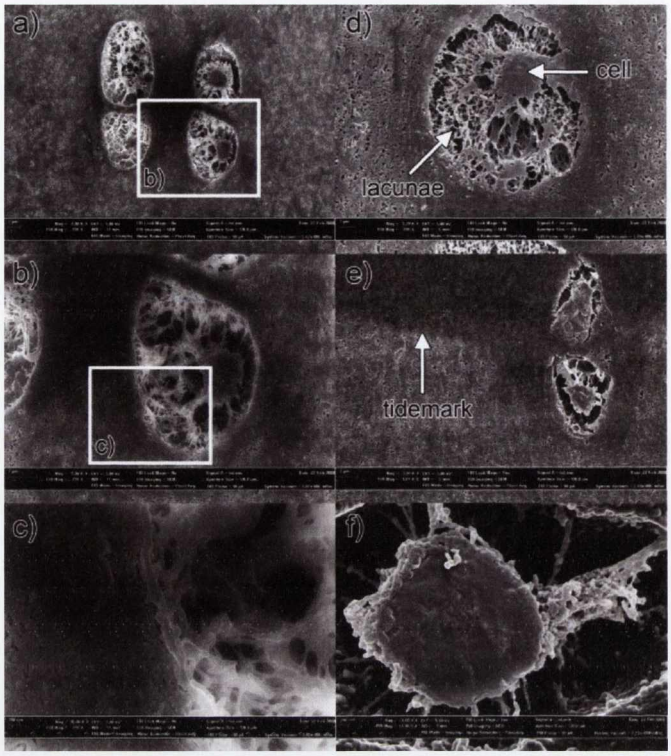

Figure 2.4. Appearance of chondrocytes in SEM imaging after levelling with a focussed ion beam (FIB) inside the lacunae in articular cartilage as (a) isogenous group of four elongated chondrocytes (2000×), (b) magnification of (a) at 5000×, (c) magnification of (b) at 20,000×, (d) single round-shaped lacunae with chondrocyte at 5290×, (e) isogenous group near the tidemark at 3000×, and (f) magnification of cell inside the lacunae at 15,000×. Adapted from (Zehbe et al., 2012).

2.2 Depth Dependent Properties of Articular Cartilage

Adult articular cartilage demonstrates a depth dependent heterogeneous composition and ultra-structure, traditionally divided into three distinct zones (Benninghoff, 1925, Julkunen et al., 2009), see Figure 2.5. The delineation between these zones is often determined on the basis of the orientation of the collagen fibrils, which may be determined via polarised light microscopy (PLM) (Julkunen et al., 2010, Király et al., 1997, Rieppo et al., 2008, Rieppo et al., 2009, Xia, 2008), magnetic resonance imaging (MRI) (Xia, 2008, Cohen et al., 1999), or Fourier transform infra-red imaging (FRIRI) (Saarakkala et al., 2010, Rieppo et al., 2009, Xia, 2008).

Each zone has a distinct cell morphology, with the shape and arrangement of the chondrocytes believed to be related to the local architecture of the collagen fibrils within the solid matrix (Guilak et al., 1995). In the superficial tangential zone (STZ), the collagen fibrils are densely packed and orientated parallel to the articular surface (Weiss et al., 1968, Rieppo et al., 2008). In this layer the matrix consists of a relatively low PG content (Stockwell, 1970) and provides a lower permeability to fluid flow (Setton et al., 1993), limiting fluid flow when cartilage is compressed (Mow and Guo, 2002). A high density of oblong shaped chondrocytes, with their long axis parallel to the articular surface (Stockwell, 1970) reside in this region. These chondrocytes have relatively low metabolic rates (Poole et al., 1987), but uniquely secrete molecules that may aid in boundary lubrication, including proteoglycan 4 (PRG4) (Klein et al., 2007).

In the middle zone (MZ), the collagen fibrils are larger, less dense and arcade from a parallel to a perpendicular orientation resulting in a random organisation (Benninghoff, 1925). The concentration of PG aggregates increases to a maximum in the middle zone, negatively correlating to decreases in water content and thus resulting in higher swelling pressures (Chen et al., 2001). Furthermore, the middle zone contains cells that are rounded with seemingly higher synthetic activities (Guilak et al., 1995). Collagen content increases with depth from the articular surface (Williamson et al., 2003) whilst water content generally decreases (Schinagl et al., 1997).

Fibrils in the deep layer form large bundles and are orientated perpendicular to the layer of subchondral bone (Benninghoff, 1925, Xia, 2008). These bundles cross the tidemark to insert into the calcified cartilage and subchondral bone, thus securely anchoring the cartilage onto the bone ends (Mow and Huiskes, 2005, Mow and Guo, 2002). This heterogeneity in the ultra-structural organisation of the collagen matrix is

reflected in the heterogeneity of tensile and compressive properties through the tissue depth (Ateshian and Hung, 2006), as will be discussed in section 2.4.

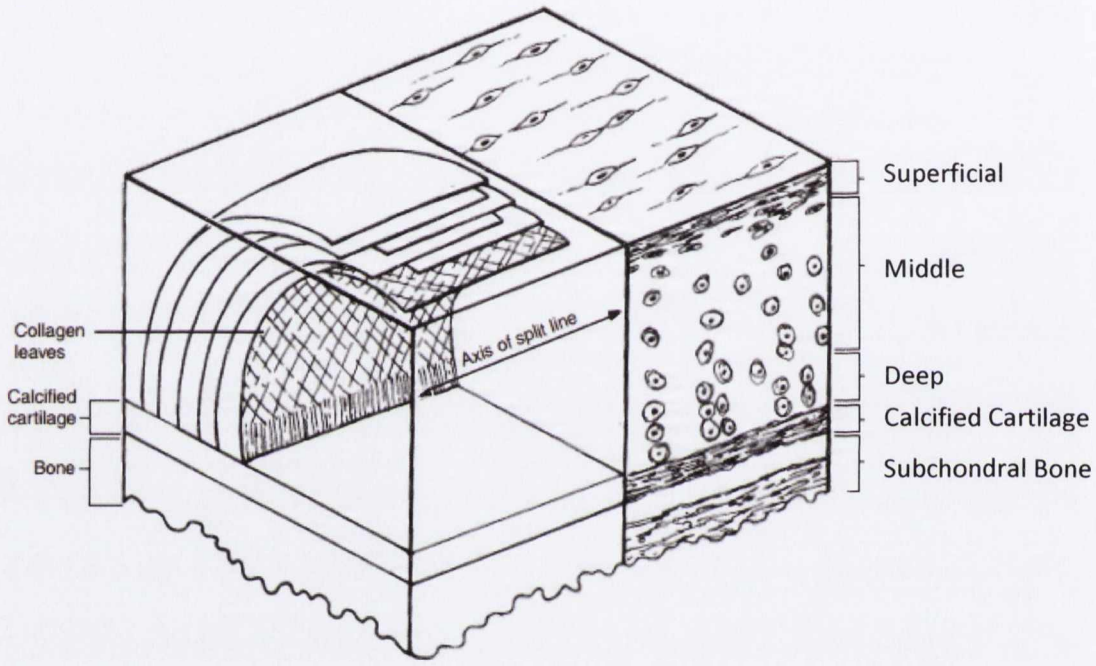

Figure 2.5. Cross sections cut through the thickness of articular cartilage on two mutually orthogonal planes. These planes are oriented parallel and perpendicular to split lines on the cartilage surface. The background shows the four zones of the cartilage: superficial, intermediate, radiate, and calcified. The foreground shows the organization of collagen fibrils into "leaves" with varying structure and organization through the thickness of the cartilage. The leaves of collagen are connected by small fibrils not shown in the figure. Adapted from (Mansour, 2003)

2.3 Cartilage Mechanics

The main extracellular matrix components of articular cartilage, proteoglycans (PG) and collagens, provide biomechanical properties that vary with growth, aging, and depth from the articular surface. The negatively charged PG contribute to compressive resistance and provide a high Donnan osmotic fluid pressure within the tissue. In contrast, the collagen network provides the restraining stress that counter balances osmotic pressure at rest or during loading (Figure 2.6, A and B), and the high resistance of cartilage to tension, as discussed in sections 2.1.3 and 2.1.4 respectively. In articular cartilage, water is distributed between collagen fibrils (intrafibrillar (IF)) and PG (extrafibrillar (EF); Figure 2.6, C and E), and this water distribution varies with external stress applied to the tissue (Basser et al., 1998, Han et al., 2011, Maroudas et al., 1991, Katz et al., 1986).

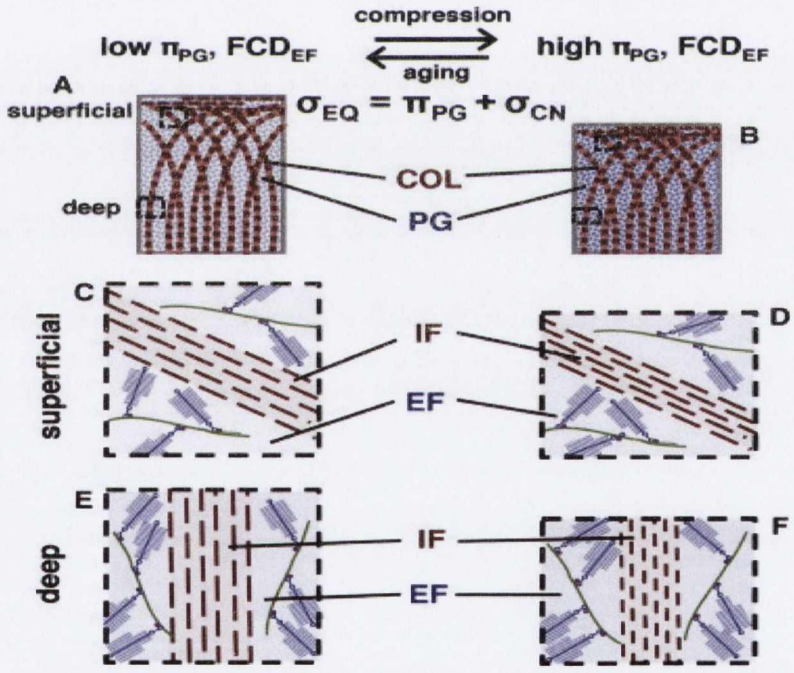

Figure 2.6. Multi-scale schematic of the effects of FCD and π_{PG} on the collagen network. (A and B) At the macroscopic tissue scale, compression (A->B) leads to increased FCD and osmotic pressure π_{PG}. (C–F) At the micro-scale, both compression (C->E and D->F) and increasing depth (superficial C, E to deep D, and F) lead to higher FCD and π_{PG}, and a fluid shift from IF space into EF space. Adapted from (Han et al., 2011).

In addition to the Donnan osmotic pressure arising from physicochemical effects, the interstitial fluid of cartilage will pressurize as a result of mechanical loading of the tissue. The biomechanical behaviour of articular cartilage can be best understood by considering it to be a fluid-filled, porous-permeable material. Fluid movements in cartilage loaded in compression are governed by the hydraulic permeability of the solid matrix. This permeability is in turn related to the extracellular matrix pore size and connectivity. The concentration of PGs affects tissue permeability as the negative charges have been shown to impede hydraulic fluid flow (Mow and Guo, 2002). As the permeability of the tissue to fluid flow is low, when cartilage is loaded, a volumetric change or a pressure gradient will be created within the tissue. As a result, the interstitial fluid will begin to flow within the tissue or be extruded from the tissue, see Figure 2.7. The fluid passing through the porous solid matrix generates very high frictional resistance and therefore is the primary mechanism giving rise to the frictional dissipation responsible for the viscoelastic behaviour of articular cartilage in compression. This phenomenon is best expressed using the biphasic theory developed by (Mow et al., 1980).

According to the biphasic theory, three major internal forces act in concert within the loaded tissue to balance externally applied forces:

- The stress developed within the deformed collagen-PG solid matrix
- The pressure that is developed within the fluid phase
- The frictional drag acting between the fluid phase and the solid phase as they flow past each other.

Permeability of normal hyaline cartilage is extremely small ($\sim 10^{-16}$ $m^4 \cdot N^{-1} \cdot s$), indicating that immense interstitial fluid pressures and dissipations are occurring inside the tissue during compression. These mechanisms for deformation and high energy

dissipation provide an efficient method to shield the collagen-PG solid matrix and embedded chondrocytes from high stresses and strains associated with joint loading during daily activities.

Several experimental measurements of interstitial fluid pressurization in articular cartilage have been reported in confined and unconfined compression (Park et al., 2003, Soltz and Ateshian, 1998, Soltz and Ateshian, 2000). In confined compression, where a cylindrical cartilage plug is loaded in a confining chamber of the same diameter using a free-draining porous indenter, the interstitial fluid pressure has been measured on the circular specimen face abutting the bottom impermeable wall of the chamber. In a stress relaxation test, upon application of a ramp loading phase, the pressure was observed to rapidly rise to a value equal to the applied compressive stress, before slowly subsiding back to zero during the relaxation phase of the test (Figure 2.7). Since the fluid pressure is equal to the applied stress up on initial load application whereas the displacement is zero (Figure 2.7, O), it is possible to conclude that the entire applied load is initially supported by the pressurized interstitial fluid, and none by solid matrix deformation (Ateshian, 2009). As time progresses however, the pressurized interstitial fluid flows out of the tissue, through the porous indenter, leading to a progressive reduction in fluid pressure and increase in solid matrix deformation. Thus, over time, the load becomes progressively more supported by the solid matrix. This concept of load sharing between the solid and fluid matrix (Ateshian, 2009, Ateshian et al., 2004, Soltz and Ateshian, 2000), which may be called the interstitial fluid load support, plays an important role in the frictional response of articular cartilage.

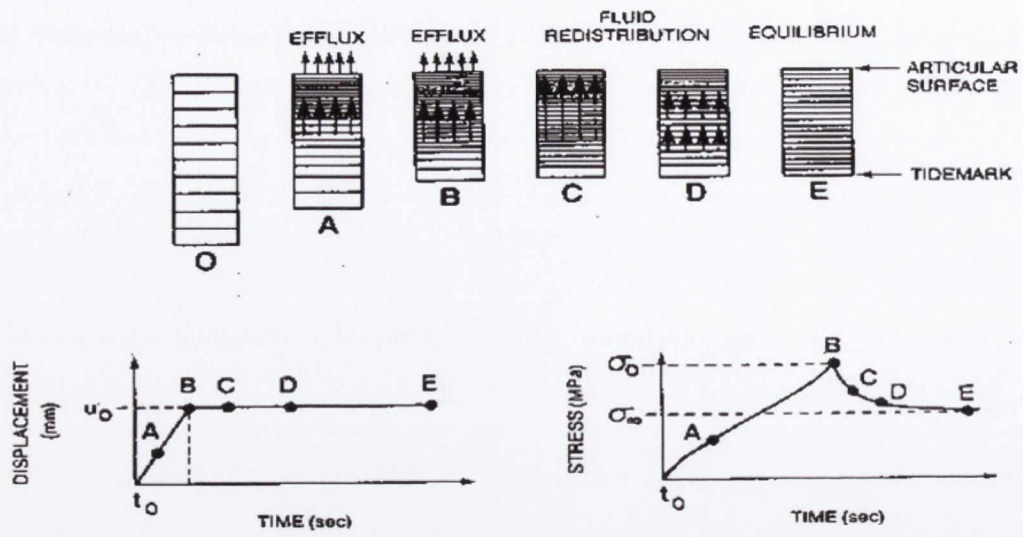

Figure 2.7. Schematic representation of fluid exudation and redistribution within cartilage during a rate-controlled compression stress-relaxation experiment. The horizontal bars in the upper figures indicate the distribution of strain in the tissue. The lower graph shows the stress response during the compression phase (O, A, B) and the relaxation phase (B, C, D, E). Adapted from (Mow and Huiskes, 2005).

Comparisons of experimental measurements with theoretical predictions from the biphasic theory have shown very good agreement in confined compression creep, stress-relaxation, and dynamic loading (Soltz and Ateshian, 1998, 2000b), providing confidence in the predictive ability of the biphasic theory for this testing configuration (Fig. 1). Good agreement between theory and experiment also lends confidence in the physical interpretation of observed phenomena using the context of that theoretical frame- work. Thus, according to the biphasic theory, the reason that the interstitial fluid load support initially matches 100% of the applied stress in confined compression occurs because the solid and fluid constituents of articular cartilage are nearly incompressible (in the range of pressures encountered in diarthrodial joints, typically less than 20MPa). Since interstitial fluid cannot escape from cartilage instantaneously, the cartilage specimen must maintain its volume immediately following the application of a step load. In confined compression the specimen is surrounded by rigid walls; thus, an isochoric (volume-conserving) deformation cannot occur initially, implying that the only manner by which the tissue can

resist the applied load is via interstitial fluid pressurization. In unconfined compression, it was found that good agreement between theoretical predictions and experimental measurements of the load response (Ateshian, 2009, Cohen et al., 1998, Soulhat et al., 1999) and interstitial fluid pressurization (Ateshian, 2009, Park et al., 2003, Soltz and Ateshian, 2000) could be achieved only after incorporating tension–compression non linearity in the modelling of the solid matrix of cartilage; as discussed in subsequent sections.

For normal articular cartilage compressive modulus and permeability, this high percentage of fluid support can last more than 500s due to its large characteristic time constant τ; hence for all practical purposes, in vivo, as a consequence of cartilages intrinsic biphasic properties, interstitial fluid pressurization shields the collagen-PG solid matrix from the high stresses that the diarthrodial joints normally experience during the normal activities of daily life. One can measure only the true mechanical properties of the collagen-PG solid matrix at equilibrium, when the fluid pressure or frictional drag effects vanish. See Table 2.1 for bulk equilibrium aggregate moduli (MPa) from a range of species.

	Human[a]	Bovine[b]	Canine[c]	Monkey[d]	Rabbit[e]
Lateral Condyle	0.701 ± 0.228	0.894 ± 0.228	0.603 ± 0.237	0.778 ± 0.176	0.537 ± 0.258
Medial Condyle	0.588 ± 0.114	0.899 ± 0.427	0.904 ± 0.218	0.815 ± 0.180	0.741 ± 0.101
Patellar Groove	0.530 ± 0.094	0.472 ± 0.147	0.555 ± 0.144	0.522 ± 0.159	0.516 ± 0.202

Table 2.1. Bulk equilibrium aggregate modulus (MPa) obtained from nonlinear regression curve fits of in situ biphasic creep indentation experiments of lateral condyle, medial condyle and patellar groove cartilage. Age groups are as indicated; (a) Young normal, (b) 18 months to 2 years old, (c) mature beagles and greyhounds, (d) mature cynomologus monkeys, (e) mature New Zealand White rabbits. Numbers indicate mean ± SD. Adapted from (Athanasiou et al., 1991).

Because of the fibrillar nature of the collagen matrix, and since fibrils can resist tensile loads much better than compressive loads, cartilage exhibits a much higher stiffness in tension than compression (Chahine et al., 2004, Khalsa and Eisenberg, 1997, Kempson et al., 1968), a phenomenon that is called tension-compression non-linearity (Soltz and Ateshian, 2000). Furthermore, studies have shown that Poisson's ratio under uniaxial tension, generally between 0.5 and 2, are considerably larger than the equilibrium compressive Poisson's ratio which ranges from 0.02 to 0.4 (Chahine et al., 2004, Jurvelin et al., 1996, Wang et al., 2003).

Under cyclic loading at physiological frequencies (e.g. 0.01-2 Hz), the interstitial fluid pressure is maintained at elevated values (Huang et al., 2001, Lee et al., 1981, Park et al., 2004, Soltz and Ateshian, 2000) and the tissues dynamic modulus is considerably higher than the equilibrium modulus (Buschmann et al., 1999, Kim et al., 1995, Lee et al., 1981, Park et al., 2004, Sah et al., 1989). This is due to the fact that the equilibrium modulus is reliant on flow-independent properties of the tissue whilst the dynamic modulus is reliant on flow-dependent properties i.e. the frictional drag of interstitial fluid flow through the porous permeable solid matrix (Setton et al., 1993). As aforementioned, hydraulic permeability which is inversely correlated to collagen content and fixed charge density (Maroudas, 1976), is lowest in the superficial region. This is speculated to be due to the collagen fibrils tightly packed organisation and their tangential orientation to the articular surface (Mansour and Mow, 1976, Maroudas and Bullough, 1968, Setton et al., 1993). In unconfined compression cyclic loading the dynamic modulus of bovine articular cartilage at 1 Hz has been measured at 13, 20, and 37 MPa under strain amplitudes of 0.5, 1, and 2.5%, respectively (Buschmann et al., 1999, Kim et al., 1995, Park et al., 2004, Sah et al., 1989); despite the fact that these results were reported in different studies, they

suggest that the dynamic response of cartilage in unconfined compression is nonlinear with respect to compressive strain (Park et al., 2004).

Cartilage has also been shown to be anisotropic in tension, with the tensile stiffness exhibiting a higher value parallel to the split line direction, see Table 2.2; the preferred orientation of the collagen fibrils in the articular surface when pricked with a needle dipped in India ink (Benninghoff, 1925) see Figure 2.8, than perpendicular to it (Kempson et al., 1968). Furthermore, more recent studies have demonstrated that cartilage exhibits material properties consistent with orthotropic symmetry when taking into account its tension-compression non linearity and inhomogeneity (Wang et al., 2003), with the planes of symmetry defined locally by the direction parallel to the local split lines (1-direction) and perpendicular to the split lines (2-direction) and normal to the articular surface (3-direction).

	Bovine		Canine		Human	
	Glenoid	Humerus	Femoral Groove	Femoral Condyle	Femoral Groove	Femoral Condyle
Surface	5.9 (2.4)	13.4 (4.6)	27.4 (8.4)	23.3 (8.5)	13.9 (2.4)	7.8 (1.7)
Middle	0.9 (0.5)	2.7 (1.6)			2.4 (1.4)	4.0 (1.1)
Deep	0.2 (0.2)	1.7 (0.8)			1.0 (0.5)	

Table 2.2. Equilibrium tensile modulus (MPa) of normal human, bovine, and canine articular cartilage, inhomogeneous variations through the depth of the cartilage layer. All samples harvested in a direction parallel to the split line direction. Data are expressed as mean (SD). Data adapted from (Akizuki et al., 1986, Mow and Huiskes, 2005, Setton et al., 1998)

The existence of complex mechanical properties such as tension-compression nonlinearity, anisotropy, and inhomogeneity, bestow a specialised load bearing capacity on articular cartilage. For example, the high stiffness in tension versus compression allows cartilage to resist radial expansion under axial compressive loading and results in increased fluid pressurisation and dynamic stiffness (Chahine et al., 2004). Specifically, in the superficial region, due the tangential orientation of the collagen fibrils limiting radial expansion during compressive loading (Ateshian et al., 2009, Kiviranta et al., 2006, Wong et al., 2000).

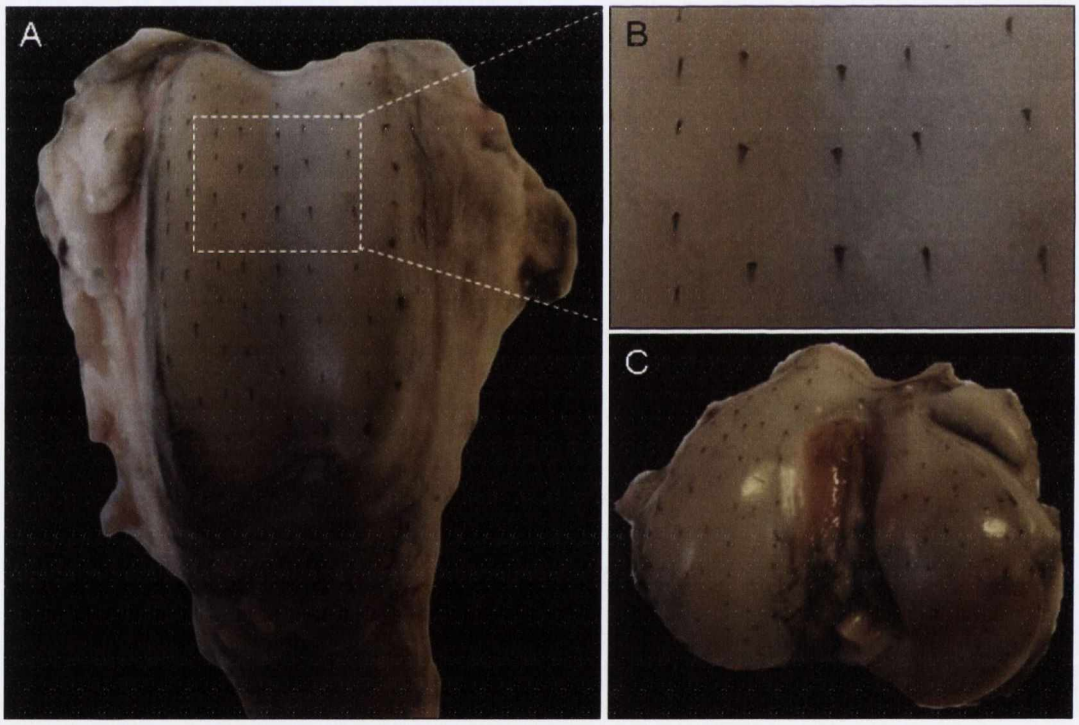

Figure 2.8. Split line pattern of porcine (a) femoropatellar groove and (c) femoral condyles. Image (b) shows a magnification of a region in (a).

2.4 Inhomogeneity of Articular Cartilage Properties

As indicated in section 2.2 and 2.3 it is well established that the composition and structure of articular cartilage vary through the depth of the tissue. These variations are closely related to the inhomogeneous mechanical properties of the tissue. Confined and unconfined compression tests are commonly used to determine the compressive material properties of articular cartilage at equilibrium. When cartilage is loaded in compression, a loss of tissue volume occurs due to fluid exudation from the tissue. These effects give rise to time-dependent viscoelastic behaviours such as creep and stress relaxation (Mow and Guo, 2002). During stress relaxation testing, upon reaching equilibrium no hydraulic fluid pressurisation exists within the tissue and the intrinsic elastic or "flow independent" properties of the porous-permeable solid matrix can be determined (Setton et al., 1993). Driven by the apparent implications of these characteristic differences in layer specific cartilage properties for cartilage function, a multitude of experimental approaches have been employed to quantify layer specific properties in full thickness cartilage samples (Armstrong and Mow, 1982, Basser et al., 1998, Bevill et al., 2010, Canal et al., 2008, Chahine et al., 2007, Chen et al., 2001, Erne et al., 2005, Guilak et al., 1999, Guilak et al., 1995, Hunziker et al., 2007, Julkunen et al., 2009, Julkunen et al., 2008, Julkunen et al., 2008b, Jurvelin et al., 1996, Khalsa and Eisenberg, 1997, Kiviranta et al., 2006, Laasanen et al., 2002, Mow et al., 1980, Rolauffs et al., 2010, Schinagl et al., 1997, Setton et al., 1993).

Recently, microscopy techniques have been developed to determine the depth varying compressive properties of articular cartilage (Guilak et al., 1995, Canal Guterl et al., 2010, Wang et al., 2002a, Schinagl et al., 1997, Schinagl et al., 1996). For example, (Schinagl et al., 1997) employed video microscopy and fluorescently labelled chondrocyte nuclei, which were used as fiducial markers to quantify the inhomogeneous

equilibrium strain fields within osteochondral cores during confined compression. At low levels of compression (8% and 16%), the compressive strains were large in the superficial layers (~0.2 – 0.5) and near 0 in the deeper layers ($\ll 0.05$). As compression was increased (24 and 32%), the strains generally increased in all layers. Their reported finding gave an average aggregate modulus of 0.079 MPa in the very superficial layer, increasing to 2.1 MPa in the deepest layer.

More recently, (Wang et al., 2002a) incorporated a digital image correlation (DIC) algorithm and the triphasic theory to determine the continuous depth-distribution of the aggregate modulus and FCD. This technique allows a non-invasive methodology to determine the intrinsic compressive stiffness (H_A) of the extracellular matrix and the depth-dependent FCD distribution for articular cartilage. They concluded that the depth dependent elastic modulus and Poisson's ratio were found to be smallest at the superficial layer and increased with depth. The apparent compressive modulus was further found to decrease with increasing compressive strain; this is known as strain softening (Ateshian et al., 2009, Chahine et al., 2004, Bursac et al., 1999). Micro-structural models have physically interpreted this phenomenon as a release of tension and buckling of the collagen fibrils during compression, as the applied compressive strain overcomes the osmotic swelling pressure (Chahine et al., 2004, Basser et al., 1998, Shirazi and Shirazi-Adl, 2008, Bursac et al., 2000). The smaller Poisson's ratio in the STZ of the tissue has also been seen by (Kiviranta et al., 2006). They postulated this decrease in the Poisson's ratio was due to the parallel orientation of the collagen fibrils limiting radial expansion of the tissue.

Less dramatic but qualitatively similar results were reported by (Guilak et al., 1995) who used confocal microscopy to measure the degree of chondrocyte deformation in the superficial, middle and deep layers of canine femoral cartilage. When full-thickness

explants were compressed to 15% surface to surface strain, a 19.1% deformation of superficial chondrocytes was observed compared to 14.8% and 15.7% for the middle and deep zones, respectively. The authors concluded that the compressive modulus on the surface zone is approximately 27% less than that of the middle and deep zones.

Tensile stiffness of normal articular cartilage in the STZ has been reported to be significantly greater than in the deep zone (Table 2.2) (Woo et al., 1976, Roth and Mow, 1980) and is mainly attributed to organisation of the fibrils in the STZ (Roth and Mow, 1980, Williamson et al., 2003). Hydraulic permeability, inversely correlated to fixed charge density (Maroudas, 1976) is lowest in the STZ. This is speculated to be due to the collagen fibrils tightly packed organisation and their tangential orientation to the articular surface (Mansour and Mow, 1976, Maroudas and Bullough, 1968, Setton et al., 1993).

2.5 Changes with Age

During foetal life, the epiphyseal region of bones is comprised initially of cartilage and a network of blood vessels, housed in cartilage canals. During foetal maturation, the cartilaginous epiphysis has a dual structure: the superficial component becomes the articular cartilage and the deeper part develops into an ossification centre (growth cartilage); combined they are called the articular-epiphyseal cartilage complex (AECC) (Lecocq et al., 2008), see Figure 2.9. In utero and postnatal growth, articular cartilage appears as a relatively homogeneous, very dense mixture of cells in a highly hydrated matrix of proteoglycan and collagen. The matrix is much softer than in mature tissue; ranging from (0.11 ± 0.03 MPa) in foetal tissue to (+182%, 0.31 ± 0.03 MPa) in adult (Williamson et al., 2001), while the collagen network is more isotropic in structure and bears little resemblance to that of mature articular cartilage (Bank et al., 1998, Hunziker

et al., 2007, Klein et al., 2007). Furthermore, the immature articular cartilage acts as an articulating layer and as a surface growth plate for the longitudinal, radial and lateral growth of the epiphyseal bone. The true growth plate, comprised of hyaline cartilage and located between the epiphysis and the metaphysis, is responsible for the longitudinal growth of the metaphysis and the diaphysis (Hunziker et al., 2007, Mow and Huiskes, 2005). Although the dual functionality of immature mammalian articular cartilage is generally recognised, the mechanisms underlying its postnatal growth activities and structural reorganisation remain obscure (Hunziker et al., 2007). It could be a process whereby the adult articular cartilage structure is gradually formed by the division and activity of the stem (progenitor) cells of the cartilage surface and that this involves simultaneous tissue resorption and structural neoformation (Hunziker et al., 2007, Julkunen et al., 2009), or one of internal tissue remodelling and reorganisation.

In a study conducted by Hunziker et al. 2007 on the development and growth of New Zealand white rabbits; knee-joint articular cartilage of rabbits attains structural maturity at the time of sexual maturity (3 months), whereas the true growth plates are still open and active at this juncture, closing only after 7-8 months meaning that during postnatal development, the growth activities of the articular cartilage layer and of the growth plate proper are hormonally regulated by different mechanisms and at different levels. Furthermore, they found that during the growth phase, when articular cartilage is undergoing structural reorganization, the net length gain in the epiphyseal bone exceeds the height of the articular cartilage layer, see Figure 2.10. Hence, these results indicate that immature cartilage is subject to the complete resorption of all zones except the superficial (stem-cell) one and their replacement by appositional growth from the latter.

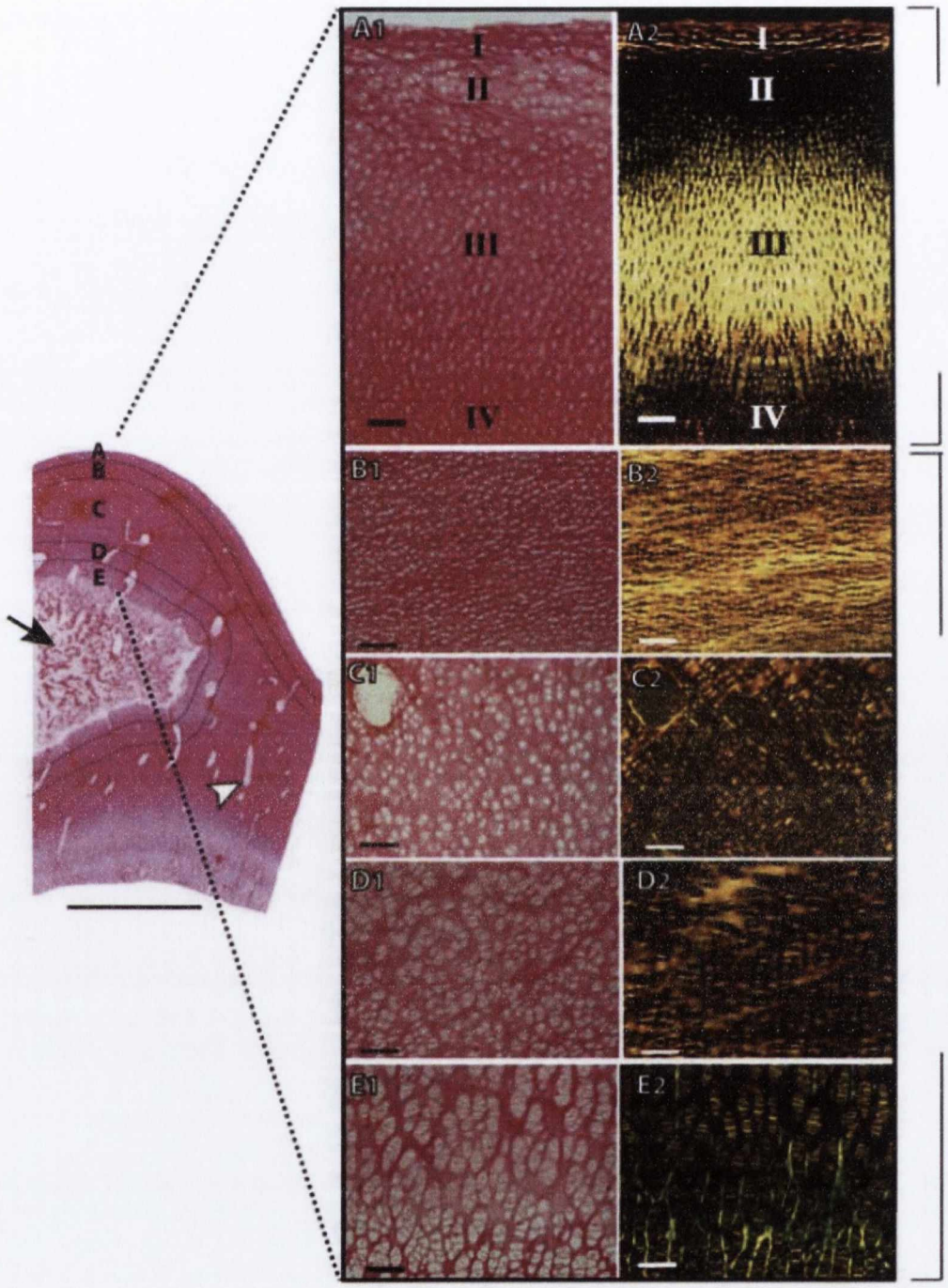

Figure 2.9. Collagen network organisation in the articular-epiphyseal cartilage complex of the distal tibia from a 9 month fetus. In the section of the epiphysis stained with picrosirius red and observed with the naked eye (left picture), the different histological zones of the cartilage corresponding to the pictures A to E are shown by dotted lines. The secondary centre of ossification is visible in the middle of the section (arrow). (Lecocq et al., 2008)

Additionally, these findings correlate with that of Lecocq et al. 2008. They compared picrosirius red stained histological sections viewed with and without polarised light respectively in eight month old equine foetuses. Reporting that the dense tangential collagen network corresponded to a resting zone with small dispersed chondrocytes, the intermediate zone corresponded to a proliferative zone with flat chondrocytes organised in pairs and nests and the radial collagen region corresponded to the zone of hypertrophy with columnar arrangement of large chondrocytes.

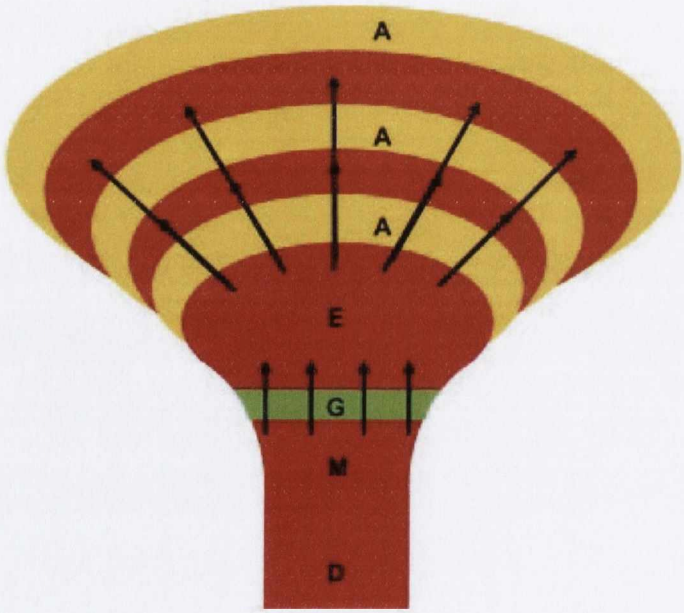

Figure 2.10. (A) Scheme representing postnatal growth of the epiphysis (E) of a long bone. The articular cartilage (A, yellow) acts not only as an articulating layer, but also as a surface growth plate for the longitudinal, radial and lateral growth of the epiphyseal bone (radially oriented arrows). The true growth plate (G, green), which is located between the epiphysis (E) and the metaphysis (M), is responsible for the longitudinal growth of the metaphysis (M) and the diaphysis (D). Longitudinal bone growth is achieved both by rapid clonal expansion in the vertical direction and by cell hypertrophy. Adapted from (Hunziker et al., 2007).

During development and maturation compositional and architectural changes occur in articular cartilage. The collagen synthesis rate is highest at a young age and as maturation proceeds; the collagen synthesis rate reduces in parallel with a decrease in the matrix metalloproteinase levels, possibly also slowing down the rate of cartilage remodelling (Rieppo et al., 2008). It has been reported that collagen content (% dry weight) and cross-linking increase with age, whereas proteoglycan (PG) (% dry weight) content remains largely unchanged (Grushko et al., 1989, Venn, 1978, Wachtel et al., 1995, Wang et al., 2001, Williamson et al., 2003). Furthermore with age, the exclusively fine collagen fibrils of young cartilage (≥10% collagen IX, ≥10% collagen XI, ≤ 80% collagen II) develop into the thicker and more varied fibril diameters of mature articular cartilage (~1% collagen IX, ~3% collagen XI, ≥ 90% collagen II) (Eyre, 2002). In addition, the collagen architecture changes from a predominantly isotropic structure in immature articular cartilage to a mature arcade-like zonal structure first described by Benninghoff (1925) (Benninghoff, 1925, Buckwalter et al., 2005, Redler et al., 1975, Rieppo et al., 2009), see Figure 2.11.

Such changes in the biochemical composition and organization of articular cartilage with age likely lead to changes in the mechanical functionality of the tissue. For example, Julkunen et al. (2009) used creep indentation testing to investigate the biomechanical to the articular cartilage of New Zealand White rabbits from 0 days to 18 months. They observed a steady increase in equilibrium modulus (0 days -18 months: ~0.5 - 2.5 MPa), positively correlated with collagen content and cross-linking (Julkunen et al., 2009). These results agree with other studies that investigated the bulk compressive modulus of articular cartilage during development in a range of different testing modalities (Brommer et al., 2005, Klein et al., 2007, Williamson et al., 2001).

Immature cartilage seems to be more vulnerable to injurious compression than more mature tissue; this could possibly be due to the fact that young immature cartilage shows less zonal differentiation but higher permeability. (Levin et al., 2005) carried out cyclic confined compression at different loading magnitudes over a range of time periods on cartilage explants from immature (4-8 weeks old) and mature (1.5-2 years old) bovine humeral heads and found that the depth of cell death was greater in immature cartilage than in the mature cartilage.

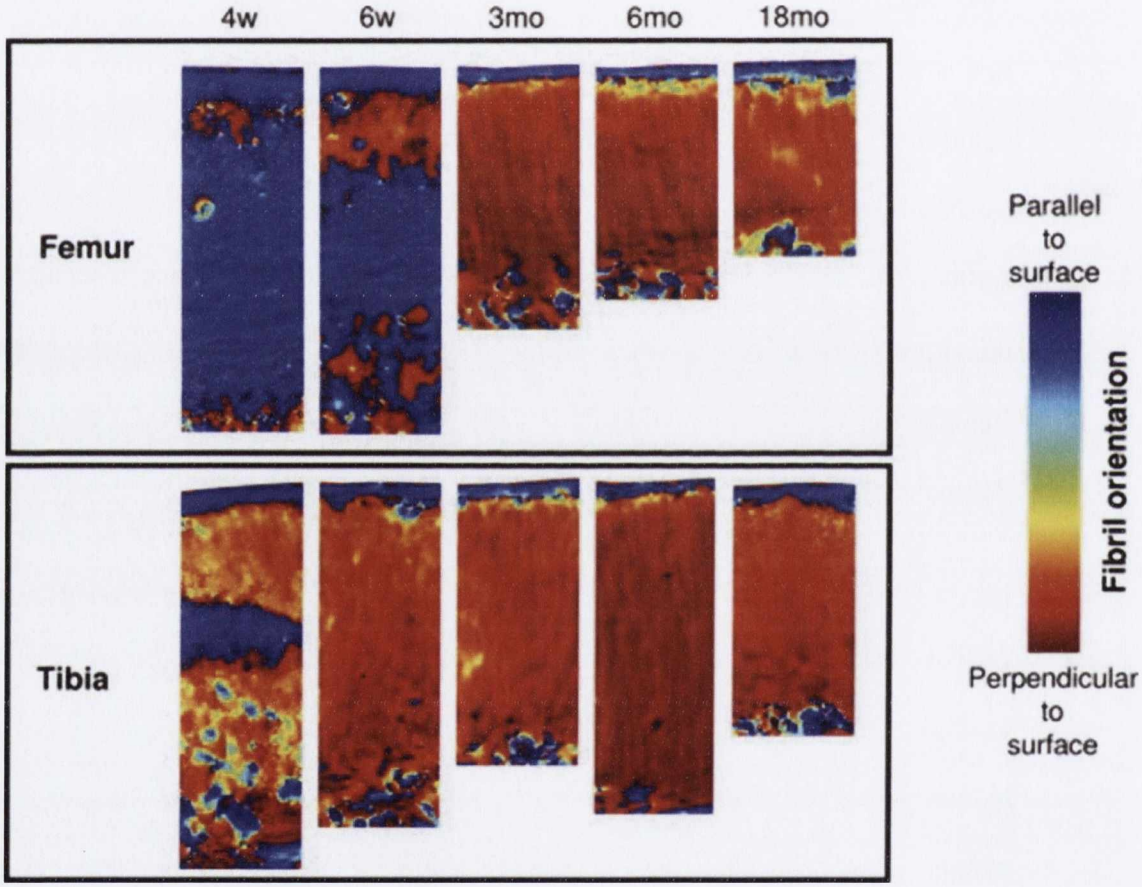

Figure 2.11. PLM images (fibril orientation) of characteristic cartilage samples from femur and tibia in each age-group are presented to show the development of the collagen architecture. Collagen architecture in tibia appeared to mature earlier than that in the femur. After 3 months of age, no significant changes occur in the collagen architecture of the rabbit cartilage (Julkunen et al., 2009).

2.6 Summary

While the relationship between the depth dependent composition of articular cartilage and its equilibrium mechanical properties have been well established, less is known about the dynamic properties of the tissue and how they depend on the tissue's spatial composition and structural organisation. A review of the literature has demonstrated a clear link between the articular cartilage permeability and the tissues ability to generate fluid load support. Furthermore, previous studies have demonstrated that the depth dependent properties of the tissue adapt with age, and that the highly organized STZ observed in skeletally mature articular cartilage has a lower permeability than the remainder of the tissue. Therefore the first hypothesis of this thesis is that removal of the superficial region will influence the flow dependent properties of articular cartilage, leading to a reduction in the dynamic modulus of the remaining tissue. Elucidating the role of this region of the tissue in determining the functional properties of articular cartilage is critically important given that disruption to the superficial zone is often associated with the initiation and/or progression of osteoarthritis.

During development and maturation compositional and architectural changes occur in articular cartilage; such changes in the biochemical composition and organization of articular cartilage with age likely lead to changes in the mechanical functionality of the tissue, yet to date this temporal and spatial relationship remains poorly understood. Therefore the second objective of the thesis was to explore how the equilibrium and dynamic compressive properties of articular cartilage change during postnatal development. I was particularly interested in determining how changes to the superficial region of articular cartilage during skeletal development impact its functional properties, as biomechanical failure of this region of the tissue is postulated by many to be related to

the development of osteoarthritis (Bank et al., 1998, Buckwalter et al., 2005, Setton et al., 1993). It was hypothesised was that a functional superficial region is not present in skeletally immature articular cartilage, and hence removal of this zone of the tissue would only negatively impact the dynamic modulus of the tissue with the attainment of skeletal maturity.

Articular cartilage is known to possess complex depth dependent mechanical properties (Wang et al., 2002a), which cannot be evaluated through commonly used bulk mechanical testing protocols. Given that we know articular cartilage changes from a relatively isotropic tissue at birth to one displaying significant complexity in its spatial composition and organization at adulthood, it would seem reasonable to assume that the depth-dependent mechanical properties of the tissue change dramatically during postnatal development. The final objective of this thesis was to elucidate how the structure and composition of articular cartilage change during postnatal development and maturation using a unique combination of histological, biochemical and imaging techniques and to relate this evolution to changes in the depth dependent compressive mechanical properties of the tissue.

Chapter 3 Methods

3.1 Mechanical Testing Protocol

In chapter 6, semi-cylindrical samples were tested in unconfined compression in a custom made stainless steel compression rig (Figure 3.1a) that was designed to sit on the stage of an inverted fluorescent Olympus IX 51 microscope equipped with a 100W xenon arc lamp, a DAPI filter cube and a 0.4 NA Universal Plan Super Apochromat 10x objective (Mason Technology, Dublin, Ireland). The unconfined compression rig incorporated Perspex loading platens; one rigidly connected to a precision miniature load cell (Model 31, 10 lbs., RDP Electronics Ltd., Wolverhampton, UK); amplified by a 4-Ch 24-Bit Half/Full Bridge Analogue Input (NI 9237, National Instruments UK & Ireland, Berkshire, UK) and connected to a standard laptop (Dell XPS M1330; Intel Core 2 Duo Processor) interfaced using LabVIEW software (National Instruments UK & Ireland, Berkshire, UK). The semi-cylindrical cartilage sample was bathed in PBS in a testing chamber with a glass microscopic slide window at its base, sandwiched between the two loading platens with its rectangular cross section facing down toward the microscope objective; enabling the visualisation of the tissue during testing. Compression was manually applied to the articular surface of test specimens by advancement of a micrometre attached to the remaining Perspex platen (Mitutoyo, Radionics, Dublin, Ireland; resolution 0.01 mm). Images were recorded with a 12-bit Olympus DP70 camera (Mason Technology, Dublin, Ireland; view 1360 × 1024) and Analysis imaging software (Mason Technology, Dublin, Ireland). The 1360 × 1024 pixel image represented a 583 μm×438 μm sampling of the specimen focal plane at 0.428 μm/pixel.

Cartilage thickness was determined using bright field microscopy at 4x magnification in the uncompressed state (Chen et al., 2001). A tare load of ~1N was applied to ensure union between the platen and the articular surface after which the sample was allowed to

fully relax. The samples were compressed up to 10%, in 2.5% strain increments, and then to 15% and 20% offset strain based on the initial sample thickness at a strain rate of 0.5%/s. After each loading increment the sample was allowed to relax for 60 minutes or until the stress changed by less than 0.001 MPa in 5 min (Chen et al., 2001), and the equilibrium force was measured. Images were captured prior to loading and after the sample had reached equilibrium at each loading stage to quantify the spatial magnitudes of deformation with the tissue.

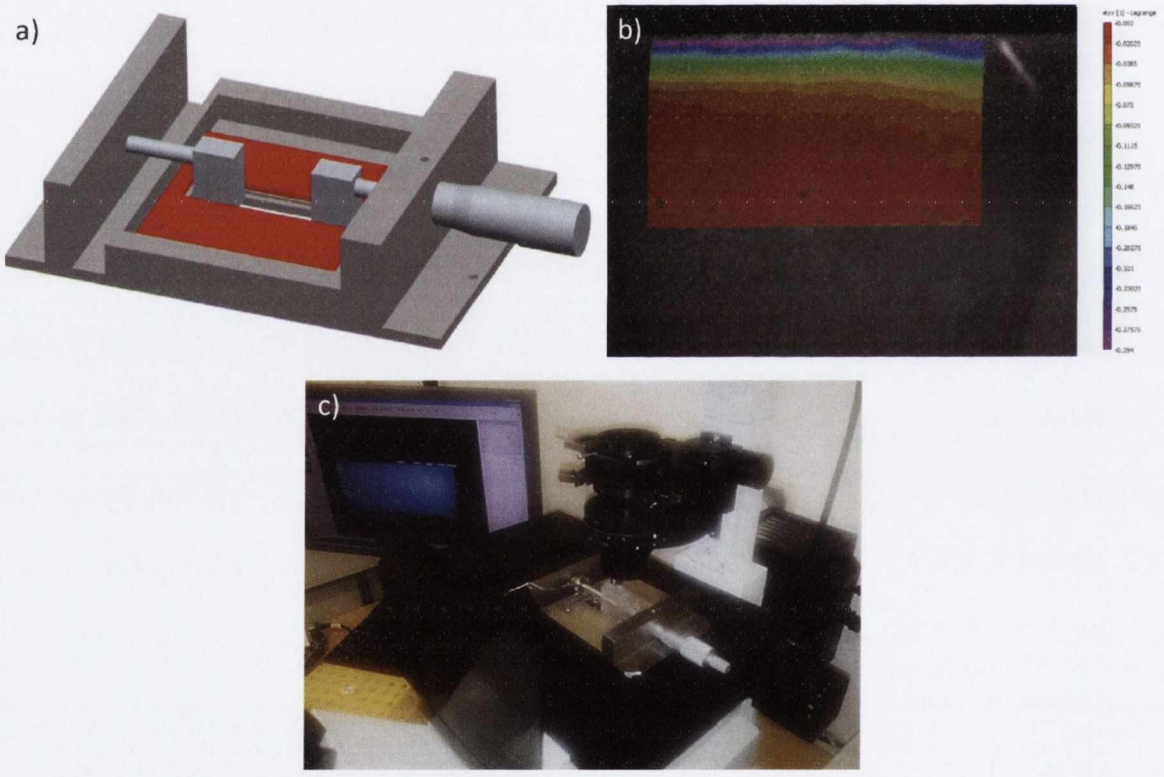

Figure 3.1. (a) Schematic of custom designed unconfined compression rig, (b) example of a typical strain ε_{yy}correlation for a one year old sample for a selected region of interest (ROI), (c) image of experimental set up.

3.2 Digital image correlation (DIC)

The intra tissue displacement field was calculated using the digital image correlation software VIC 2D 2009 (Correlated Solutions, Columbia, SC, USA). The input for the strain calculation is the grid of data points from the correlation of the undeformed reference image taken prior to loading and subsequent deformed images. A cloud of X and Y points is extracted and corresponding U and V displacement vectors are calculated for a selected region of interest (ROI) spanning from the articular surface to the deep zone (Figure 3.1b). The estimated separation between these points, in pixels, is input as the step size. With the grid as the input, each point is considered separately and a local mesh of triangles is created (Figure 3.2a). Each triangle is considered separately (Figure 3.2b); from the vector data, the rigid body motion can be removed to calculate the deformation between the reference and the deformed configuration (Figure 3.2c). The remaining deformation of the triangle is then used to compute a strain tensor for this triangle; this process is repeated for each triangle (Figure 3.2d). Thereafter the strain for each existing data point X and Y is interpolated from the surrounding strains (Figure 3.2e) until each initial data point has a corresponding strain tensor (Figure 3.2f). Due to the small size of each local triangle, smoothing functions are applied over groups of points to account for noise errors. The size of this smoothing group is dictated by the filter size (Figure 3.2g). All analyses utilised subset window sizes of 33×33 pixels surrounding data analysis points which were incrementally chosen at every third pixel (step size) horizontally and vertically throughout the chosen region of interest.

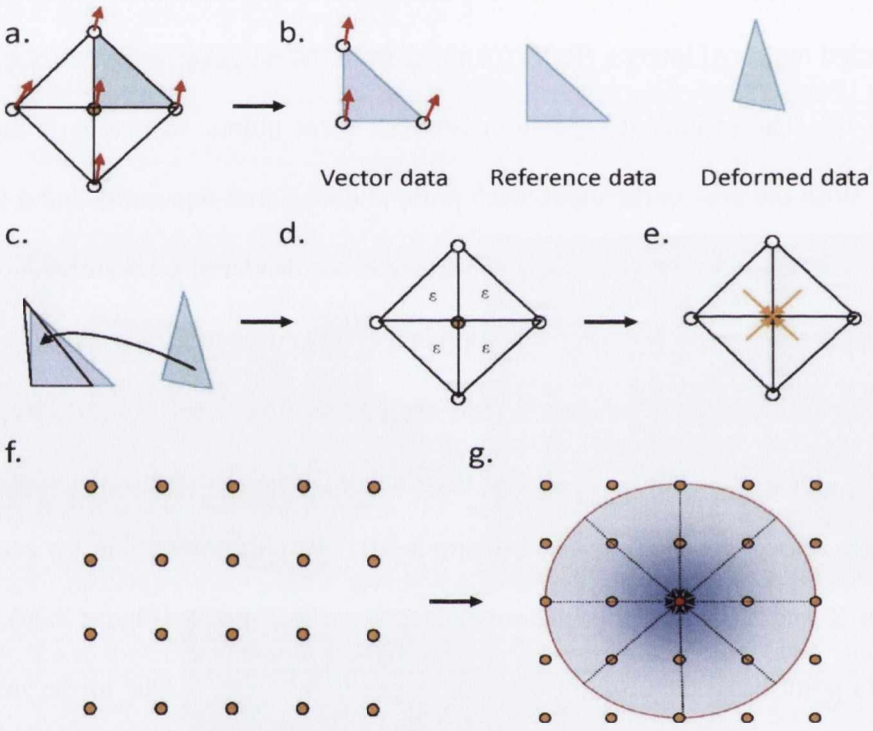

Figure 3.2. Stages of digital image correlation pattern matching technique utilised by VIC 2D software. Schematic courtesy of Correlated Solutions Inc, Columbia, SC, USA.

Localised in-plane deformation was calculated by the software, smoothed over 15 point segments to create a continuous field and differentiated spatially to yield the Lagrangian strain tensor as outlined below. In DIC, as described above, multiple images are acquired of a ROI that may be undergoing deformation. These images may be labeled I_k $(k = 0 - n)$, where I_0 represents the reference configuration X. Let x_k represent the current configuration for the deformation, where $x_0 = X$. The displacement field from I_0 to I_k is given by $u_k(X) = (X) - X$ and the deformation gradient at the current configuration is given by $F_k(X) = I + \partial u_k/\partial X$, where I is the identity tensor, from which the Lagrangian strain $E_k = (F_k^T \cdot F_k - I)/2$ may be evaluated in a material frame (Canal Guterl et al., 2010, Sutton et al., 2009).

When the deformation is sufficiently large, the DIC analysis is unable to provide the displacement u_k accurately. In that case, it is more convenient to evaluate the incremental displacement $\Delta u_k(x_{k-1}) = x_k(x_{k-1}) - x_{k-1}$ from two consecutive images I_{k-1} and I_k $(k = 1 - n)$. The corresponding incremental deformation gradient is given by $\Delta F_k(x_{k-1}) = I + \partial u_k/\partial x_{k-1}$; the cumulative deformation gradient at X is given by $F_k(X) = \Delta F_k(X) \cdot \Delta F_{k-1}(X) \llcorner \Delta F_1(X)$. To obtain $\Delta F_k(X)$ from $\Delta F_k(x_{k-1})$, an algorithm was developed to track X forward by performing suitable interpolations (Canal Guterl et al., 2010, Sutton et al., 2009).

The average axial (ε_{yy}), lateral (ε_{xx}) and shear strain (ε_{xy}) were computed within three distinct zones; the superficial tangential zone (STZ), the middle zone (MZ) and the deep zone (DZ). These regions were assumed to be 0-6%, 7-18% and 19-30% respectively of the total cartilage thickness from the articular surface. Data distributed in the direction transverse to the loading direction were averaged to create a one-dimensional array of axial deformation, and corresponding strain values in each region in

the zonal direction through the depth of the sample were determined, see Figure 3.3. Local strains were computed for a range of different global offset strains (2.5%, 5%, 10% and 15% strain). The depth dependent nominal Young's modulus (E_{yy}) [MPa] was taken as the equilibrium force divided by the specimens cross-sectional area divided by the computed averaged strain (ε_{yy}) within each zone for each nominal applied global offset strain. Likewise Poisson's ratio was calculated as computed averaged strain in the radial direction (ε_{xx}) divided by the averaged axial strain (ε_{yy}), all computed for each applied global offset strain; 2.5%, 5%, 10% and 15% strain.

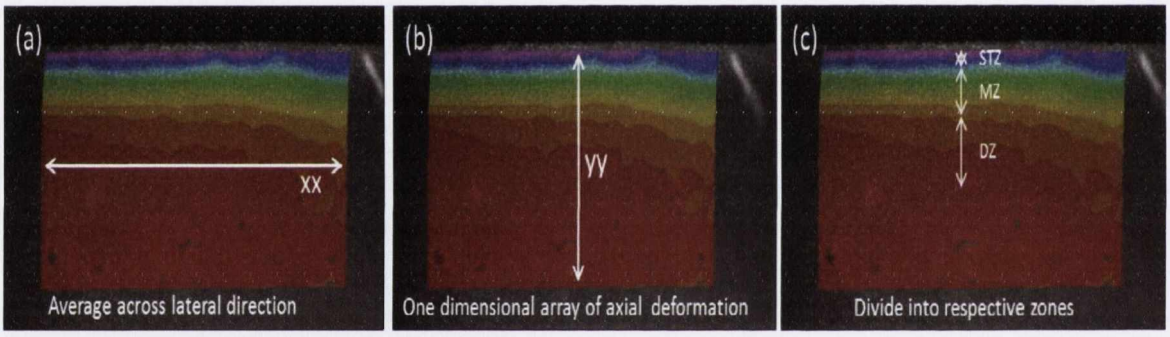

Figure 3.3. (a) Data computed from a selected region of interest (ROI) distributed in the direction transverse to loading direction was averaged to create (b); a one-dimensional array of axial deformation. The average axial strain (ε_yy) and nominal Young's moduli (E_yy) were then computed within three distinct zones (c); the superficial tangential zone (STZ), the middle zone (MZ) and the deep zone (DZ). These regions were assumed to be 0-6%, 7-18%, 19-30% respectively of the total region of interest.

3.3 Helium Ion Microscopy

In chapters 5 and 6, the collagen network was imaged using a HIM (Orion® Plus, Carl Zeiss NTS) with an Everhart-Thornley detector producing an image from the secondary electrons generated by the incident helium ions. All helium ion microscopy was carried out with the expert help of Dr. Alan Bell. In order to provide an unobstructed view of the collagen fibrils, serial enzymatic digestion was used to remove glycosaminoglycan from the cartilage specimens. This protocol is based on a modified version of (Vanden Berg-Foels et al., 2012). All processing solutions included a broad spectrum protease inhibitor cocktail [10 mM ethylenediaminetetraacetic acid (EDTA), 1% (v/v) protease inhibitor cocktail (P8340, Sigma)] and antibiotic-antimycotic [100 U mL^{-1} penicillin, 100 µg/ mL^{-1} streptomycin and 0.25 µg mL^{-1} amphotericin B (A5955, Sigma)] unless otherwise noted. The digestions were performed at 37°C with gentle agitation. Briefly, chondroitin sulfate and dermatan sulfate were removed by incubating the samples in 0.6 U mL^{-1} chondroitinase ABC (C2905, Sigma) in a buffer of 0.05 M tris HCL and 0.06 M sodium acetate at pH 8.0 for 24 h. Hyaluronic acid was removed by incubating the samples in 20.4 U mL^{-1} hyaluronidase (H3506, Sigma) in phosphate buffered saline (PBS) with 10mM sodium acetate at pH 6.0 for 24 h. Residual DNA due to cell lysis was removed by incubating the samples in 1082 Kunitz UmL^{-1} DNase I (D4527, Sigma) in phosphate buffered saline with 1 mM $CaCl_2$ and 6mM $MgCl_2$ at pH 7.7 for 1 h. EDTA was not included in the dilution buffer because it inhibits DNase activity. The samples were rinsed in PBS for 12 h, then fixed in gluteraldeyhyde, dehydrated in a graded ethanol series (30-100%) and dried at critical point (E3000, Quorum Technologies Ltd., East Sussex). All samples were stored in a desiccator prior to imaging. Conductive coatings were not applied to the samples for HIM imaging.

Helium ion microscopy works in similar manner to a scanning electron microscope with the main difference between the two techniques being helium ions replace electrons as the incident particle. The helium ions are generated using a gas field ion source technique. An atomically sharp single crystal metal tip under a high positive bias is cooled to liquid nitrogen temperatures. Helium gas at a pressure of ~5 x 10^{-6} Torr is introduced to the area around the tip. The helium gas is ionized at the apex of the tip where the fields are highest and accelerated down the column where it interacts with the specimen and various interactions occur. The main signal of interest is the generation of secondary electrons. Helium ions generate a higher quantity of secondary electrons compared to electrons in an SEM (Joy, 2012). Owing to the lower velocity of the ions compared to electrons at identical accelerating voltages the signal for HIM is concentrated at the surface, giving higher surface detail.

HIM images were acquired in secondary electron mode with an acceleration voltage of 34.9kV, a beam current of 0.2-0.5 pA and a dwell time of 0.5-2.0 µs. An electron flood gun was used to neutralise the positive charging of the sample by the helium ion beam. All images were acquired using a pixel resolution of 2048x2048 or 1024x1024. The pixel spacing for a 1 µm field of view corresponds to a pixel dimension spacing of 0.49-0.98 nm px^{-1}. The brightness and contrast of all images were optimised; no other post processing procedures were performed. Fibril diameters were measured using ImageJ (Schneider et al., 2012).

Chapter 4 The role of the superficial region in determining the dynamic properties of articular cartilage

4.1 Introduction

Articular cartilage is a thin layer of highly specialized tissue that functions to support and redistribute joint contact forces and to reduce friction within the joint. It is comprised of a specialised cell type; chondrocytes, embedded in an abundant fluid filled extra-cellular matrix (ECM) that consists mainly of a collagen type II network containing water and the large aggregating proteoglycan aggrecan, the latter of which consists of a protein core to which numerous negatively charged glycosaminoglycan (GAG) side chains are attached (Freeman, 1973, Mow and Guo, 2002, Stockwell, 1970). Articular cartilage demonstrates a depth dependent heterogeneous composition and ultra-structure, traditionally divided into three distinct zones. Each zone has a distinct ECM composition, organisation and cell morphology, with the shape and arrangement of the chondrocytes in these zones believed to be related to the local architecture of the collagen fibrils within the solid matrix (Guilak et al., 1995). In the superficial tangential zone (STZ) collagen fibrils are densely packed and orientated parallel to the articular surface while the proteoglycan content is lowest. In the middle zone (MZ) the collagen fibrils are larger, less dense and arcade from a parallel to a perpendicular orientation resulting in a more random organisation. The concentration of PG aggregates increases with depth from the articular surface negatively correlating to decreases in water content and thus resulting in higher swelling pressures with tissue depth (Ge et al., 2012). Finally in the deep zone collagen fibrils are arranged perpendicular to the subchondral bone thus anchoring the tissue to its bony bed

(Armstrong and Mow, 1982, Benninghoff, 1925, Mow and Huiskes, 2005, Redler et al., 1975, van Turnhout et al., 2010a).

The functional properties of articular cartilage are dependent on this unique structure and biochemical composition (Ateshian, 2009, Julkunen et al., 2009, Wilson et al., 2007). Confined and unconfined compression tests are commonly used to determine the material properties of articular cartilage. When cartilage is loaded in compression, a loss of tissue volume occurs due to fluid exudation from the tissue. These effects give rise to time-dependent viscoelastic behaviours such as creep and stress relaxation (Mow and Guo, 2002). During stress relaxation testing, upon reaching equilibrium no hydraulic fluid pressurization exists within the tissue and the intrinsic elastic properties of the solid matrix can be determined (Setton et al., 1993). Previous studies have revealed that the compressive modulus increases with depth from the articular surface which correlates to an increase in sulphated glycosaminoglycan (sGAG) content (Chen et al., 2001, Julkunen et al., 2009, Maroudas, 1976, Mow et al., 1980, Schinagl et al., 1997, Wang et al., 2002a). A certain amount of strain softening has also been observed during compressive loading (Ateshian, 2009, Chahine et al., 2004) which can be attributed, at least in part, to unloading of the vertically aligned collagen fibrils that are initially pre-stressed due to tissue swelling (Nagel and Kelly, 2010). The tensile strength and stiffness of the tissue is mainly attributed to both the amount and organisation of the collagen fibrils and is highest in the superficial tangential zone (Roth and Mow, 1980, Williamson et al., 2003). Hydraulic permeability, inversely correlated to collagen content and fixed charge density (Maroudas, 1976), is lowest in the superficial tangential zone. This is speculated to be due to the zone's high collagen content, the collagen fibrils tightly packed organisation and their tangential orientation to the articular surface (Mansour and Mow, 1976, Maroudas and Bullough, 1968, Setton et al., 1993).

While the relationship between the depth dependent composition of articular cartilage and its equilibrium mechanical properties have been well established, less is known about the depth dependent dynamic properties of the tissue and how they depend on the tissue's composition and structural organisation. During dynamic loading the apparent stiffness of the tissue is dependent on fluid pressurisation, which in turn is a function of the hydraulic permeability of the solid matrix. Such fluid pressurisation has been shown to initially support over 90% of the load applied to articular cartilage (Soltz and Ateshian, 2000). While the collagen network plays a key role in determining the permeability of articular cartilage, it further contributes to the tissue's ability to generate fluid load support by limiting radial expansion during compressive loading (Andriacchi et al., 2009, Kiviranta et al., 2006). Together these findings would suggest that the superficial region of the tissue, where the collagen network is a tightly packed and highly organised structure, would play a key role in determining the dynamic properties of the tissue. While the compressive modulus of this superficial region is lower than the rest of the tissue (Bevill et al., 2010, Glaser and Putz, 2002, Torzilli, 1993, Torzilli et al., 1983), it has been demonstrated that upon removal of this layer the tissue is more susceptible to damage from impact loading (Rolauffs et al., 2010). The hypothesis of this study is that removal of the superficial region will influence both the flow dependent and independent properties of articular cartilage, leading to a reduction in the dynamic modulus of the remaining tissue. Elucidating the role of this region of the tissue in determining the functional properties of articular cartilage is critically important given that disruption to the superficial zone is often associated with the initiation and/or progression of osteoarthritis.

4.2 Materials and methods

4.2.1 Sample preparation

24 osteochondral cores were harvested from the medial and lateral trochlear ridges of the femoropatellar groove of three 4-month-old porcine knee joints within 3h of sacrifice; specimens were pooled from three different animals. Of these 24 cores, 16 were selected for mechanical testing. Cores (6mm diameter) were isolated normal to the articular surface using the Osteochondral Autograft Transfer System (Athrex, Naples, FL, USA) to a maximum depth of 20mm. After coring the subchondral bone was trimmed to approximately 2mm using a custom made cutting tool. The specimens were stored in phosphate buffered saline (PBS) solution (0.15M) and frozen at -80°C until the day of use. On each day of mechanical testing an individual core was thawed to room temperature by immersion in PBS solution and the height of the articular cartilage and respective subchondral bone was measured microscopically (Mitutoyo UK Ltd., Andover, UK) at four sites around the perimeter of the core, the cartilage-bone interface identified and marked using permanent ink. Osteochondral cores were first tested in confined or unconfined compression, and then cut into sections for layer specific testing.

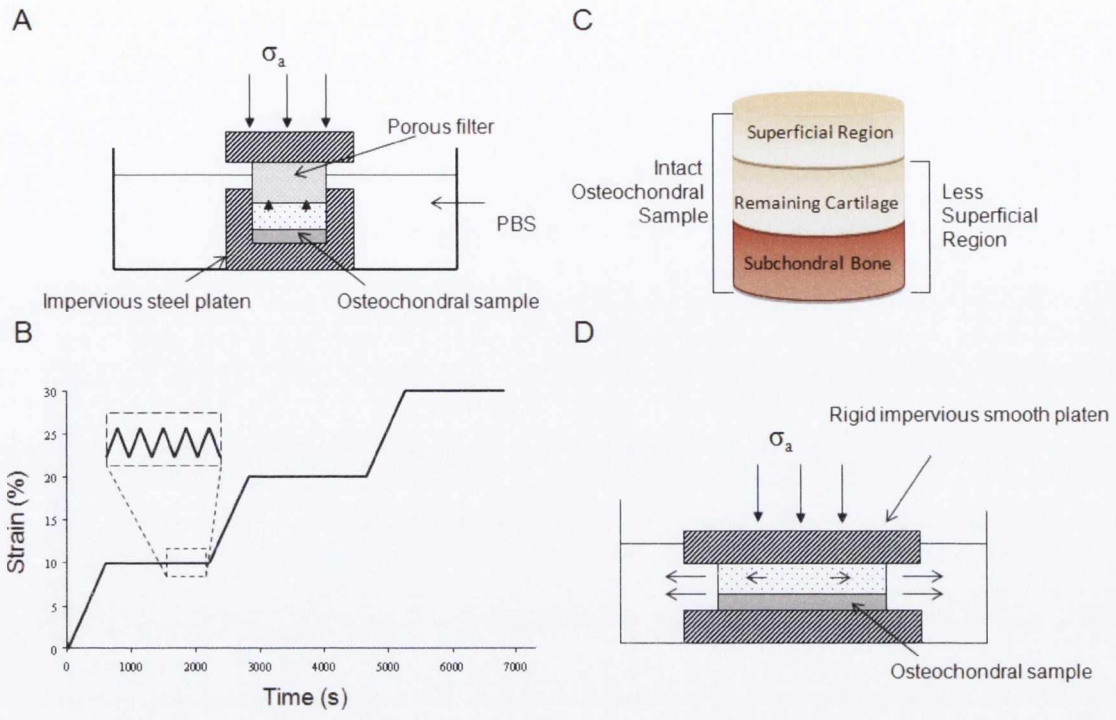

Figure 4.1. Schematic representation of testing configurations. (A) Diagram illustrating confined compression; σ_a indicating axial stress is applied in the arrow direction, (B) loading protocol at increasing strain levels (10, 20 and 30 % strain). In addition, cyclic loading was applied at each strain level after equilibrium had been reached at 1% amplitude and 1Hz frequency (C) Graphic of an osteochondral core divided into layers: intact osteochondral core, less superficial region: remaining cartilage and subchondral bone, superficial region and remaining cartilage (D) diagram illustrating unconfined compression. During unconfined compression of the osteochondral cores radial displacement of the deepest cartilage layers are prevented by the attached subchondral bone.

4.2.2 Mechanical Testing-Full Thickness Osteochondral Cores

Osteochondral cores (n=9) were transferred to a confined compression chamber (Figure 4.1a) and attached to a standard materials testing machine with a 20N pancake load cell (Zwick Roell Z005, Germany; resolution <0.5%). A preload of 0.05N was applied to ensure contact between the articular surface and the porous indenter (30μm porosity, Aegis Advanced Materials Ltd., Worcestershire, UK). Cores were kept hydrated through immersion in a PBS bath at room temperature. Stress relaxation testing was performed, where a series of compressive strains were applied in increasing steps of 10% strain to a maximum of 30% strain. At each strain increment, peak strain was achieved within 500

seconds and the equilibrium stress was recorded after a relaxation period of 1800 seconds (Figure 4.1b). Preliminary tests revealed that 1800 seconds was a sufficient relaxation period to allow the samples to fully equilibrate at all loading magnitudes previously outlined. A 1% amplitude sinusoidal strain was superimposed directly after relaxation at each static strain increment at a frequency of 1Hz for five cycles (Figure 4.1b). The aggregate modulus was calculated as the equilibrium force divided by the specimen's cross sectional area divided by the applied strain, whilst the dynamic modulus was calculated as the average force amplitude divided by the specimens cross sectional area divided by the average strain amplitude for all cycles. After dynamic testing the superficial region of the cartilage was removed (Figure 4.1c) using customised cutting tools for further testing in confined and unconfined compression. To ensure removal of the entire superficial region, and upon review of histological characterisation (Figure 4.2 and Figure 4.4), this section was taken as the top 25% of the total cartilage thickness from the articular surface (Canal et al., 2008, Mow et al., 1980, Rieppo et al., 2003, Xia, 2008). The remaining osteochondral core was then placed back into the confined compression chamber and retested using the same test sequence as outlined above.

For unconfined compression testing (Figure 4.1d), osteochondral cores (n=7) were placed between two impermeable steel platens with and without their respective superficial regions. An identical testing regime to that described for confined testing was implemented, consisting of both stress relaxation and dynamic compression testing.

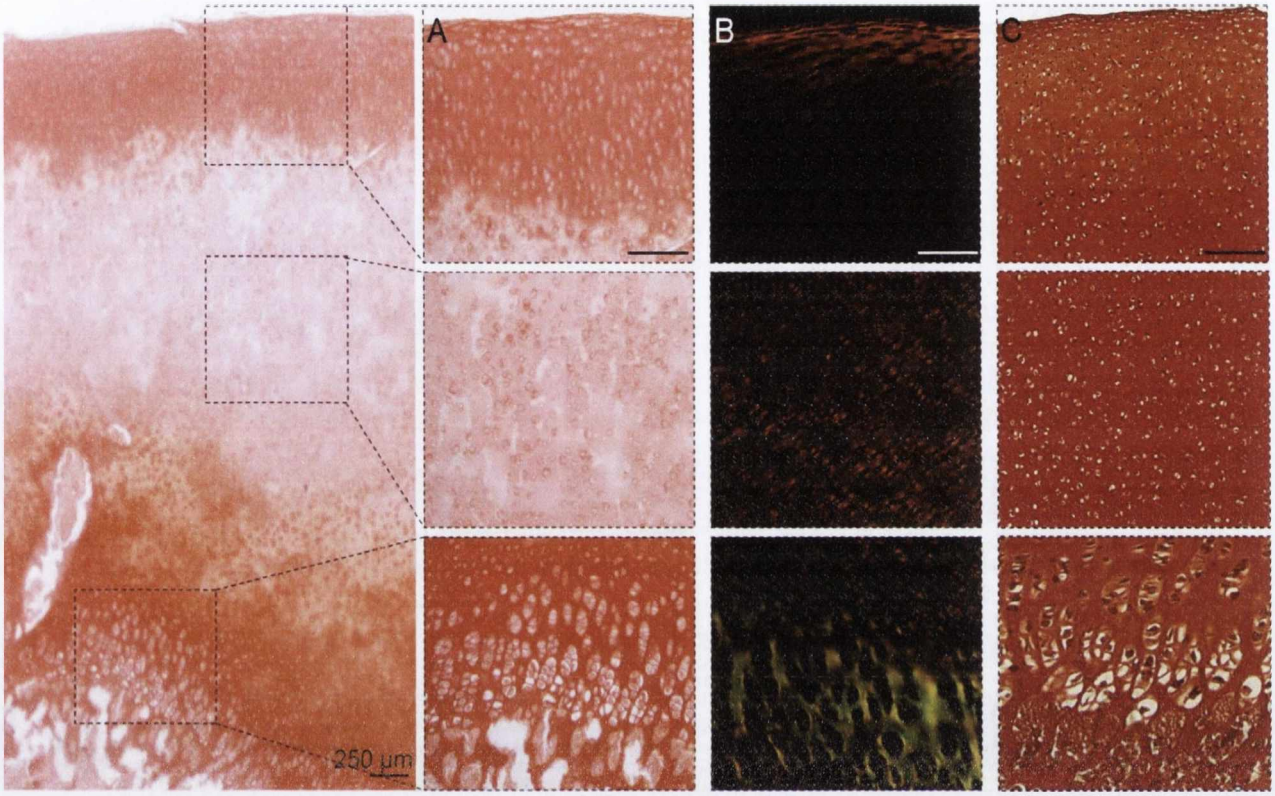

Figure 4.2. Osteochondral sections stained with picrosirius red and safranin O from the femoral trochlear ridges. (A) Picrosirius red stained magnifications of a full thickness cartilage section, scale bar 200µm (Left). (B) Picrosirius red stained magnifications imaged using polarised light microscopy (PLM). A change in the direction of the polarised light known as birefringence occurs close to the articular surface and in the deep zone, allowing the visualisation of the differentiation between the highly organised superficial and deep zone and the non-birefringent middle zone; scale bar 50µm. (C) Safranin O stained magnifications displaying an increase in staining with depth correlating to an increase in sGAG content, scale bar 50µm.

4.2.3 Layer Specific Testing

In order to elucidate the layer specific material properties individual layers were tested without the subchondral bone in confined and unconfined compression under the same testing sequence as was applied to the osteochondral cores. The superficial region, mean thickness of 0.9368 (0.71, 1.1637) mm, was taken as the cartilage section previously removed and the remainder of the articular cartilage after removal of the subchondral bone and calcified cartilage measured a mean thickness of 2.222 (2.1023, 2.3420) mm.

In a stress relaxation test under confined compression, characterised by one dimensional motion but multidimensional loading (due to the constraining sidewalls); the intrinsic material property hydraulic permeability (k, in units of $m^4/N \cdot s$) can be determined when an isotropic homogeneous biphasic constitutive theory is employed to fit to the transient stress-relaxation or creep response of the loaded specimen. The time course of the stress relaxation is determined by a characteristic time constant τ which is defined by the compressive modulus (H_A), permeability (k) and thickness (h, or distance travelled by the fluid); $\tau = h^2/H_A k$. This time constant defines the characteristic gel-time of any porous-permeable elastic solid matrix and hence describes its time-dependent deformational behaviours such as stress relaxation and creep.

Experimental data in the form of force/time stress relaxation curves were fit to a linear bi-phasic model for a known strain and aggregate modulus (H_A) in order to determine the layer specific average permeability of the different articular cartilage regions in confined compression, see Figure 4.3. To evaluate the stress strain response, the axial normal stress can be evaluated at the interface with the porous indenter during the relaxation phase ($t \geq t_0$) by:

$$\frac{\sigma_a(t)}{H_A} = -P_e^w \left\{ \frac{t_0}{\tau} + \frac{2}{\pi^2} \sum_{n=1}^{\infty} e^{-n^2\pi^2\frac{t}{\tau}} \left(e^{n^2\pi^2\frac{t_0}{\tau}} - 1 \right) \right\} \text{ , where } P_e^w = \frac{V_0 h}{H_A k} \text{ and } \tau = \frac{h^2}{H_A k}$$

Here, P_e^w represents the non-dimensional Peclet number for interstitial fluid flow through the porous tissue i.e. ratio of convective velocities to diffusive velocities. V_0 is the loading velocity and h is the specimen thickness. Optimised values of k were determined by minimising the difference between predicted and experimental stress time profiles $\sigma_a(t)$ using a least squares method (Mow et al., 1980). Details of the Matlab code are contained in appendix A.

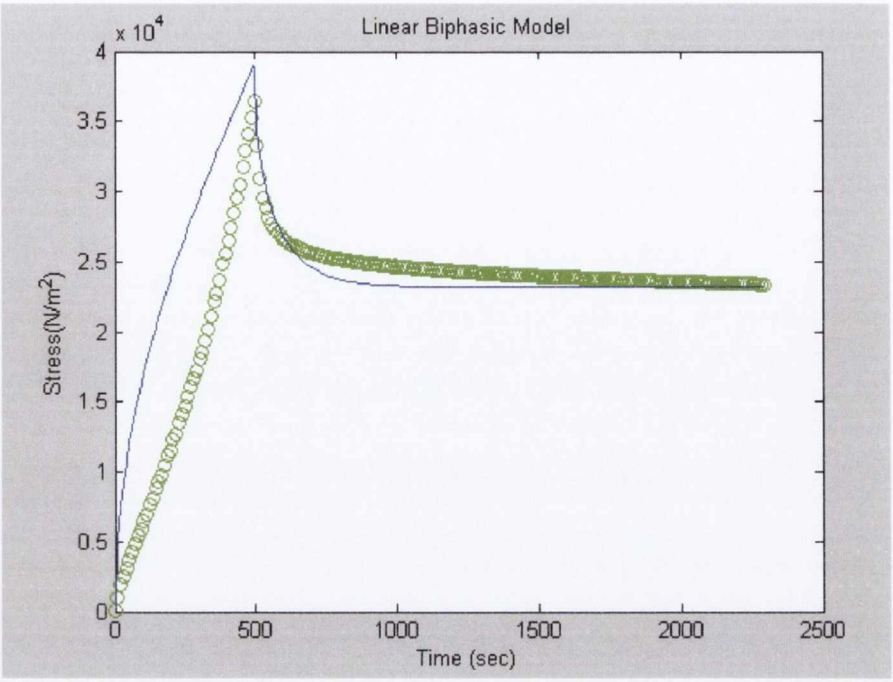

Figure 4.3.a. Example of a typical stress relaxation curve fit to a linear biphasic model for a known aggregate modulus (H_A)

4.2.4 Biochemical Analysis

The wet mass of all mechanically tested layer specific slices was recorded and the samples were frozen for subsequent biochemical analysis. Samples were digested in papain (125 lg/mL) in 0.1 M sodium acetate, 5 mM cysteine HCl, 0.05 M EDTA, pH 6.0 (all from Sigma-Aldrich, Dublin, Ireland) at 60 °C under constant rotation for 18h. Aliquots of the digested samples were assayed separately for collagen and sulphated GAG content. The proteoglycan content was estimated by quantifying the amount of sulfated GAG using the dimethylmethylene blue dye-binding assay (Blyscan, Biocolor Ltd., Northern Ireland), with a chondroitin sulfate standard. Total collagen content was determined by measuring the hydroxyproline content using a hydroxyproline-to-collagen ratio of 1:7.69 (Ignat'eva et al., 2007). Each biochemical constituent (hydroxyproline and GAG) was normalized to the tissue wet weight.

4.2.5 Histological Analysis

Osteochondral cores were fixed in 4% paraformaldehyde overnight at 4°C. Tissues were decalcified in 5% formic acid, 95% DI H_2O and secured on a gyro rocker at 40revs/min for approximately 30 days. Samples were checked each week and returned to fresh solution if not deemed completely decalcified. Once each sample appeared fully decalcified they were sliced in half along the vertical axis, dehydrated, wax embedded and sectioned at 8μm. Sections were stained with safranin O for sGAG and picrosirius red for collagen and subsequently imaged on an Olympus Bx41 microscope equipped with a 30-bit CCD camera (Mason Technology, Dublin, Ireland).

In order to quantitatively analyse these histologically stained sections, TIFF images were converted to greyscale and stored as 8 bits per sampled pixel which allows 256 intensity levels or shades of grey. Among these light intensity levels, black or complete lack of light is represented numerically as zero whilst pure white is represented as 255. Converted images were analysed for intensity levels with depth from the articular surface using MATLAB 7.0. (Mathworks, Cambridge, UK).

4.2.6 Polarised Light Microscopy (PLM)

Polarised light microscopy is an optical microscopy technique used to study structural orientation of anisotropic materials such as articular cartilage. Essentially, a polariser filter placed after the light source on a microscope ensures only linearly polarised light is transmitted to the specimen. Optically anisotropic materials change the direction of the polarised light, which is known as birefringence (Changoor et al., 2011). PLM exploits the natural birefringence of cartilage which varies through the depth of the tissue due to the orientation and the alignment of collagen fibrils. As this birefringence can be fairly weak and difficult to detect, picrosirius red staining was performed to enhance visualisation with polarised light (Király et al., 1997). In an effort to reduce birefringence

of the surrounding matrix all GAGs were digested prior to imaging. Briefly, sections were incubated for 90 min at 37°C in a 0.5% pre-warmed papain solution (pH 4.43) and then rinsed in distilled water prior to staining (Lecocq et al., 2008). In articular cartilage, PLM reveals the highly organised collagen structure of the superficial region and deep zone as two birefringent regions, separated by a non-birefringent and hence randomly organised middle zone (Changoor et al., 2011).

4.2.7 Statistical Analysis

Statistical analysis was performed using a two way ANOVA with Tukey's post-hoc test for multiple comparisons, whilst two sample t-tests were used for unpaired data sets. All tests were performed using the statistical software package MINITAB 15.1 (Minitab Ltd., Coventry, UK). Numerical and graphical results are displayed as mean with uncertainty expressed by 95% confidence intervals (CIs): mean (upper limit, lower limit). Significance was accepted at $p \leq 0.05$ or as indicated. Sample numbers varied according to respective comparison and are outlined in the results section of this manuscript.

4.3 Results

Polarised light microscopy revealed intensely birefringent and hence highly organised collagen structures in the superficial region and deep zone of the tissue; fibrils appear orientated parallel to the articular surface in the superficial region and perpendicular to the subchondral bone in the deep zone (Figure 4.2).

Biochemical analysis revealed a lower (p=0.027) sGAG content in the superficial region compared to the remaining tissue, with no significant difference (p=0.426) in the total collagen content between the two regions (Figure 4.3). Histological analysis with safranin O staining correlated with the results of the sGAG biochemical assay, displaying decreased staining in the superficial region. The picrosirius red stained sections demonstrated a more complex spatial distribution of collagen through the depth of the tissue, with the superficial and deep regions staining intensely for collagen and a more moderate staining in the middle region (Figure 4.2). Significantly higher light intensities were measured in the superficial region of the safranin O stained sections (p=0.026) (Figure 4.4), indicating less intense staining in this region of the tissue and hence a lower sGAG content. Picrosirius red stained sections displayed highest light intensity in the middle zone, with lower intensity values in the superficial and deep regions suggesting higher collagen content in these zones (Figure 4.4). Hence, removal of the superficial region exposed a low-collagen region. This observation could not have been made from bulk biochemical analysis alone.

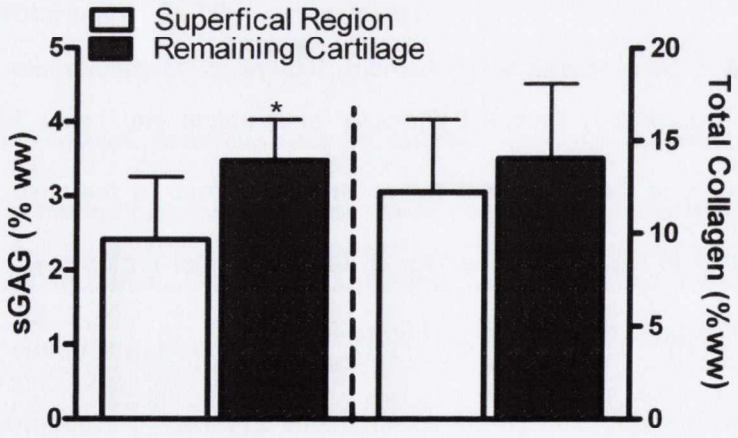

Figure 4.4b. Sulphated glycosaminoglycan (sGAG) content and total collagen content of superficial region and remaining cartilage disks of porcine articular cartilage per wet weight [%] obtained from the femoral trochlear ridges. Bars show the mean with 95% CI; n=6; donors=3. * p = 0.027.

Cartilage thickness averaged 3.051 (2.516, 3.586) mm for full thickness osteochondral cores and 2.435 (1.92, 2.95) mm after removal of the superficial region; approximately 25 (19.01, 31.95) % of the total cartilage thickness. Typical stress strain and cyclic loading data plots are presented in Figure 4.4a. The aggregate moduli determined from confined compression testing of osteochondral cores (Figure 4.5a) significantly increased ($p=0.0035$) at 10% strain after removal of the superficial region by 50.4% (from 0.76 (0.65, 0.88) MPa to 1.1 (0.88, 1.3) MPa). The compressive stiffness in unconfined compression (Figure 4.5b) also significantly increased ($p=0.0365$) by 26.6% (from 0.75 (0.66, 0.84) MPa to 0.93 (0.86, 1.01) MPa). In contrast, the confined dynamic modulus significantly decreased at each strain level of 10, 20 and 30% ($p=0.0053$, $p<0.0001$ and $p=0.0049$ respectively) upon removal of the superficial region by 24% (from 29.45 (26.64, 32.25) MPa to 22.26 (19.97, 24.54) MPa), 33.3% (from 43.75 (40.44, 47.07) MPa to 29.07 (25.91, 32.22) MPa) and 25.4% (from 42.09 (31.43, 52.76) MPa to 30.59 (26.6, 34.58) MPa) respectively. The ratio of the peak stress to equilibrium stress during stress relaxation testing (Figure 4.6) at 10% strain in unconfined compression significantly reduced ($p=0.006$) upon removal of the superficial region from 2.07 (1.89, 2.25) to 1.68 (1.47, 1.9) suggesting a reduced ability to maintain fluid load support.

Layer specific mechanical testing revealed a similar trend of increasing aggregate and equilibrium moduli with depth, whilst in general the confined and unconfined dynamic moduli of the superficial region was lower than the remaining cartilage (Figure 4.7a and Figure 4.7b). Experimental data fit to a linear bi-phasic model of articular cartilage in confined compression revealed a significantly lower hydraulic permeability in the superficial region (1.98×10^{-15} (1.03×10^{-15}, 2.93×10^{-15}) $m^4/N\cdot s$) compared to the remaining cartilage (3.22×10^{-15} (2.46×10^{-15}, 3.97×10^{-15}) $m^4/N\cdot s$) when tested in isolation ($p=0.028$). Typical example of a phase shift during dynamic loading can be seen in Fig. 8.

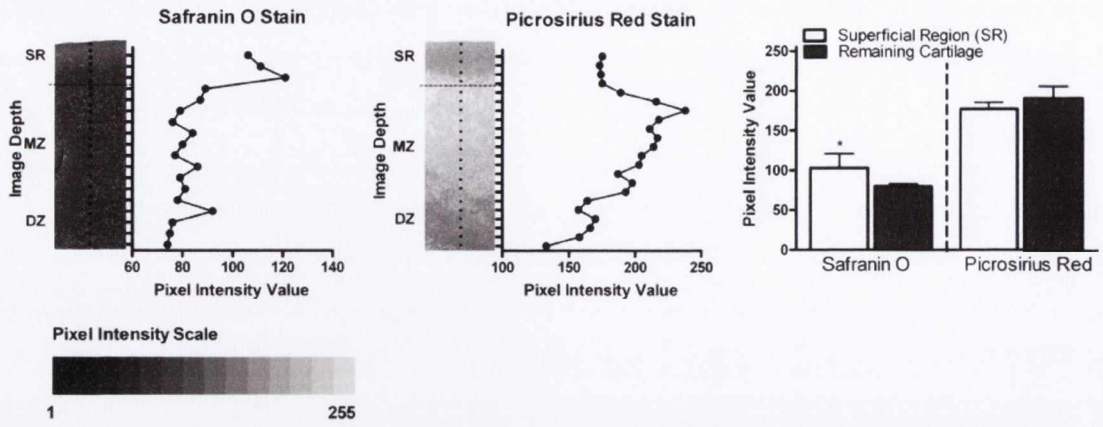

Figure 4.5a. Pixel intensity profiles of histological samples with depth from the articular surface of (A) safranin o stain and (B) picrosirius red stain. Figure (C) displays the average of these values correlating to specific regions; superficial region (SR) and the remaining cartilage. Bars show mean with 95% CI. The dashed line indicates the top 25% of the total cartilage thickness i.e. from the articular surface to the base of the cartilage. *p=0.026.

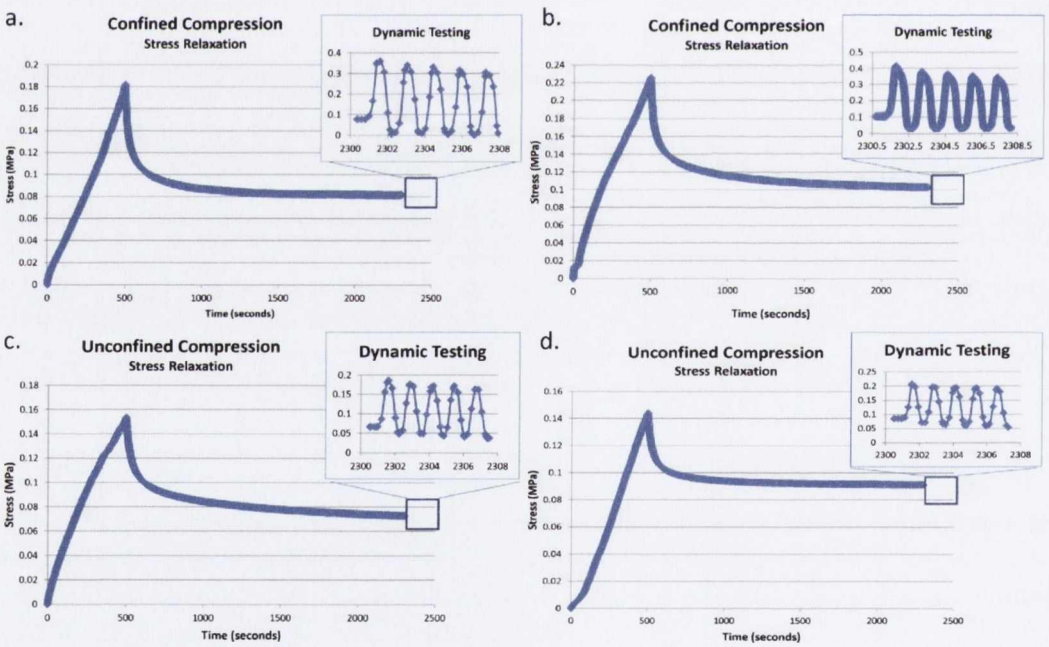

Figure 4.6b. Typical stress relaxation data plots at 10% strain and cyclic loading data plots at 1 Hz frequency and 1% amplitude. (a) Confined compression (CC) testing configuration for an intact osteochondral core, (b) CC testing configuration for an osteochondral core less its superficial region, (c) unconfined compression (UC) testing configuration for an intact osteochondral core, (d) UC testing configuration for an osteochondral core less its superficial region, (c) unconfined compression.

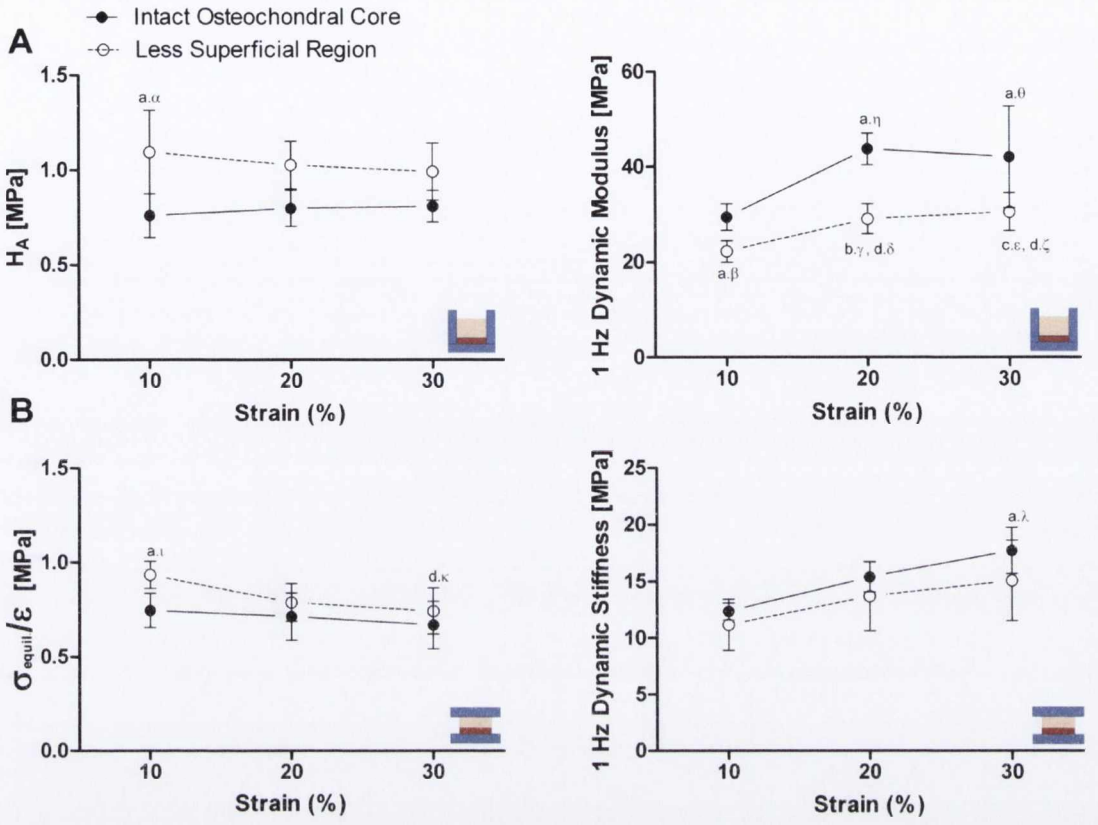

Figure 4.7. (A) Aggregate moduli and dynamic moduli in confined compression of full thickness osteochondral cores and less the superficial region of porcine articular cartilage obtained from the femoral trochlear ridges. Bars show the mean ± 95% CI, n=9. (B) Compressive stiffness (σequil/ε) and dynamic stiffness in unconfined compression of the same testing configuration as outlined above. Bars show the mean ± 95% CI, n=9. All dynamic testing was carried out at 1Hz freq. and 1% amplitude at increasing levels of offset strain ε: 10, 20 and 30%. Connecting line does not imply linear relationship with strain. In A and B, 'a' indicates a significant difference vs. 'Intact Osteochondral Core' (10% ε), 'b' indicates a significant difference vs. 'Intact Osteochondral Core' (20% ε), 'c' indicates a significant difference vs. 'Intact Osteochondral Core' (30% ε),'d' indicates a significant difference vs. 'Less Superficial Region' (10% ε). Specific p values for these differences are as follows: α:p=0.0035, β:p=0.0053, γ:p<0.0001, δ:p=0.0093, ε:p=0.0049, ζ:p=0.0015, η:p=0.0001, θ:p=0.0016, ι:p=0.0037, κ:p=0.0032, λ:p=0.0033.

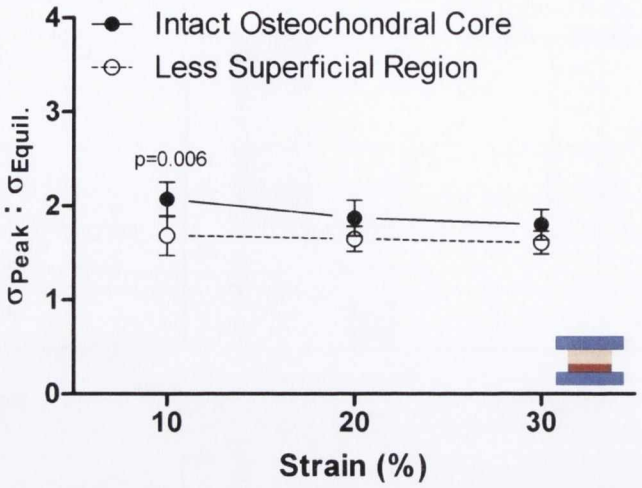

Figure 4.9a. Peak stress: equilibrium stress ratio in unconfined compression at increasing levels of offset strain ε: 10, 20 and 30% of full thickness osteochondral cores and less the superficial region of porcine articular cartilage obtained from the femoral trochlear ridges. Bars show the mean ± 95% CI, n=9. Connecting line does not imply linear relationship with strain.

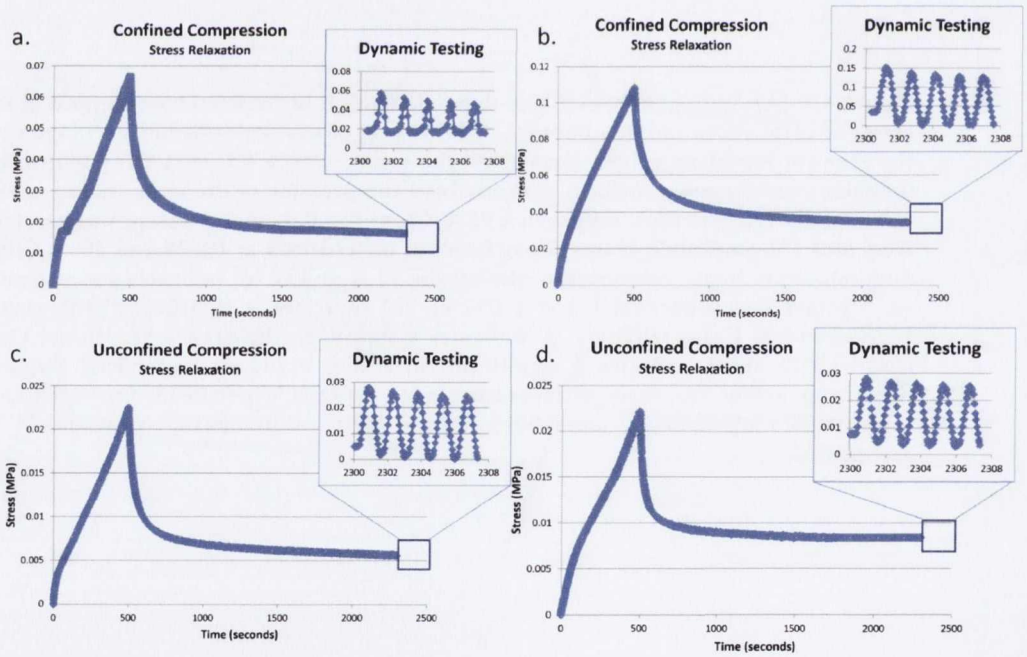

Figure 4.8b. Typical stress relaxation data plots at 10% strain and cyclic loading data plots at 1 Hz frequency and 1% amplitude. (a) Confined compression (CC) testing configuration for the superficial region, (b) CC testing configuration for the deep zone, (c) unconfined compression (UC) testing configuration for the superficial region (d) UC testing configuration for the deep zone.

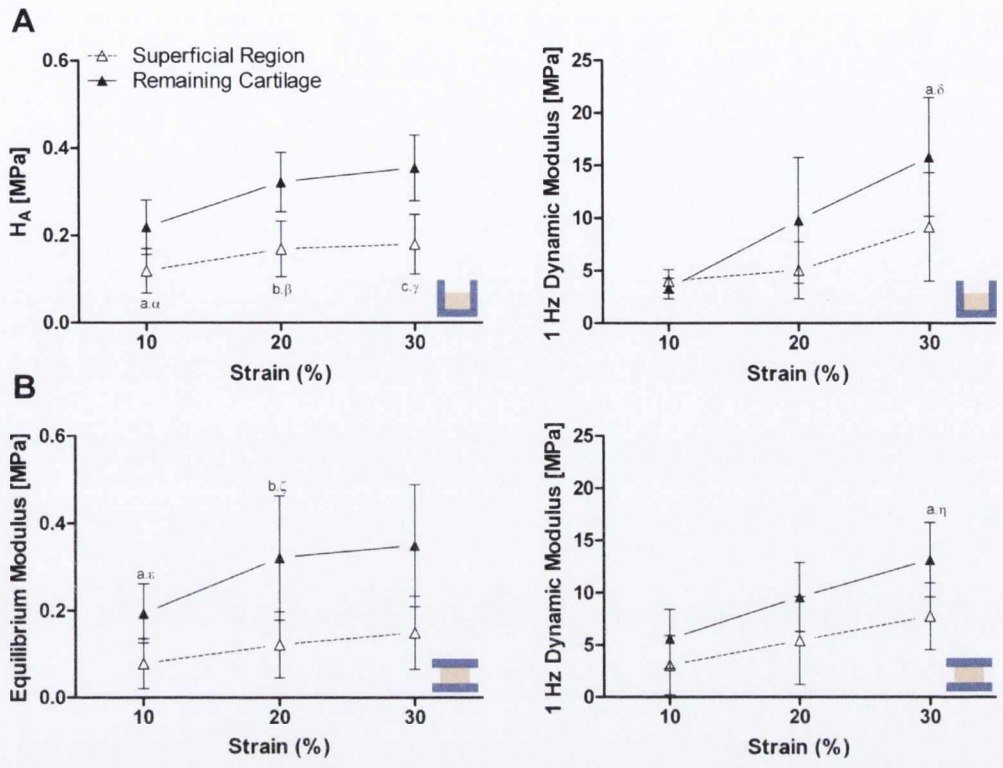

Figure 4.10. (A) Aggregate moduli and dynamic moduli in confined compression of the superficial region and remaining cartilage disks of porcine articular cartilage obtained from the femoral trochlear ridges. Bars show the mean ± 95% CI, n=7. (B) Equilibrium moduli and dynamic moduli in unconfined compression of the same testing configuration as outlined above. Bars show the mean ± 95% CI, n=7. All dynamic testing was carried out at 1Hz freq. and 1% amplitude at increasing levels of offset strain ε: 10, 20 and 30%. Connecting line does not imply linear relationship with strain. In A and B, 'a' indicates a significant difference vs. 'Superficial Region' (10% ε), 'b' indicates a significant difference vs. 'Superficial Region' (20% ε), 'c' indicates a significant difference vs. 'Superficial Region' (30% ε). Specific p values for these differences are as follows: α:p=0.05, β:p=0.0401, γ:p=0.0386, δ:p=0.0001, ε:p=0.0147, ζ:p=0.0185, η:p=0.0104.

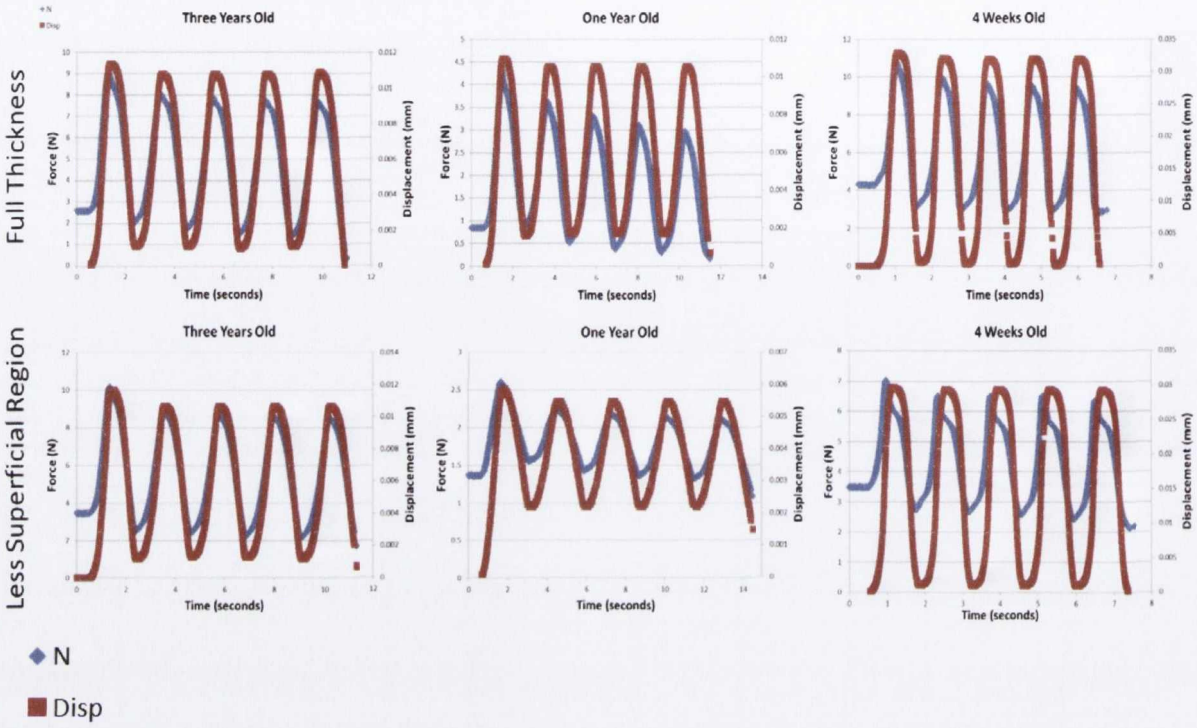

Figure 4.8. Example of phase shift during dynamic testing; displacement and force vs time graphs for all ages with and without the presence of the superficial tangential zone. The blue line represents the force curve whilst the red line represents the displacement curve with time.

4.4 Discussion

The objective of this study was to test the hypothesis that removal of the superficial region of the tissue will influence both the flow dependent and independent properties of articular cartilage, leading to an increase in the equilibrium modulus but a reduction in the dynamic modulus of the tissue. In confined compression, significant increases in the aggregate modulus (H_A) of the osteochondral cores upon removal of the superficial region were observed, which is in agreement with the literature (Julkunen et al., 2009, Kiviranta et al., 2006, Laasanen et al., 2002, Schinagl et al., 1997, Setton et al., 1993). This rise in stiffness corresponded with a significant increase in sGAG content with depth from the articular surface (Canal Guterl et al., 2010, Lu and Mow, 2008, Poole et al., 1987, Williamson et al., 2001). However, while removal of the superficial region increased the aggregate modulus of the remaining tissue, a significant reduction in the dynamic modulus was observed. This is despite the fact that when tested in isolation the dynamic modulus of this layer at high offset strains was significantly lower than the remaining tissue in both confined and unconfined compression as has been observed in previous studies (Rolauffs et al., 2010, Treppo et al., 2000), confirming that in isolation the superficial region is the softest part of the tissue in compression.

While the finding of an increased equilibrium modulus upon removal of the superficial region is intuitive, the finding that the dynamic modulus decreased with removal of this soft layer requires further discussion. The reduction in dynamic modulus may be partially explained by geometric effects. Consider first the gel diffusion time, given by $\tau_m = {\delta^2}/{H_A k}\,(s)$, where δ in confined compression is given by the height (m) of the sample, $H_A(Pa)$ is the aggregate modulus and $k(m^4N^{-1}s^{-1})$ is the hydraulic permeability (Morel and Quinn, 2004, Mow et al., 1980). By reducing the sample height,

this effectively reduces the gel diffusion time. Therefore for any given loading frequency, this would imply lower interstitial fluid pressurisation based on the assumptions of a linear biphasic model of articular cartilage (Mow et al., 1980, Suh et al., 1995). This reduction in fluid pressurisation could contribute to the lower dynamic modulus observed upon removal of the superficial region. The reduced sample height may also partially explain the lower dynamic modulus values of the isolated regions in confined compression versus the full thickness osteochondral cores.

Another explanation for this reduction in dynamic modulus is the significantly lower ($p=0.028$) permeability in the superficial region compared to the remaining cartilage (obtained from fits of the data to a linear biphasic model). This low permeability region essentially acts as a barrier to fluid flow and its removal is speculated to lead to reduced fluid pressurisation in the tissue during dynamic loading. It has previously been hypothesised that the permeability of this region of the tissue is due to the high concentration of tightly woven collagen fibrils orientated parallel to the articular surface resulting in a system of much narrower channels offering a greater resistance to fluid flow (Freeman, 1973, Maroudas and Bannon, 1981, Maroudas and Bullough, 1968, Setton et al., 1993). Once compressed this fibrillar sheet is compacted and further restricts fluid exudation (Torzilli, 1984). After removal of the superficial region, more fluid can escape during cyclic loading than in intact tissues. Histological analysis of the tissues tested as part of this study (Figure 4.2) confirmed a high collagen content in the superficial region, with PLM analysis revealing closely packed collagen fibrils orientated parallel to the articular surface (Rieppo et al., 2008). It has previously been found that with removal of the upper most 100 microns of tissue, equilibrium deformation is reached sooner compared to the intact articular cartilage specimen and furthermore removal of the top surface caused a substantial increase in the quantity of fluid exchanged

during each loading cycle, also suggesting an increase in the permeability of the tissue (Torzilli et al., 1983) and supporting the studies observations. Overall, the present results indicate that removal of the superficial region leads to a deterioration in the transient, i.e. fluid mediated, load bearing properties of cartilage tissue via both geometric and permeability effects. Decoupling these geometric and permeability effects further requires additional work.

During unconfined compression fluid will exude radially out of the sides of the cylindrical samples. As all sample diameters were identical geometric effects will play no role. It should be noted that with this testing modality the tissue is allowed to bulge radially and collagen fibrils, particularly those orientated perpendicular to the direction of loading in the superficial region, can play a key role in maintaining fluid load support by preventing lateral expansion of the tissue (Ateshian, 2009, Jurvelin et al., 1996, Kiviranta et al., 2006, Korhonen et al., 2002, Park et al., 2003). This may explain the significant drop ($p=0.006$) in the ratio of peak stress to equilibrium stress at 10% strain observed during unconfined compression upon removal of the superficial region of the tissue (Figure 4.6)

A significant increase in dynamic stiffness with increasing magnitudes of the offset compressive strain was observed in confined and unconfined compression for osteochondral tissue cores and isolated layers (Figure 4.5 and Figure 4.7). This strain dependent increase may be due to a deformation induced decrease in tissue permeability, i.e. increasing compaction of the collagen network offering increased frictional resistance to the flow of interstitial fluid (Bursac et al., 1999, Chahine et al., 2004, Chen et al., 2001, Erne et al., 2005). In a similar manner, compressive strain of the cartilage will cause compaction of the proteoglycans in the tissue which will in turn increase the fixed charge

density in the tissue further decreasing tissue permeability (Mansour and Mow, 1976, Maroudas and Bullough, 1968).

There are potential limitations associated with this study. The porcine tissue tested was not skeletally mature and therefore its collagen architecture does not equate that of fully mature samples, although analysis confirmed a tissue organisation that mimics key aspects of the architecture of adult cartilage (Figure 4.2b). Slicing the cartilage into layers may have an impact on the functional properties of the tissue by disturbing the intrinsic continuum structure (Glaser and Putz, 2002) and possibly damaging the tissue. Although scanning electron microscopy has previously demonstrated that the surface of both cut and intact articular cartilage display similar collagen fibril architecture (Torzilli, 1993), artefacts due to cutting cannot be ruled out and the isolation of specific zones may have compound effects on their functional properties. In an effort to ensure full removal of the superficial region the top 25 (19.01, 31.95) % of the total cartilage thickness was cut from the articular surface. Whilst a larger proportion than what is classically defined as the superficial zone, this percentage ratio was based on previous studies (Mow et al., 1980, Rieppo et al., 2003, Xia, 2008) and my own analysis of picrosirius red stained histological sections (Figure 4.2) and pixel intensity profiles (Figure 4.4) which show a dense collagen content in the upper ~25% of the total cartilage thickness. In tissue that has reached full skeletal maturity, the superficial zone of the tissue is thinner, pointing to the dynamic nature of collagen modelling and remodelling during skeletal development (Van Turnhout et al., 2010b). Preliminary studies whereby only the top 10% of the total cartilage thickness was removed (data not shown) showed no statistically significant decrease in the dynamic modulus of the remaining tissue upon its removal. This suggested that the entire superficial region with its high collagen content was not removed, although geometrical effects as discussed above may also play a role. Another

possible limitation to the experimental approach adopted in this study is that part of the transitional zone of the tissue may also have been removed during slicing. The biomechanical function of the transitional zone has yet to be fully elucidated. Therefore as it isn't possible to accurately separate the superficial region from the transitional zone using the present experimental setup, the possibility that removal of part of this region of the tissue is also contributing to the experimental findings cannot be excluded.

A biomechanical failure of the collagen network in the superficial tangential zone is postulated in many hypotheses as related to the development of osteoarthritis (Bank et al., 1998, Buckwalter et al., 2005, Setton et al., 1993) Computational models have also been used to demonstrate how a viable superficial zone is critical to achieving long term survival in repairing articular cartilage (Owen and Wayne, 2006, Owen and Wayne, 2010). This study demonstrates that although this layer is less stiff than the remainder of the tissue in compression, it plays a key role in elevating the dynamic material properties of the tissue. This is presumably achieved by generating higher fluid load support due to its dense collagen fibril network and organisation and hence low permeability. Taken together these studies highlight the importance of understanding the role of the superficial region in articular cartilage development and degeneration, and in the design of novel tissue engineering approaches to cartilage regeneration. Future studies will explore how and why these structural, compositional and functional changes emerge in articular cartilage with skeletal maturity and what role the local environment within the developing joint plays in driving these changes.

Chapter 5 The Changing Role of the Superficial Region in Determining the Dynamic Compressive Properties of Articular Cartilage during Postnatal Development and Skeletal Maturation

5.1 Introduction

The composition and ultra-structure of articular cartilage varies through the depth of the tissue and is typically described as consisting of three distinct zones; the superficial tangential zone (STZ), the middle zone (MZ) and the deep zone (DZ). Each zone has a distinct extracellular matrix (ECM) composition, organisation and cell morphology. Interstitial water decreases with depth from the articular surface (Mow and Huiskes, 2005) whilst proteoglycan content (% dry weight) increases with distance from the articular surface (Julkunen et al., 2009). During development and maturation compositional and architectural changes occur in articular cartilage; it has been reported that collagen content (% dry weight) and cross-linking increase with age, whereas proteoglycan (PG) (% dry weight) content remains largely unchanged (Grushko et al., 1989, Venn, 1978, Wachtel et al., 1995, Wang et al., 2001, Williamson et al., 2003). Furthermore with age, the exclusively fine collagen fibrils of young cartilage ($\geq$10% collagen IX, $\geq$10% collagen XI, $\leq$ 80% collagen II) develop into to the thicker and more varied fibril diameters of mature articular cartilage (~1% collagen IX, ~3% collagen XI, $\geq$ 90% collagen II) (Eyre, 2002). In addition, the collagen architecture changes from a predominantly isotropic structure in immature articular cartilage to a mature arcade-like zonal structure first described by Benninghoff (1925) (Benninghoff, 1925, Buckwalter et al., 2005, Redler et al., 1975, Rieppo et al., 2009).

Such changes in the biochemical composition and organization of articular cartilage with age likely lead to changes in the mechanical functionality of the tissue, yet to date this temporal and spatial relationship remains poorly understood. The primary mechanical functions of collagen fibrils in cartilage are twofold. First, they provide tensile stiffness and strength to the tissue. Second, the collagen network functions to restrain the swelling pressure of the embedded proteoglycans, which provides compressive stiffness to the tissue (Mow and Huiskes, 2005). These trapped proteoglycans contain large amounts of glycosaminoglycans (GAG), particularly chondroitin sulphate and keratin sulphate that carry negative electrical charges in the physiological environment (Ateshian et al., 2004, Maroudas, 1979). The density of these fixed charges is known as the fixed charge density (FCD) (Lu et al., 2009). The swelling pressure exerted by FCD, known as the Donnan osmotic fluid pressure, plays a key role in maintaining cartilage hydration and in determining the ability of the tissue of support compressive loads (Donnan, 1995, Lu et al., 2009, Maroudas, 1979, Soltz and Ateshian, 2000, Tanaka et al., 2006). The heterogeneous composition and structure of articular cartilage results in a tissue with depth dependent mechanical properties (Schinagl et al., 1997). The compressive equilibrium modulus of articular cartilage increases with depth from the articular surface, which correlates to increases in FCD in the deeper regions of the tissue, whereas dynamic properties have been shown to correlate with interstitial water and collagen content (Julkunen et al., 2009, Kiviranta et al., 2006). What remains to be fully elucidated is how these functional properties vary with age as a result of temporal changes to the biochemical composition and structural organization of articular cartilage.

The objective of this study was to explore how the equilibrium and dynamic compressive properties of articular cartilage change during postnatal development. In particular, we were interested in determining how changes to the superficial region of

articular cartilage during skeletal development impact its functional properties. It has previously been demonstrated that although this layer, in isolation, is less stiff in axial compression than the remainder of the tissue, it plays a key role in elevating the dynamic material properties of the entire tissue (Gannon et al., 2012). It was speculated that this was due to the presence of the superficial region facilitating the generation of higher fluid load support during dynamic loading, which can be attributed to its high collagen fibril density and architectural organisation and hence low permeability. The question arises as to whether such functionality is present at birth, and if not, when these structural and compositional changes emerge in the SR of articular cartilage with skeletal maturity, and furthermore how they influence the biomechanical properties of the tissue. To address this fundamental question, the equilibrium and dynamic compressive properties of articular cartilage from birth to skeletal maturity were measured before and after removal of the SR of the tissue. Furthermore, the changing composition and organization of the tissue were characterised using biochemical, histological and microscopic techniques. The hypothesis of this study was that a functional superficial region is not present in skeletally immature articular cartilage, and hence removal of this zone of the tissue would only negatively impact the dynamic modulus of the tissue with the attainment of skeletal maturity.

5.2 Materials and Methods

5.2.1 Sample preparation

Osteochondral cores were obtained as described previously (Gannon et al., 2012). Briefly, cores were isolated from the medial and lateral trochlear ridges of the femoropatellar groove of porcine knee joints within 3h of sacrifice (n=62). The samples were collected and divided into three age groups representing different stages of maturation: 4 weeks, 1 year, and 3 years. Each respective age group contained cartilage cores derived from three

different pigs. These samples were prepared for mechanical (n=27), biochemical (n= 47), histological (n=6) and helium ion microscopy (n=9). All specimens for mechanical testing were stored in phosphate buffered saline (PBS) solution (0.15M) and frozen at -80°C until the day of use. On each day of mechanical testing an individual core was thawed to room temperature by immersion in PBS solution and the height of the articular cartilage and respective subchondral bone was measured microscopically (Mitutoyo UK Ltd., Andover, UK) at four sites around the perimeter of the core, the cartilage-bone interface identified and marked using permanent ink.

5.2.2 Mechanical testing

Osteochondral cores were transferred to a confined compression chamber and attached to a standard materials testing machine with a 200N XForce HP load cell (Zwick Roell Z005, Germany; resolution <0.2%). A preload of 0.05N was applied to ensure contact between the articular surface and porous indenter (30 μm pore size, Aegis Advanced Materials Ltd., Worcestershire, UK). Cores were kept hydrated through immersion in a PBS bath at room temperature. Stress relaxation testing was performed, where a series of compressive strains were applied in increasing steps of 10% to a maximum of 30%. At each strain increment, peak strain was achieved within 500 seconds and the equilibrium stress was recorded after a relaxation period of 1800 seconds, see Figure 5.1. Preliminary tests revealed that 1800 seconds was a sufficient relaxation period to allow the samples to fully equilibrate at all loading magnitudes previously outlined. A 1% amplitude sinusoidal strain was superimposed directly after relaxation at each static strain increment at a frequency of 1Hz for five cycles. The aggregate modulus at each strain increment was calculated as the equilibrium force divided by the specimen's cross sectional area divided by the applied strain, whilst the dynamic modulus was calculated as the average force amplitude divided by the specimens cross sectional area divided by the average strain

amplitude for all cycles. After dynamic testing the superficial region of the cartilage was removed, taken as the top 15% of the total cartilage thickness, using customised cutting tools for further testing in confined and unconfined compression. The remaining osteochondral core was then placed back into the confined compression chamber and retested using the same test sequence as outlined above.

For unconfined compression testing, osteochondral cores were placed between two impermeable steel platens, with and without their respective superficial regions. An identical testing regime to that described for confined compression testing was implemented, consisting of both stress relaxation and dynamic compression testing.

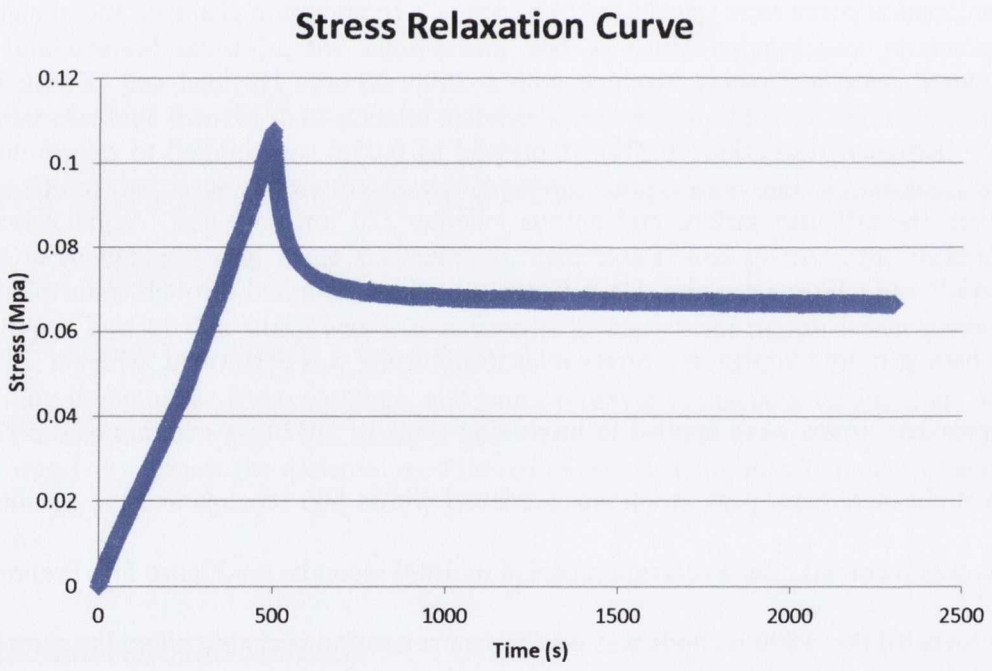

Figure 5.1. Example of a typical stress relaxation curve

5.2.3 Permeability fits

Experimental data in the form of force/time stress relaxation curves were fit to a linear bi-phasic model (Mow et al., 1980) for a known strain, cross-sectional area and aggregate

modulus (H_A) in order to estimate the average permeability of the different articular cartilage regions in confined compression. See (Gannon et al., 2012) for further details.

5.2.4 Biochemical analysis

All biochemical analyses in this study were carried out by Mr Nick Avery. The wet mass of all annuli of the mechanically tested cores were recorded and the samples were frozen for subsequent biochemical analysis as mentioned previously. The frozen samples were freeze dried (RVT4104 Thermo Scientific) for 48 hours or until a constant dry weight was obtained. They were then recovered, weighed and sub-divided to yield separate aliquots for sulphated GAG and collagen determinations and cross-link analyses.

5.2.5 Sulphated glycosaminoglycan determination

Aliquots of (c.10mg) dry material were placed in 1ml 50 mM phosphate buffer, 2 mM EDTA, pH 6.5 (Sigma) and hydrated overnight. Samples were then digested with papain 0.5ml (0.5mg/ml) at 60°C under constant rotation for 18h. The proteoglycan content was estimated by quantifying the amount of sulfated GAG using the dimethylmethylene blue dye-binding assay (Sigma Aldrich), with a chondroitin sulfate standard (Farndale et al., 1982). Data was normalized to tissue dry weight.

5.2.6 Hydroxyproline analysis

The samples were rehydrated with phosphate buffered saline overnight at 4°C, then treated with sodium borohydride as described elsewhere (Avery et al., 2009). Next they were acid hydrolysed, lyophilised, separated into (5µl) aliquots and analysed for hydroxyproline content (Burkhard Scientific, Uxbridge, UK) utilising Bannister & Burns adaptation (Bannister and Burns, 1970) of the Bergman & Loxley technique (Bergman and Loxley, 1963). Total collagen content was determined by assuming an

hydroxyproline conversion factor of 7.14 (Etherington and Sims, 1981). Data acquisition and manipulation was via Dionex AI 450 software. Data was normalized to tissue dry weight.

5.2.7 Histological analysis and PLM

Osteochondral cores were fixed in 4% paraformaldehyde overnight at 4°C. Tissues were decalcified in 5% formic acid, 95% DI H_2O and secured on a gyro rocker at 40revs/min for approximately 30 days. Samples were checked regularly and returned to fresh solution if not deemed completely decalcified. Once each sample was deemed fully decalcified they were sliced in half along the vertical axis, dehydrated, wax embedded and sectioned at 8μm. Sections were stained with safranin O for sGAG and picrosirius red for collagen and subsequently imaged on an Olympus Bx41 microscope equipped with a 30-bit CCD camera (Mason Technology, Dublin, Ireland).

Additionally, in order to visualise the orientation of the collagen fibril architecture these picrosirius red stained sections were imaged using a polarised light microscope (Nikon Eclipse E400 POL). In an effort to enhance visualisation of the collagen architecture all sulphated glycosaminoglycans were removed from the tissue sections by bovine testicular hyaluronidase (Sigma) for 18h. The enzyme was prepared in 0.1 M phosphate buffer, pH 6.9, containing hyaluronidase 1000 U ml^{-1} at 37°C (Király et al., 1997).

5.2.8 Helium ion microscopy

The collagen network was imaged using a helium ion microscope (HIM) (Orion® Plus, Carl Zeiss NTS) with an Everhart-Thornley detector producing an image from the secondary electrons generated by the incident helium ions. In order to provide an unobstructed view of the collagen fibrils serial enzymatic digestion was used to remove

glycosaminoglycan from the cartilage specimens, this protocol was based on a modified version of (Vanden Berg-Foels et al., 2012) and is described in detail in chapter 3 of this thesis. HIM images were acquired in secondary electron mode with an acceleration voltage of 34.9kV, a beam current of 0.2-0.5 pA and a dwell time of 0.5-2.0 µs. An electron flood gun was used to neutralise the positive charging of the sample by the helium ion beam. High resolution images were acquired in the superficial zone of the articular cartilage tissue classified as the top 100 µm of the tissue from the articular surface across age groups in order to visualise the changing morphology of individual network fibrils and fibril connections in this region and during maturation. All images were acquired using a pixel resolution of 2048x2048 or 1024x1024. The pixel spacing for a 1µm field of view corresponds to a pixel dimension spacing of 0.49-0.98 nm px^{-1}. The brightness and contrast of all images were optimised; no other post processing procedures were performed. Fibril diameters were measured using ImageJ (Schneider et al., 2012).

5.2.9 Statistical Analysis

Statistical analysis was performed using a two way ANOVA with Tukey's post-hoc test for multiple comparisons, whilst two sample t-tests were used for unpaired data sets where appropriate. All tests were performed using the statistical software package MINITAB 15.1 (Minitab Ltd., Coventry, UK). Graphical results are displayed as mean with uncertainty expressed by 95% confidence intervals (CIs): mean (lower limit, upper limit). Numerical results are displayed as mean ± SD. Significance was accepted at $p \leq 0.05$ or as indicated. Sample numbers varied according to respective comparison and are outlined in the results section of this manuscript.

5.3 Results

5.3.1 Removal of the superficial region negatively impacts the dynamic modulus of skeletally mature but not immature articular cartilage

The aggregate modulus at 10% strain (determined from confined compression tests) significantly increased after removal of the superficial region for every age group (Figure 5.2); four weeks, one year and three years old (P=0.0424, P=0.0073 and P=0.0463) respectively. The equilibrium Young's modulus (determined from unconfined compression tests) did not significantly change after removal of the SR (Figure 5.2), although the general trend was similar to the findings from confined compression testing. In contrast to the equilibrium results, the confined dynamic modulus (determined by dynamically loading tissue in confined compression) significantly decreased in the mature one year (P=0.0166, P=0.0152 at 20% and 30% applied strains respectively) and three year (P=0.0023 at 10% applied strain) old tissue after removal of the SR, whilst no significant change was observed after its removal in the four week old tissue (Figure 5.3). A similar result was seen in the unconfined dynamic tests where a significant decrease in dynamic modulus was seen in the one (P=0.0106, P=0.0011, P<0.0001 at 10%, 20% and 30% applied strains) and three year (P=0.0177 and P=0.0112 at 10% and 30% applied strains) old tissue after removal of the SR, with no significant change observed after its removal in the four week old tissue (Figure 5.3). The ratio of peak stress to equilibrium stress during stress relaxation testing (Figure 5.4) also significantly decreased in the one (P=0.0007 and P=0.0044 at 10% and 30% applied strains) and three year (P<0.0001, P=0.0488 and P=0.025 at 10%, 20% and 30% applied strains) old tissue after removal of the SR in confined compression. This was also observed for the one (P=0.0044, P=0.001 and P=0.0147 at 10%, 20% and 30% applied strains) and three year (P=0.011 at 10% applied strain) old tissue respectively in unconfined compression, whilst no significant difference was observed in the four week old tissue for either testing configuration.

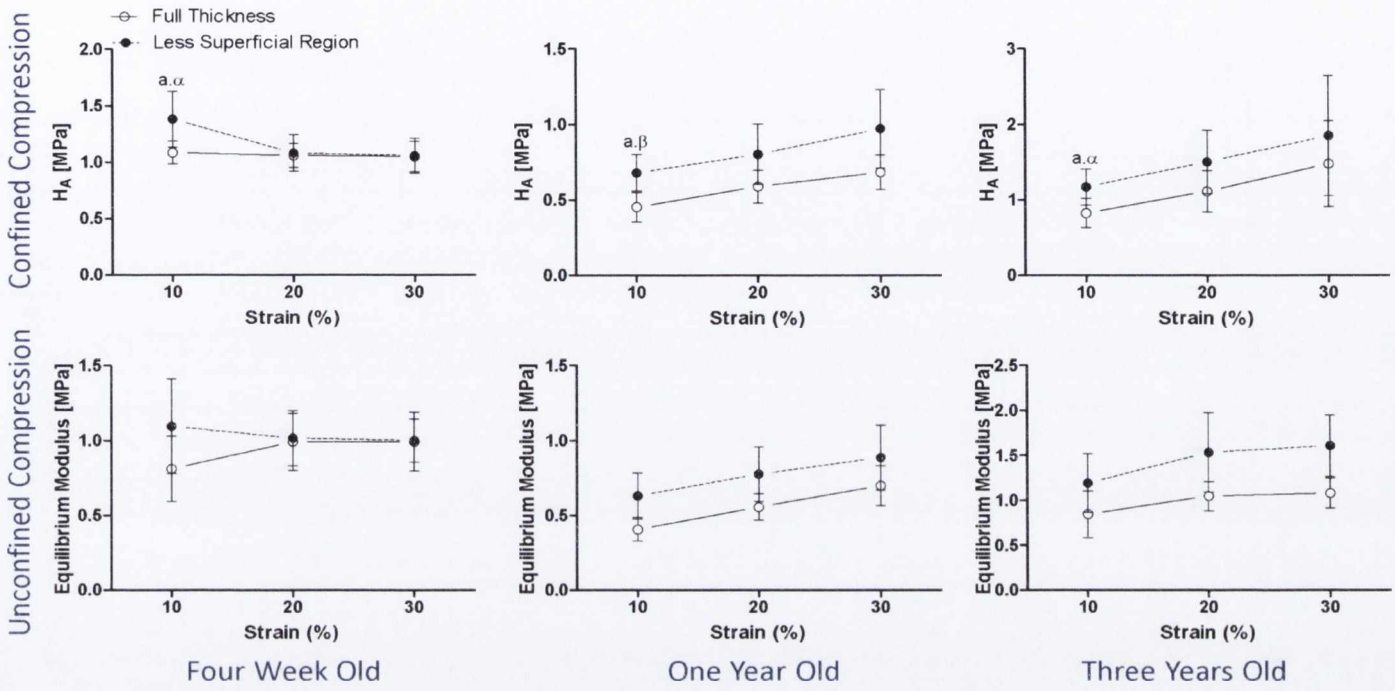

Figure 5.2. Equilibrium aggregate moduli HA (MPa) and equilibrium Young's moduli (MPa) in confined compression and unconfined compression respectively of full thickness osteochondral cores and cores less their superficial region. Cores were obtained from the femoral trochlear ridges for different age groups: four weeks, one year and three years old. Bars show the mean ± 95% CI, n=9/group. All testing was carried out at increasing levels of applied strain: 10, 20 and 30%. Connecting line does not imply linear relationship with strain. 'a' indicates a significant difference vs. 'Intact Osteochondral Core' (10% strain). P value ranges for these differences are as follows: α: $P<0.05$, β: $P<0.01$.

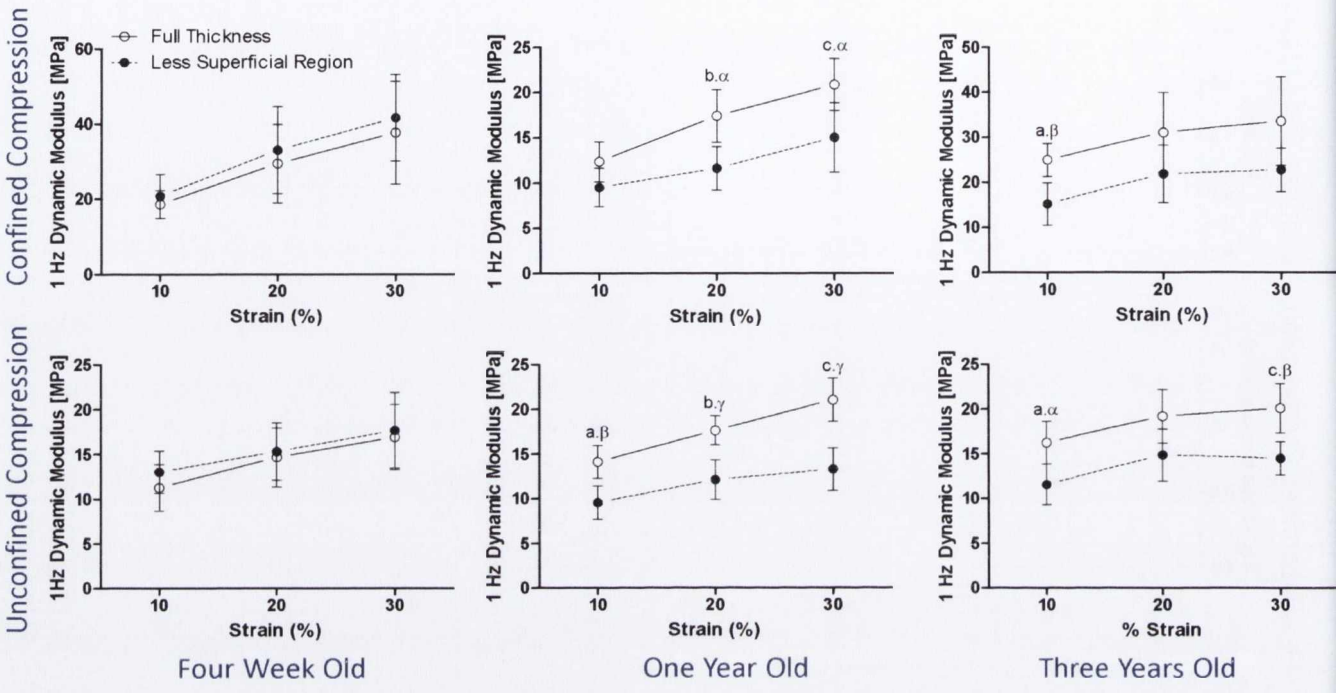

Figure 5.3. Dynamic moduli (MPa) in confined compression and unconfined compression respectively of full thickness osteochondral cores and cores less the superficial region. Cores were obtained from the femoral trochlear ridges for different age groups: four weeks, one year and three years old. Bars show the mean ± 95% CI, n=9/group. All dynamic testing was carried out at 1Hz freq. and 1% amplitude at increasing levels of applied strain: 10, 20 and 30%. Connecting line does not imply linear relationship with strain. 'a' indicates a significant difference vs. 'Intact Osteochondral Core' (10% strain), 'b' indicates a significant difference vs. 'Intact Osteochondral Core' (20% strain), 'c' indicates a significant difference vs. 'Intact Osteochondral Core' (30% strain). P value ranges for these differences are as follows: α: P<0.05, β: P<0.01, γ: P<0.001.

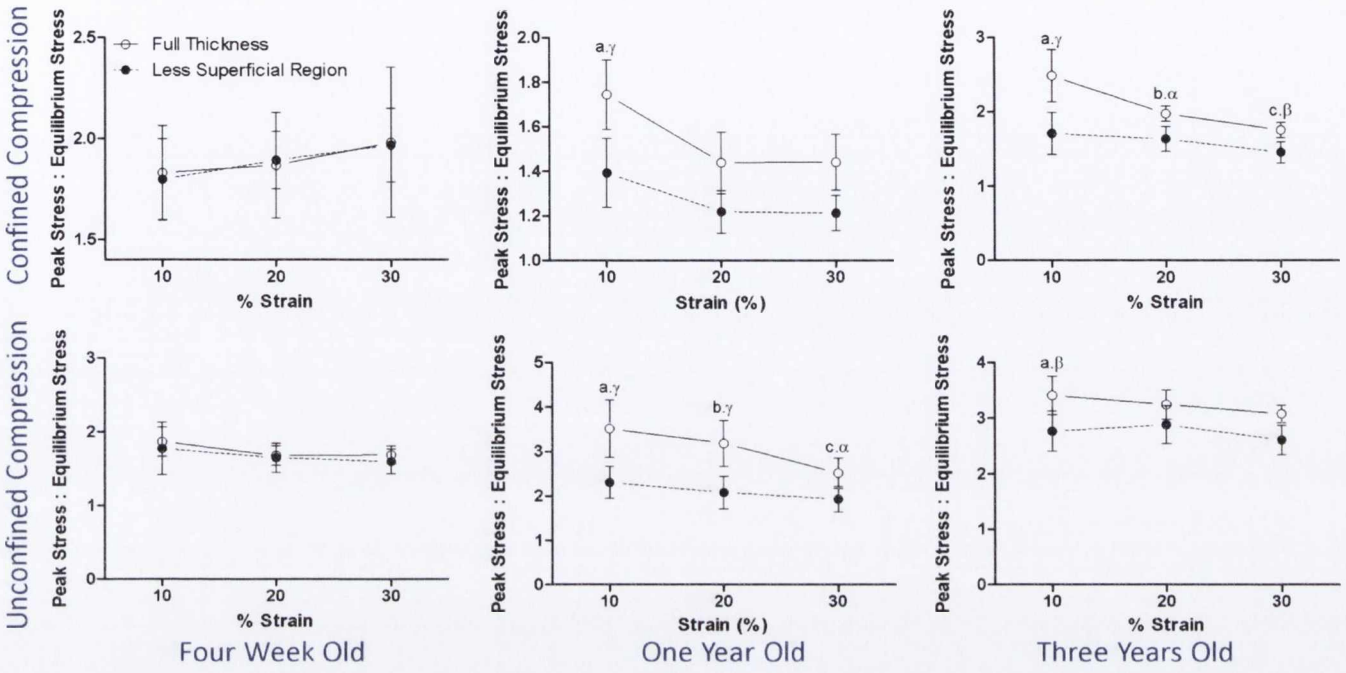

Figure 5.4. Peak stress:equilibrium stress ratio in confined compression and unconfined compression respectively of full thickness osteochondral cores and cores less their superficial region. Cores were obtained from the femoral trochlear ridges from different age groups: four weeks, one year and three years old. Bars show the mean ± 95% CI, n=9/group. All testing was carried out at increasing levels of applied strain: 10, 20 and 30%. Connecting line does not imply linear relationship with strain. 'a' indicates a significant difference vs. 'Intact Osteochondral Core' (10% strain), 'b' indicates a significant difference vs. 'Intact Osteochondral Core' (20% strain), 'c' indicates a significant difference vs. 'Intact Osteochondral Core' (30% strain). P value ranges for these differences are as follows: α: P<0.05, β: P<0.01, γ: P<0.001.

The incremental aggregate modulus (Figure 5.5), defined as the slope of the equilibrium stress-strain curve in confined compression from 10%-30% applied strain, significantly changed with age (P<0.0001). Specifically, the full thickness three year old mature tissue was significantly stiffer than the full thickness one year old tissue (P=0.0268), whilst the three year old tissue, less its superficial region, was significantly stiffer than all the 4 week and one year old tissues either with or without their SR (P=0.0078, P=0.0021, P=0.0002 and P=0.0017 respectively). The incremental Young's modulus (Fig.7) in unconfined compression revealed a similar overall significant change with age (P=0.014) however no individual significant effects were observed. Comparing the dynamic properties of intact samples (at 10% offset strain) across different ages groups, it can be seen that the dynamic modulus in unconfined compression is significantly higher for the 3 year (P=0.0044) old tissue compared to 4 week old tissue (Figure 5.6).

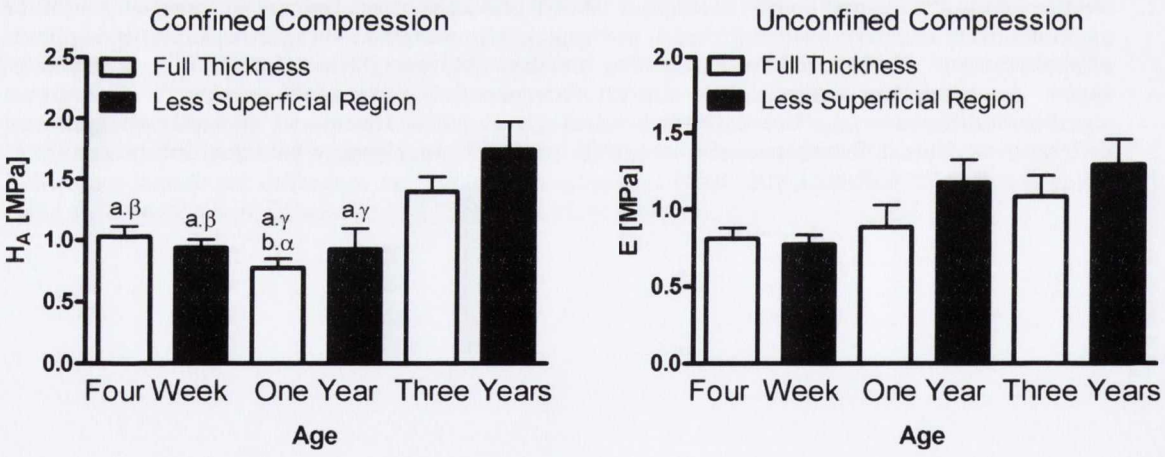

Figure 5.5. Incremental aggregate and Young's modulus (MPa) of full thickness porcine osteochondral cores and cores less the superficial region in confined and unconfined compression taken as the slope of the stress strain curve for all applied strains (10, 20 and 30% ε) from different age groups: four weeks, one year and three years. Bars show the mean ± 95% CI, n=8. 'a' indicates a significant difference vs. 'Three year old core less its superficial region', 'b' indicates a significant difference vs. 'Full thickness three year old tissue'. P value ranges for these differences are as follows: α: P<0.05, β: P<0.01, γ: P<0.001.

Experimental data fit to a linear bi-phasic model of articular cartilage in confined compression revealed that the hydraulic permeability of the mature three year old full thickness cartilage ($7.2\times10^{-16} \pm 2.23\times10^{-16}$ $m^4/N\cdot s$) was significantly lower (P=0.039) than after removal of the SR ($1.54\times10^{-15} \pm 5.48\times10^{-16}$) $m^4/N\cdot s$. The predicted permeability was over an order of magnitude higher in four week old tissues, increasing from $2.33\times10^{-14} \pm 1.29\times10^{-14}$ $m^4/N\cdot s$ to $5.06\times10^{-14} \pm 3.54\times10^{-14}$ $m^4/N\cdot s$ upon removal of the SR.

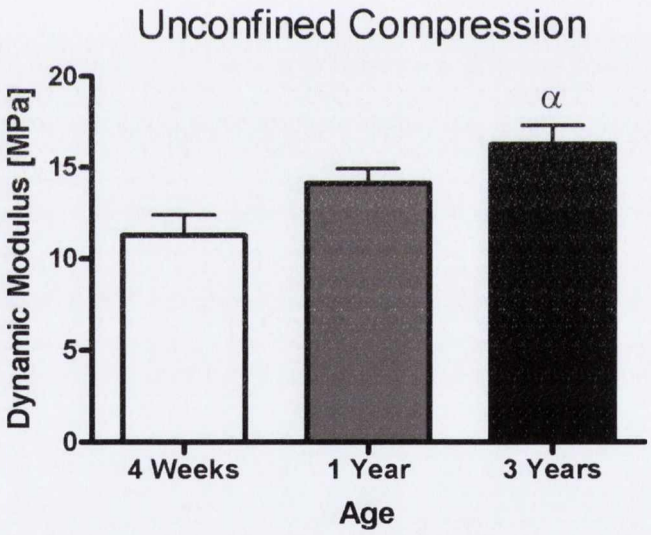

Figure 5.6. Dynamic moduli (MPa) of full thickness osteochondral cores in unconfined compression at 10% applied strain for all age groups; 4 week old, one year old and three year old. α indicates a significant difference vs. 4 week old core, P=0.0044.

5.3.2 Spatial changes in tissue composition with age cannot fully explain the functional role played by the superficial region of mature articular cartilage during dynamic compressive loading

Biochemical analysis revealed a significant age effect ($P<0.0001$) in sGAG content when normalised to percentage dry weight (Figure 5.76b). The superficial region and the remaining cartilage tissue of the one and three year old skeletally mature joints contained significantly less sGAG than the four week old immature superficial region ($P=0.0137$, $P=0.0038$, $P=0.05$ and $P=0.0136$) and the remaining cartilage tissue ($P=0.0088$, $P=0.0021$, $P=0.041$ and $P=0.0087$ respectively). Furthermore, the overall sGAG content (SR + remaining tissue) was significantly lower in the 1 (P=0.0016) and 3 (P=0.0001) year old tissue compared to the 4 weeks old tissue (data not shown). In contrast, collagen content (when normalised to % dry weight) significantly increased with age ($P<0.0001$). Both the superficial and remaining regions of the mature full thickness three year old tissue contained significantly higher amounts of collagen compared to the SR of the 4 week old tissue ($P=0.006$ and $P=0.0055$ respectively) (Figure 5.76a). Furthermore, the overall collagen content (SR + remaining tissue) was significantly higher in the 3 (P=0.0016) year old tissue compared to the 4 weeks old tissue (data not shown). In terms of changes in spatial tissue composition with age (% dry weight), no significant difference in collagen or sGAG content was observed between the SR and the remainder of the tissue within any given age group. Together these results suggest that relative changes in spatial tissue composition with age may not fully explain why removal of the SR leads to a reduction in the dynamic modulus in the mature articular cartilage.

These biochemical results are generally reflected in the histological analyses. Picrosirius red stained sections (Figure 5.76a) point to an increase in staining between the four week old immature and one year and three year old mature tissue, correlating with the significant increase in collagen content with age. Safranin O staining (Figure 5.76b)

demonstrated a decrease in staining between four weeks and one and three years, which again can be related to the significant decrease in sGAG concentration with age.

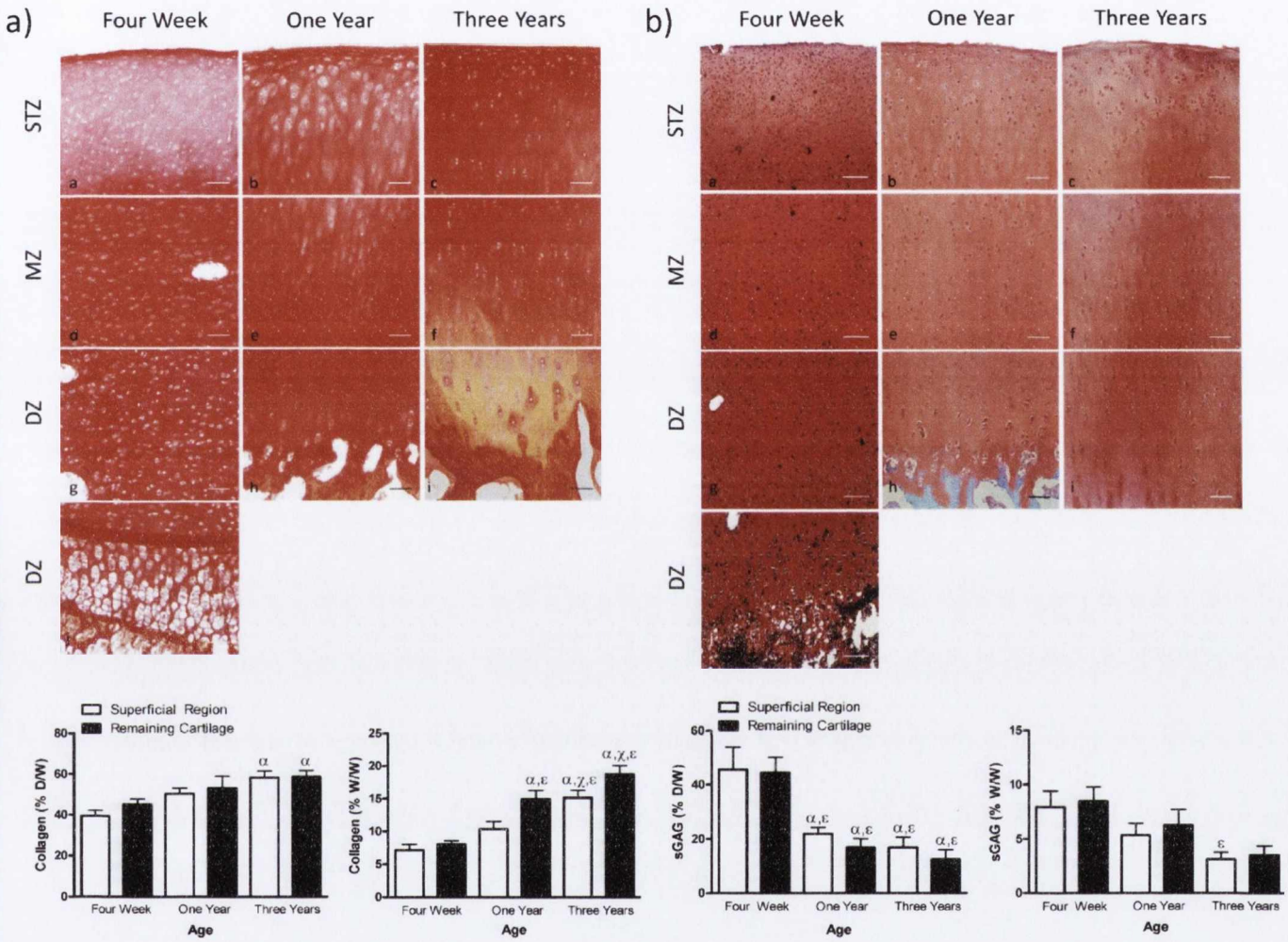

Figure 5.7 . Full thickness cartilage sections stained with picrosirius red-collagen (A) and safranin O-sGAG (B) from the femoral trochlear ridges. Images are taken at each respective zone - STZ, MZ and DZ with developing ages; four weeks, one year and three years old. It should be noted that four week old cartilage is significantly thicker than the more mature tissue. Scale bars 100μm. Biochemical analysis of total collagen content (C) and sulphated glycosaminoglycan (sGAG) content (D) expressed per sample dry weight (%) and wet weight (%) respectively of the superficial region of the tissue taken as the top 15% of full thickness cores and the remaining cartilage once this layer has been removed from developing age groups: four weeks, one year and three years. Bars show mean with SEM, statistical significance is taken at $p \leq 0.05$. Statistical differences are indicated as follows: α vs. 4 week old SR, ε vs. 4 week old core less its respective superficial region, χ vs. one year old SR.

5.3.3 The collagen network within the superficial region of articular cartilage dramatically reorganises with skeletal maturity

Given that the overall collagen content of SR of mature articular cartilage is not significantly different than the remaining tissue, it was next sought to determine if changes to the organization of the SR during postnatal development might explain why removing this zone of the tissue negatively impacts its dynamic mechanical properties. A thin, intensely birefringent and hence highly organised layer can be seen in the superficial region of the immature four week old tissue (Figure 5.8), suggesting that even at this early age some level of organization exists in the superficial region. The majority of the remainder of the tissue displays large bands of non-birefringence, illustrating that the majority of the tissue is isotropic in structure. The one year old tissue demonstrates the beginning of a skeletally mature architecture. The highly birefringent superficial region displays the parallel orientation of the collagen fibrils. In the middle zone these fibrils arcade to a perpendicular orientation. Interestingly, an extra lamina or zone is visible in the deep zone of the tissue (Nieminen et al., 2002, Rieppo et al., 2008), with an isotropic orientation, possibly relating to growth and maturation of the articular cartilage (Hunziker et al., 2007). In the three year old, fully mature tissue, intense birefringent regions exist in the superficial and deep zone, clearly illustrating a fully developed Benninghoff architecture.

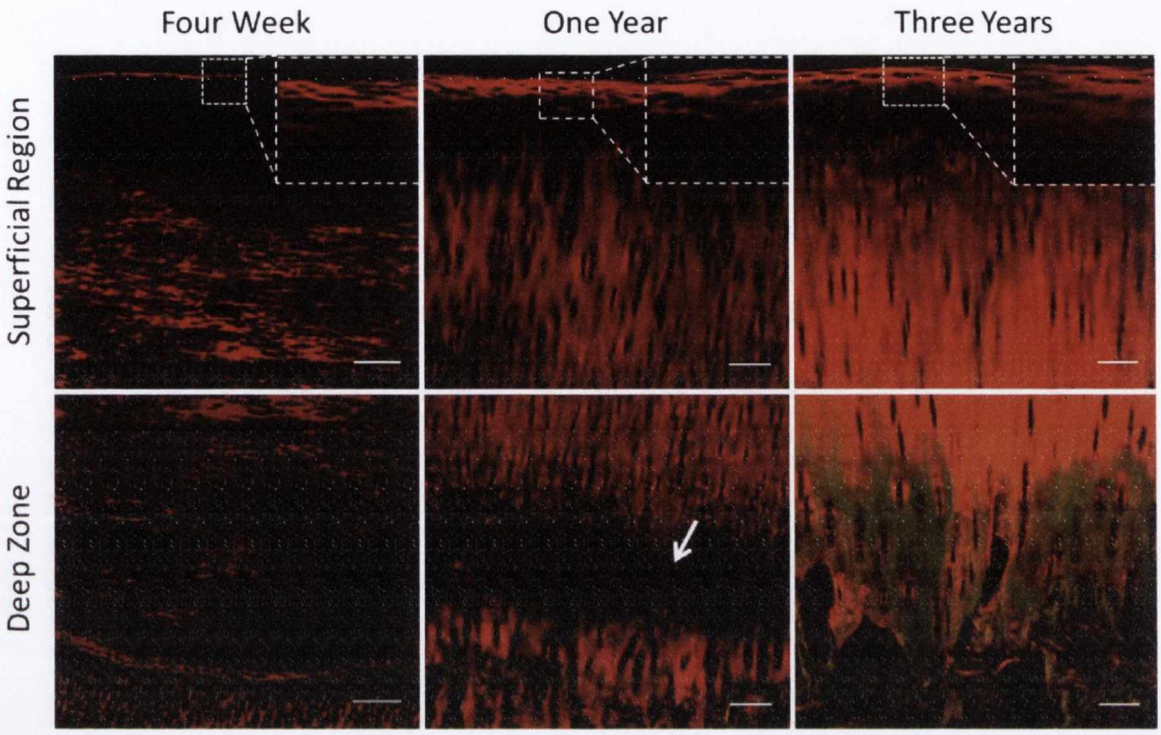

Figure 5.8. Picrosirius red stained sections imaged using polarised light microscopy (PLM) of the superficial region and deep zone of articular cartilage. A change in the direction of the polarised light known as birefringence occurs close to the articular surface and in the deep zone, allowing the visualisation of the dramatic differentiation between the highly organised superficial and deep zone in the three year old mature tissue; scale bar 100-250μm. Arrow highlights what appears to be an extra lamina in the deep zone of the one year old tissue.

In order to further investigate the changing internal environment of the collagen architecture in the superficial region of the tissue, HIM was employed. These high resolution images taken 100 microns from the articular surface revealed detailed information about the individual collagen fibrils and fibril connections in the superficial region. The fibrils appear randomly organised in the 4 week old tissue, but appear more aligned parallel to the articular surface in the one and three year old tissue. A significant increase was observed in fibril diameter with age ($P<0.0001$) (Figure 5.9). Average fibril diameter increased from 14.37±7.28 nm in the four week old tissue significantly ($P<0.0001$) to 22.91±11.41 nm in the one year old tissue, with a further significant

increase (P<0.0001) to 75.91±30.47 nm in the three year old tissue. In addition, a decrease in the number of collagen fibrils and fibril branching can be seen with age; this is most apparent between the 4 week old and three year old tissue, see (Figure 5.9).

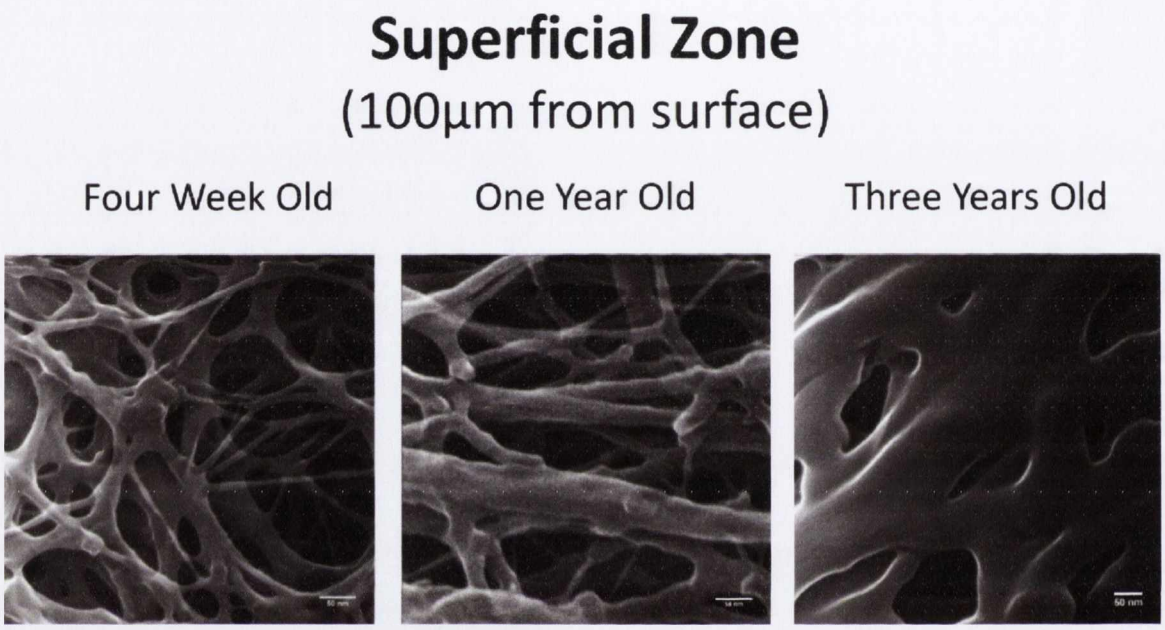

Figure 5.9. Helium ion microscopy images from the superficial region of porcine articular cartilage (taken from the top 100µm of the tissue) across developing age groups: four weeks, one year and three years old. Scale bar 50nm.

5.4 Discussion

The hypothesis of this study was that the superficial region of articular cartilage develops into a functionally important region of the tissue during postnatal development, and hence removal of this region would only lead to a reduction in the dynamic modulus of the tissue when it has reached a certain level of skeletal maturity. In agreement with previous studies that explored the depth dependent compressive equilibrium properties of articular cartilage (Julkunen et al., 2009, Schinagl et al., 1997, Setton et al., 1993), a significant increase in the aggregate modulus upon removal of the SR (at 10% applied strain) was

observed for all age groups in confined compression (Figure 5.2). In contrast to the equilibrium results, the dynamic modulus significantly decreased after removal of the SR in confined and unconfined compression for the one and three year old mature tissue (Figure 5.3). Overall, sulphated GAG content (% dry weight) decreased significantly with age whilst collagen content (% dry weight) significantly increased, however no significant difference was observed between the bulk biochemical composition of the SR and the remaining cartilage for any age-group. This suggests that temporal changes in the relative spatial biochemical composition of the tissue cannot fully explain why the superficial region of articular cartilage becomes so mechanically important with age. The results of this study would suggest that organizational changes to the collagen network of the SR of the tissue with age play a key role in determining the dynamic properties of the tissue. This was revealed using PLM which demonstrated the development of a Benninghoff architecture in the three year old mature tissue, while helium ion microscopy illustrated a change in fibril alignment, a significant increase in fibril diameter from immature to mature tissue and a decrease in fibril branching.

In confined compression, characterised by one dimensional deformation, fluid flux occurs in the axial direction, forcing interstitial fluid through the SR of the tissue. An explanation for the reduction in the dynamic moduli in confined compression upon removal of the SR in mature articular cartilage may therefore be that the SR acts as a low permeability barrier to fluid flow, where its removal results in a reduced ability to maintain fluid load support. This argument is reinforced by the finding that the ratio of peak stress to equilibrium stress also significantly reduces after removal of the SR. This is consistent with previous interpretations that the tangential zone acts to limit fluid flow out of and into articular cartilage (Glaser and Putz, 2002, Setton et al., 1993, Wayne, 1995). In contrast, removal of the SR did not influence the dynamic properties of the immature

four week old tissue, which is likely due to the fact that the tissue is predominantly isotropic in structure and has yet to obtain a Benninghoff architecture (Figure 5.8). Fibrils in the four week old tissue are approximately five times smaller than three year old mature fibrils and less organised (Fig. 6), which likely explains the finding of an overall higher permeability in immature cartilage. Furthermore, the densely packed and highly aligned collagen fibrils observed in the superficial region of mature articular cartilage are hypothesized to reduce the axial permeability of the tissue to a greater degree than in the immature tissue.

Geometric differences between mature and immature tissue (specifically that mature tissue is significantly ($P<0.001$) thinner than immature tissue) were also considered as a possible alternative explanation for the fact that removal of the SR (defined as the top 15% of total tissue thickness) only negatively impacted the dynamic modulus of mature articular cartilage. In order to investigate this further; cylindrical cores of articular cartilage were modelled (Mow et al., 1980) as homogeneous, linear elastic and linear biphasic in confined compression, with the same material properties[1] but different tissue thicknesses. Modelling was carried out by Dr. Thomas Nagel. The simulated loading rates and magnitudes corresponded to the experimental protocol outlined in the methods section of this manuscript. Mature tissue was modelled with a thickness t = 1 mm, whilst the immature tissue was modelled with t = 3 mm. The results of these simulations indicate that as flow path length decreases with decreasing tissue thickness (i.e. as occurs with age), fluid flow induced viscous effects become less apparent relative to (thickness independent) elastic effects. Comparing dynamic moduli values in "thin" (mature) and "thick" (immature) tissue, removal of the superficial region induced a 5.46% drop in the dynamic modulus in the mature tissue compared to a 12.71%

[1] E 0.5 MPa, υ 0.2, μ 10^{-9} MPas, k $7.5*10^{-12}$ mm^2, ϕ 0.8

drop in the immature tissue, demonstrating that removal of the top 15% of a thick tissue (i.e. an immature tissue) has a more dramatic effect than removal of 15% of a thin tissue (i.e. the mature tissue). Experimentally, the opposite observation was made: the mature tissue was affected more than the immature tissue. Therefore, the reduction of the dynamic modulus observed experimentally after removal of the SR in mature tissue is not due to geometric differences between the different age groups. This model prediction also at least partially explains why the dynamic modulus of the thicker immature articular cartilage in confined compression is higher that mature tissue (i.e. due to a greater flow path length in thicker tissue), and demonstrates that it is inappropriate to directly compare the absolute values of dynamic moduli in confined compression across different age groups.

Similar to the confined compression results, a significant drop in both the dynamic moduli (Figure 5.3) and the ratio of peak stress to equilibrium stress (Figure 5.4) was observed during unconfined compression testing after removal of the SR (for most strain levels) in mature articular cartilage. This was not observed in the immature tissue. This is speculated to be due to the mature superficial region acting to limit radial expansion during instantaneous loading (Kiviranta et al., 2006, Schinagl et al., 1997), therefore increasing fluid load support in the tissue (Ateshian et al., 2009) and hence increasing the tissue dynamic modulus. Unlike the confined compression testing configuration, no inherent thickness effects exist in unconfined compression due to the orthogonal direction of the fluid path. In this case the gel diffusion time depends on the sample radius instead of its thickness, which was identical for all age groups.

A finite element simulation was also used to confirm that removal of the superficial region in skeletally mature articular cartilage could reduce the dynamic modulus of the tissue due to increased radial expansion (and hence reduced fluid load

support) during unconfined compressive loading. A tissue plug with a fully developed Benninghoff architecture as described in (Nagel and Kelly, 2010) (Figure 5.10.9a) was assumed for mature articular cartilage (Görke et al., 2010). These finite element simulations demonstrated a 34.34% decrease in the dynamic modulus after removal of the superficial region in the mature tissue. The effect of the mature SR can be seen most clearly by examining the radial displacement (mm) at the edge of the tissue in the superficial region and deep zone of the sample (Figure 5.10.9b). Here much smaller sample displacements are visible in the superficial region of the tissue during stress relaxation and dynamic testing. This further supports the theory that the SR can play a key role in unconfined compression by limiting radial expansion and thus maintaining fluid load support.

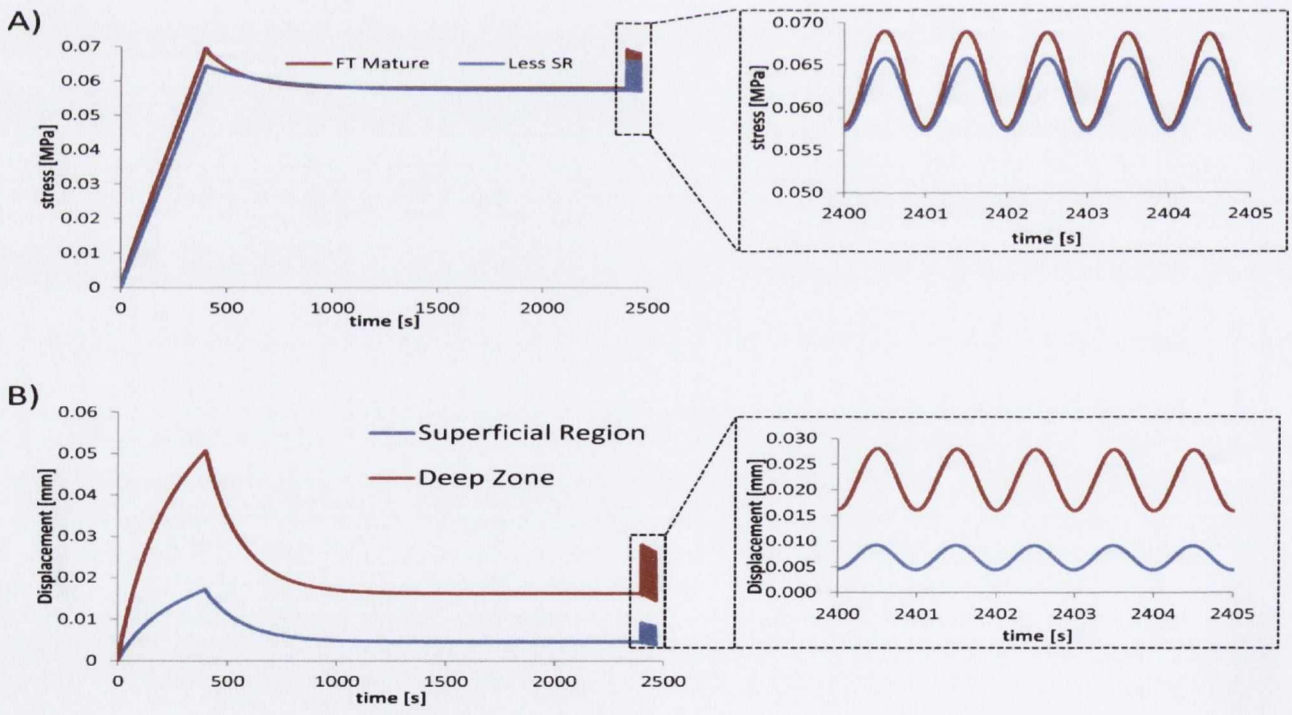

Figure 5.10. Finite element simulations of an osteochondral core with a fully developed mature Benninghoff architecture in unconfined compression. (A) Stress relaxation curve for the full thickness section (FT Mature) and after removal of the respective superficial region (Less SR) and subsequent dynamic loading of the sample (B) Radial displacement (mm) at the edge of the tissue in the superficial region and deep zone of the sample during stress relaxation and dynamic loading.

The incremental aggregate and Young's modulus (MPa) of the cartilage cores in confined and unconfined compression (taken as the slope of the equilibrium stress-strain curve) were found to increase with age (Figure 5.5). No significant changes in the bulk tissue mechanical properties between 4 week old and 1 year old tissue were observed, despite a significant drop in sGAG/dry weight content with age. Furthermore, the bulk equilibrium properties of the three year old tissue were significantly higher than other groups. This is in agreement with previous studies that found an increase in compressive modulus between foetal bovine (0.11 ± 0.03 MPa) and adult bovine (0.31 ± 0.03 MPa) articular cartilage (Williamson et al., 2001), whilst other studies have observed an increase in equilibrium compressive modulus of New Zealand White rabbits in new-born (~0.5 MPa) to 18 months of age (~2.5 MPa) using creep indentation testing (Julkunen et al., 2009). In addition, the dynamic modulus (at 10% offset strain) in unconfined compression was significantly higher for the 3 year (P=0.0044) old tissue compared to 4 week old tissue (Figure 5.6). These results highlight the importance of both increases in collagen (dry weight) content and attainment of a Benninghoff architecture to the equilibrium and dynamic compressive properties of articular cartilage.

A pig reaches puberty at six months of age (Rieppo et al., 2009, Swindle and Smith, 1998), therefore animals at the age of one year have passed puberty but full skeletal maturity is not yet attained. At three years, porcine articular cartilage could be considered a model of skeletally mature human tissue, while the 4 week time point might be more representative of human articular cartilage in the first months or years of life. A change in collagen organisational development can be seen in the polarised light microscopy images (Figure 5.8). The four week old tissue demonstrates very little organisational evidence bar a thin birefringent region in the superficial tangential zone, which may be due in part to the lamina splendens. The one year old tissue demonstrates

the onset of skeletal maturity, with the presence of what appears to be an extra isotropic lamina visible in the deep zone of the tissue, which has also been observed previously (Nieminen et al., 2002, Rieppo et al., 2008). Finally the three year old tissue demonstrates a fully developed Benninghoff architecture with the highly organised fibrils in the superficial region orientated parallel to the articular surface and the vertical orientation of the fibrils in the deep zone. A significant increase in collagen fibril diameter with age was also observed, which is in agreement with previous studies (Gardner, 1992, Hwang et al., 1990, Provenzano and Vanderby Jr, 2006, Wachtel et al., 1995). This increase in fibril diameter is thought to be attributable to the aggregation of smaller individual fibrils (Wachtel et al., 1995). One reason for this sequence may be a reduction in proteoglycan monomer size (Gardner, 1992) and overall decrease in sGAG/dry weight with age.

There are limitations associated with this study. Slicing the tissue into layers may affect the intrinsic continuity of the tissue. In addition, whilst classifying the superficial region as the top 15% of the tissue is within traditional definitions, age related changes in the tissue structure could mean that some of the transitional zone may also have been removed. However, for the purpose of investigating what role the presence of the superficial region plays in determining the dynamic properties of the tissue, it's of higher importance that the entire superficial tangential zone be removed.

A fully developed superficial region has been shown to be of vital importance in maintaining the mechanical integrity of articular cartilage under a range of loading regimes (Bevill et al., 2010, Glaser and Putz, 2002, Hosseini et al., 2013). The findings of this study demonstrate that the superficial region of articular cartilage undergoes structural adaptation with age, which in turn plays a key role in determining the dynamic compressive properties of the tissue. Understanding such mechanisms will play a key role in furthering our understanding of articular cartilage development and degeneration and

has important implications for the field of functional cartilage tissue engineering, highlighting the significance of recapitulating the native cartilage organization in tissue engineered constructs for supporting *in vivo* loads.

Chapter 6 Changes to the Depth Dependent Mechanical Properties of Articular Cartilage from Birth to Skeletal Maturity are driven by the temporal Evolution of its Collagen Network

6.1 Introduction

Articular cartilage consists of an extracellular matrix made up of water (80% wet weight), proteoglycans (25-35% dry weight) and collagen (60% dry weight) together with a small concentration of non-collagenous matrix proteins and glycoproteins (15-20% dry weight) (Brama et al., 2000, Buckwalter et al., 2005). The tissue is synthesized and remodelled by chondrocytes which vary in organisation and phenotype with depth from the articular surface (Stockwell, 1970). During postnatal development and skeletal maturation, the biochemical composition of articular cartilage changes both spatially and temporally. Collagen concentration and pyridinoline cross-link concentration is reported to increase with maturation, whilst the glycosaminoglycan concentration and percentage water content remain unchanged or decrease slightly (Williamson et al., 2003). The specific composition of the matrix also changes; chondroitin-4 sulphate is reported to be the predominant glycosaminoglycan (GAG) in immature cartilage, while chondroitin-6 sulphate is predominant in mature tissue (Torzilli et al., 1998). Structurally, significant alterations of the collagen network also take place during postnatal development. This network transitions from a predominantly isotropic architecture in immature tissue to the mature arcade-like zonal structure first described by Benninghoff (Benninghoff, 1925).

Understanding how such compositional (Bank et al., 1998, Brama et al., 2000, Stockwell, 1970, Wachtel et al., 1995), and architectural changes (Hyttinen et al., 2009, Julkunen et al., 2010, Rieppo et al., 2009) alter the mechanical properties of articular

cartilage during postnatal development is central to understanding how the tissue achieves its function. Surprisingly, relatively little is known about how the biomechanical properties of articular cartilage evolve during postnatal development and maturation (Brommer et al., 2005, Julkunen et al., 2009, Williamson et al., 2001). In terms of bulk mechanical properties, an increase in tensile stiffness has been reported with maturation (Roth and Mow, 1980, Williamson et al., 2003), with more subtle changes reported in the compressive properties of the tissue with age (Brommer et al., 2005, Julkunen et al., 2009, Williamson et al., 2001). However, articular cartilage is known to possess complex depth dependent mechanical properties (Wang et al., 2002a), which cannot be evaluated through commonly used bulk mechanical testing protocols. Given that we know articular cartilage changes from a relatively isotropic and homogeneous tissue at birth to one displaying significant complexity in its spatial composition and organisation at adulthood, it would seem reasonable to assume that the depth-dependent mechanical properties of the tissue change dramatically during postnatal development. Recently, digital image correlation techniques have been developed to determine the depth varying compressive properties of articular cartilage (Canal Guterl et al., 2010, Schinagl et al., 1997, Schinagl et al., 1996, Wang et al., 2002a). The objective of this study was to elucidate how the structure and composition of articular cartilage change during postnatal development and maturation using a unique combination of histological, biochemical and imaging techniques and to relate this evolution to changes in the depth dependent compressive mechanical properties of the tissue.

6.2 Methods

6.2.1 Sample preparation

Tissue explants were isolated and stored as described previously (Gannon et al., 2012). Osteochondral cores (Ø6 mm) were harvested from the femeropatellar groove of healthy

porcine knee joints within 3 h of sacrifice. Specimens collected were divided into groups representing different stages of postnatal development; 4 week and 8 week old- immature articular cartilage, 1 year old – approaching skeletal maturity and 3 years old - representing fully mature articular cartilage. These samples were analysed using mechanical, biochemical and histological techniques, in addition to helium ion microscopy. Specimens harvested for mechanical testing were placed in phosphate buffered saline (PBS) solution and stored at -80°C until the day of use. On each respective day of mechanical testing, cores were thawed to room temperature by immersion in PBS and sub-punched from Ø6 mm to Ø3 mm. These cores were then sliced in half along the zonal direction to create two semi-cylindrical osteochondral specimens in order to obtain a flat surface on which to image cells (that acted as fiducial markers) within the mechanically compressed tissue. The annulus of each sample was wet weighed and frozen at -80°C for later biochemical analysis. The fiducial markers were created by fluorescent staining of chondrocyte DNA. Chondrocytes are essentially affixed within the dense extracellular matrix because they are three orders of magnitude larger than the effective pore size of the matrix (Maroudas, 1979) and the movement of these cells can thus reflect the deformation of the sample within the imaging plane (Wang et al., 2002a). Samples were immersed in 1ml PBS with 5µl/ml Hoechst 33342 for 1.5 h at 22°C to allow diffusion of the dye into the cartilage and reaction with the cellular DNA (Schinagl et al., 1996).

6.2.2 Mechanical Testing Protocol

Semi-cylindrical samples were tested in unconfined compression in a custom made stainless steel compression rig (Figure 6.1a) that was designed to sit on the stage of an inverted fluorescent Olympus IX 51 microscope equipped with a 100W xenon arc lamp, a DAPI filter cube and a 0.4 NA Universal Plan Super Apochromat 10x objective (Mason

Technology, Dublin, Ireland). Details of this rig can be found in chapter 3. The semi-cylindrical cartilage sample was bathed in PBS in a testing chamber with a glass microscopic slide window at its base, sandwiched between the two loading platens with its rectangular cross section facing down toward the microscope objective; enabling the visualisation of the tissue during testing. Compression was manually applied to the articular surface of test specimens by advancement of a micrometre attached to the remaining Perspex platen (Mitutoyo, Radionics, Dublin, Ireland; resolution 0.01 mm). Images were recorded with a 12-bit Olympus DP70 camera (Mason Technology, Dublin, Ireland; view 1360 × 1024) and Analysis imaging software (Mason Technology, Dublin, Ireland). The 1360 × 1024 pixel image represented a 583 μm×438 μm sampling of the specimen focal plane at 0.428 μm/pixel.

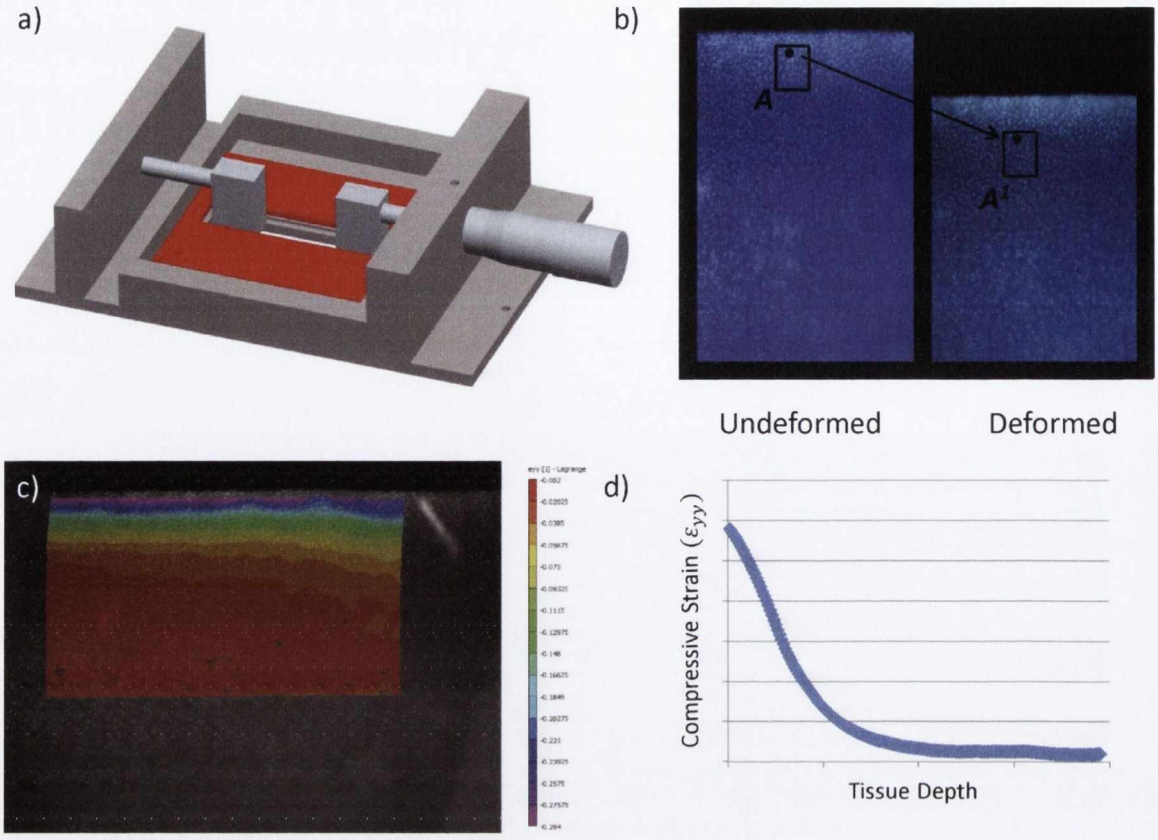

Figure 6.1. (a) Schematic of custom designed unconfined compression rig, (b) example of an undeformed reference and subsequent deformed fluorescent image taken prior to and after loading illustrating the way in which strain is tracked at every loading increment, (c) example of a typical strain ε_{yy}correlation for a one year old sample for a selected region of interest (ROI), (d) graphical representation of the strain output of image (c) displayed as the compressive strain in the zonal direction (ε_{yy}) plotted versus depth from the articular surface (pixels).

Cartilage thickness was determined using bright field microscopy at 4x magnification in the uncompressed state (Chen et al., 2001). A tare load of ~1N was applied to ensure union between the platen and the articular surface after which the sample was allowed to fully relax. The samples were compressed up to 10%, in 2.5% strain increments, and then to 15% and 20% offset strain based on the initial sample thickness at a strain rate of 0.5%/s. After each loading increment the sample was allowed to relax for 60 minutes or until the stress changed by less than 0.001 MPa in 5 min (Chen et al., 2001), and the equilibrium force was measured. Images were captured prior to loading and after the sample had reached equilibrium at each loading stage to quantify the

spatial magnitudes of deformation with the tissue (Figure 6.1b). The intra tissue displacement field was calculated using the digital image correlation software VIC 2D 2009 (Correlated Solutions, Columbia, SC, USA)

The average axial (ε_{yy}), lateral (ε_{xx}) and shear strain (ε_{xy}) were computed within three distinct zones; the superficial tangential zone (STZ), the middle zone (MZ) and the deep zone (DZ). These regions were assumed to be 0-6%, 7-18% and 19-30% respectively of the total cartilage thickness from the articular surface. Local strains were computed for a range of different global offset strains (2.5%, 5%, 10% and 15% strain). The depth dependent nominal Young's modulus (E_{yy}) [MPa] was taken as the equilibrium force divided by the specimens cross-sectional area divided by the computed averaged strain (ε_{yy}) within each zone for each nominal applied global offset strain. Likewise Poisson's ratio was calculated as computed averaged strain in the radial direction (ε_{xx}) divided by the averaged axial strain (ε_{yy}), all computed for each applied global offset strain; 2.5%, 5%, 10% and 15% strain.

6.2.3 Biochemical analysis

All biochemical analyses in this study were carried out by Mr Nick Avery. The wet mass of all annuli of the mechanically tested cores were recorded and the samples were frozen for subsequent biochemical analysis as mentioned previously. The frozen samples were freeze dried (RVT4104 Thermo Scientific) for 48 hours or until a constant dry weight was obtained. The samples were then recovered, weighed and sub-divided to yield separate aliquots for sulphated GAG, collagen content and cross-link analyses.

6.2.3.1 Sulphated glycosaminoglycan determination

Aliquots of dry material (c.10 mg) were placed in 1ml 50 mM phosphate buffer, 2 mM EDTA, pH 6.5 (Sigma) and hydrated overnight. Samples were then digested with papain

0.5ml (0.5mg/ml) at 60°C under constant rotation for 18h. The proteoglycan content was determined by quantifying the amount of sulfated GAG using the dimethylmethylene blue dye-binding assay (Sigma Aldrich), in comparison with a chondroitin sulfate standard (Farndale et al., 1982). Data was normalized to the tissue dry weight.

6.2.3.2 Collagen cross-link determination

The samples were rehydrated with phosphate buffered saline overnight at 4°C, then treated with sodium borohydride as described elsewhere (Avery et al., 2009). After 1h reduction at room temperature they were acid hydrolysed for 24h at 115°C, lyophillised and pre-fractionated using strong cation exchange solid phase extraction (SPE) cartridges (Biotage Ltd, Kungsgatan, Sweden), prior to cross-link analysis. Cross-links were quantified using a Dionex Ultimate 3000 auto-sampler (Thermo Scientific) linked to a Dionex ICS 3000 ion chromatography system (Thermo Scientific) configured for post-column analysis of the eluate from a 15x0.46cm sodium cation exchange column (Pickering Laboratories, CA, USA). Column eluate was reacted with ninhydrin in a post column reactor at 125°C (CRX400, Pickering Laboratories, CA, USA) and assayed using a variable wavelength detector set at 570 nm (Dionex Ultimate 3000, Thermo Scientific). System control and data acquisition was via Dionex Chromeleon software. The cross-links were quantified; by comparison with standards prepared in-house, after resolution using an analytical program also developed in-house, and are expressed as moles per mole of collagen. The mature cross-links hydroxylysyl pyridinoline, lysyl pyridinoline and histidino-hydroxylysinonorleucine could all be detected, although lysyl pyridinoline predominated in all samples. The immature cross-links hydroxylysino-ketonorleucine and hydroxylysinonorleucine were also detected in some samples but at appreciably lower levels. Cross-links are expressed as molecule per mole.

6.2.3.3 Hydroxyproline analysis

Prior to treatment with SPE an aliquot (5µl) of the above hydrolysates was analysed for hydroxyproline content (Burkhard Scientific, Uxbridge, UK) utilising Bannister & Burns adaptation (Bannister and Burns, 1970) of the Bergman & Loxley technique (Bergman and Loxley, 1963). Total collagen content was determined by assuming a hydroxyproline conversion factor of 7.14 (Etherington and Sims, 1981). Data acquisition and manipulation was via Dionex AI 450 software. Data was normalized to the tissue dry weight.

6.2.4 Polarised Light Microscopy

Osteochondral cores were fixed in 4% paraformaldehyde overnight at 4°C. Tissues were decalcified in 5% formic acid, 95% DI H_2O and secured on a gyro rocker at 40revs/min for approximately 30 days. Samples were checked regularly and returned to fresh solution if not deemed completely decalcified. Once each sample was deemed fully decalcified they were sliced in half along the vertical axis, dehydrated, wax embedded and sectioned at 8µm. In order to visualise the orientation of the collagen fibril architecture picrosirius red stained sections were imaged using a polarised light microscope (Nikon Eclipse E400 POL). In an effort to enhance visualisation of the collagen architecture all sulphated glycosaminoglycans were removed from the tissue sections by bovine testicular hyaluronidase (Sigma) for 18h. The enzyme was prepared in 0.1 M phosphate buffer, pH 6.9, containing hyaluronidase 1000 U ml^{-1} at 37°C (Király et al., 1997).

6.2.5 Helium Ion Microscopy

The collagen network was imaged using a HIM (Orion® Plus, Carl Zeiss NTS) with an Everhart-Thornley detector producing an image from the secondary electrons generated by the incident helium ions. In order to provide an unobstructed view of the collagen fibrils, serial enzymatic digestion was used to remove glycosaminoglycan from the

cartilage specimens. This protocol is based on a modified version of (Vanden Berg-Foels et al., 2012) and is described in detail in chapter 3 of this thesis. HIM images were acquired in secondary electron mode with an acceleration voltage of 34.9kV, a beam current of 0.2-0.5 pA and a dwell time of 0.5-2.0 µs. High resolution images were acquired in the superficial zone of the articular cartilage (classified as the top 100 µm of tissue from the articular surface), in the middle zone (taken between 100-250 µm from the articular surface) and in the deep zone (taken below 500 µm from the articular surface) across age groups in order to visualise the changing morphology of individual network fibrils and fibril connections in this region and during maturation. In the 4 week old and 8 week old immature tissue samples an extra region was imaged due to the increased thickness of the immature samples; this region was labelled the lower deep zone and taken as approximately 1mm from the articular surface. All images were acquired using a pixel resolution of 2048x2048 or 1024x1024. The pixel spacing for a 1µm field of view corresponds to a pixel dimension spacing of 0.49-0.98 nm px-1. The brightness and contrast of all images were optimised; no other post processing procedures were performed. Fibril diameters were measured using ImageJ (Schneider et al., 2012).

6.2.6 Statistical Analysis

Statistical analysis was performed using a general linear model for analysis of variance with Tukey's *post-hoc* test for multiple comparisons used to compare regional/zonal differences and age affects. All tests were performed using the statistical software package MINITAB 15.1 (Minitab Ltd., Coventry, UK). Graphical results are displayed as mean with standard error, whilst numerical results are displayed as mean ± SD. Significance was accepted at $p \leq 0.05$ or as indicated. Sample numbers varied according to respective comparison and are outlined in the results section of this manuscript.

6.3 Results

6.3.1 Dramatic changes to the depth dependent mechanical properties of articular cartilage are observed during skeletal development

The average local strain (ε_{yy}) in the STZ, MZ and DZ of porcine articular cartilage (from 4 week old, 8 week old, one year old and three year old donors) was determined using DIC for increasing magnitudes of global applied strain (2.5%, 5%, 10% and 15%). Similar local strains were measured in the 4 week old and 8 week old tissues (Figure 6.2). There was a strong trend towards lower strains in the deeper regions of the one year old and three year old tissues compared to the STZ for lower levels of global applied strain, whilst at higher global applied strains similar levels of strain were observed in all regions and age groups. No significant changes in the local Young's moduli (E_{yy}) were observed with depth from the articular surface in 4 week old and 8 week old immature articular cartilage (Figure 6.3 and Table 6.1), irrespective of the applied global strain. In contrast, the DZ was found to be significantly stiffer that the STZ in one year old cartilage for all applied strains. In addition, significant differences were observed between the depth dependent mechanical properties of the immature (4 weeks old) and skeletally mature (1 and 3 year old) tissue, with dramatic increases observed in the Young's modulus of articular cartilage during postnatal development. For example, at low global offset strains (2.5% applied strain), the DZ of the one year old (6.01 ± 2.7 MPa) and three year old (9.4 ± 9.1 MPa) tissue were significantly stiffer than corresponding region in the 4 week old (0.97 ± 0.89 MPa) tissue (P=0.0315 and P=0.0052 respectively). At high global offset strains (15% global applied strain), all regions of the three year old tissue (STZ, MZ and DZ: 1.1 ± 0.66 MPa, 0.97± 0.33 MPa and 1.92 ± 1.28 MPa) were significantly stiffer than the immature 4 week old (STZ, MZ and DZ: 0.33 ± 0.1 MPa, 0.27 ± 0.08 MPa and 0.28 ± 0.19 MPa) tissue (P=0.0133, P=0.0019 and P<0.0001 respectively). Similarly, the DZ of the one year old tissue (6.01 ± 2.7, 7 ± 4.85, 5.68 ± 2.98, 4.1 ± 1.26 MPa for 2.5%, 5%,

10% and 15% strain respectively) was significantly stiffer than DZ of the 4 week old tissue (0.97 ± 0.89, 0.71 ± 0.66, 0.17 ± 0.08, 0.28 ± 0.19 MPa for 2.5%, 5%, 10% and 15% strain respectively) tissue (P=0.0315, P=0.0084, P<0.0001 and P<0.0001) for all applied strains.

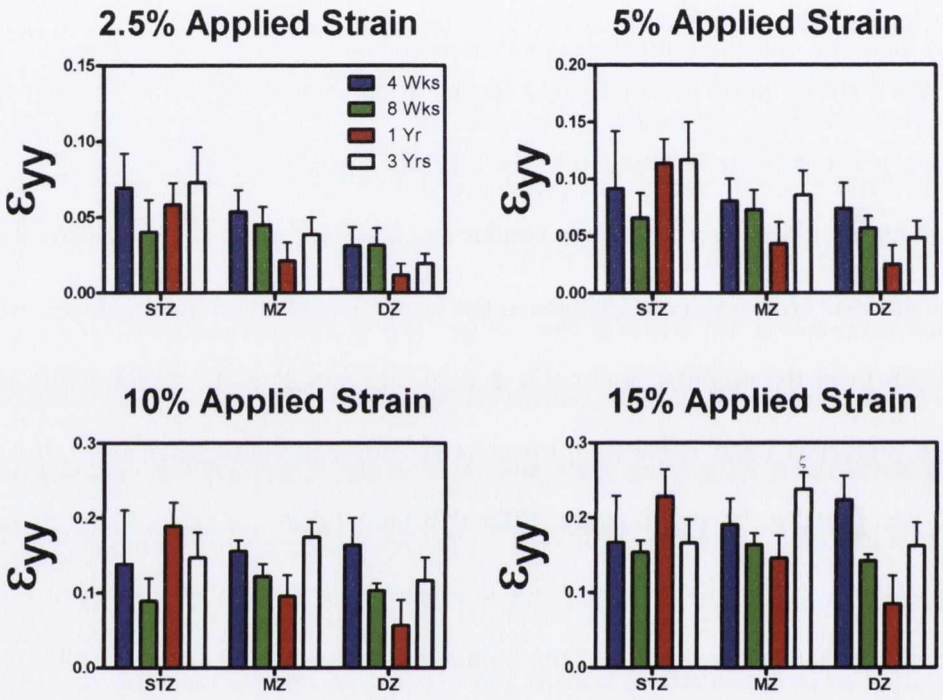

Figure 6.2. Compressive strain ε_{yy} in the zonal direction plotted versus depth from the articular surface divided into three distinct zones-the superficial tangential zone (STZ), the middle zone (MZ) and the deep zone (DZ). The results displayed are of different stages of postnatal development: 4 weeks old, 8 weeks old, one year old and three years old. In addition the graphs are displayed at increasing global offset strains: 2.5%, 5%, 10% and 15%. This analysis only considers the top 40% of the entire thickness of the tissue. Bars show mean with SEM, statistical significance is taken at $p \leq 0.05$. ς indicates significant difference vs. 1Y DZ.

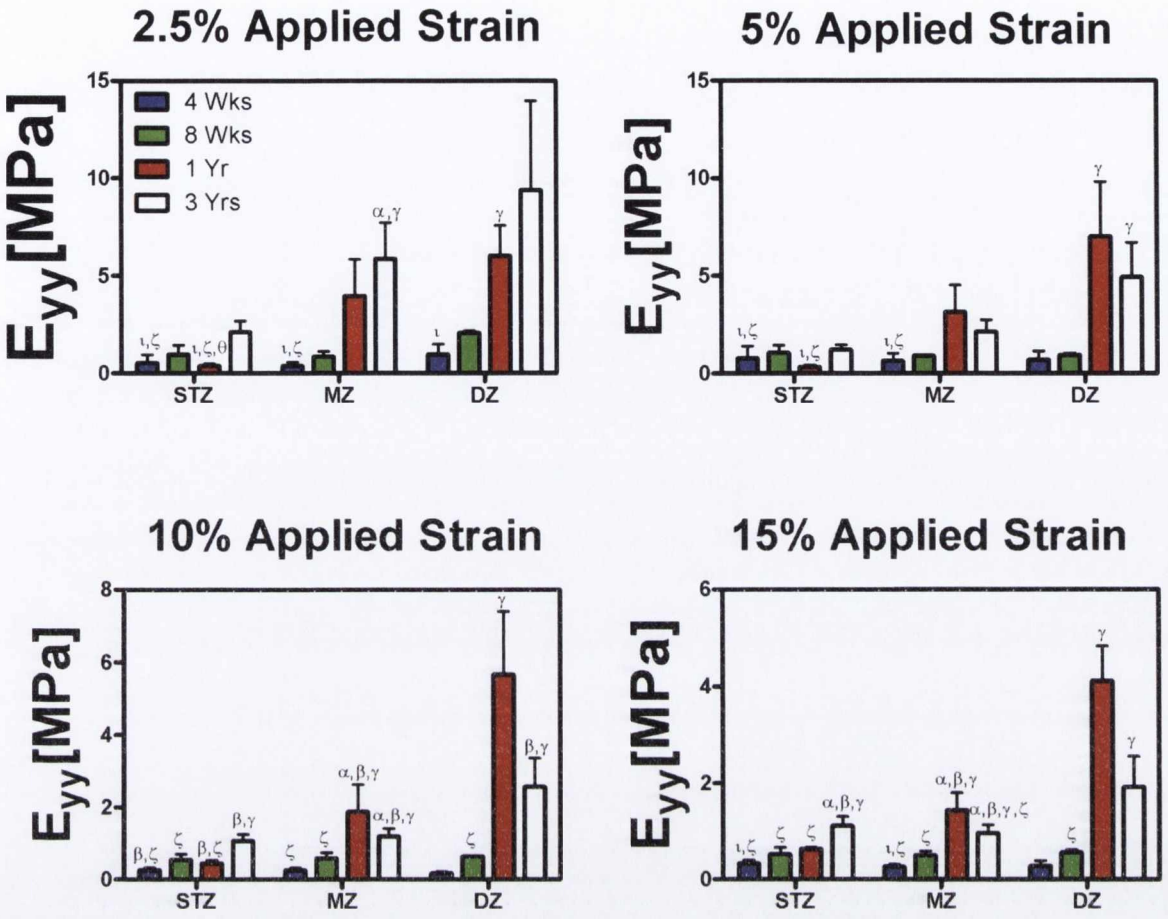

Figure 6.3. Incremental Young's Modulus E_{yy} (MPa) in the zonal direction plotted versus depth from the articular surface divided into three distinct zones-the superficial tangential zone (STZ), the middle zone (MZ) and the deep zone (DZ). The results displayed are of different stages of postnatal development: 4 weeks old, 8 weeks old, one year old and three years old. In addition the graphs are displayed at increasing global offset strains: 2.5%, 5%, 10% and 15%. Bars show mean with SEM, statistical significance is taken at $p \leq 0.05$. Statistical differences are indicated as follows: α vs. 4 Wks STZ, β vs. 4 Wks MZ, γ vs. 4 Wks DZ, ς vs. 1Y DZ, θ vs. 3Y MZ, ι vs. 3Y DZ.

Applied Strain	Age	Zone		
		STZ	MZ	DZ
		E_{yy}(MPa)	E_{yy}(MPa)	E_{yy}(MPa)
2.5%	4 Weeks	0.5272 ± 0.49	0.3716 ± 0.34	0.9730 ± 0.89
	8 Weeks	0.9695 ± 0.50	0.8412 ± 0.27	2.0543 ± 0.13
	1 Year	0.3715 ± 0.20	3.9629 ± 3.26	6.0144 ± 2.70
	3 Years	2.1046 ± 1.30	5.8725 ± 4.13	9.3994 ± 9.11
5%	4 Weeks	0.7748 ± 0.72	0.6398 ± 0.59	0.7096 ± 0.66
	8 Weeks	1.0501 ± 0.56	0.9013 ± 0.08	0.9393 ± 0.12
	1 Year	0.3306 ± 0.17	3.1485 ± 1.94	7.0049 ± 4.85
	3 Years	1.2168 ± 0.57	2.1407 ± 1.35	4.9329 ± 3.94
10%	4 Weeks	0.2629 ± 0.08	0.2588 ± 0.10	0.1690 ± 0.08
	8 Weeks	0.5405 ± 0.16	0.5817 ± 0.23	0.6355 ± 0.04
	1 Year	0.4426 ± 0.15	1.8816 ± 1.31	5.6793 ± 2.98
	3 Years	1.0623 ± 0.38	1.1816 ± 0.49	2.5726 ± 1.77
15%	4 Weeks	0.3280 ± 0.10	0.2673 ± 0.08	0.2804 ± 0.19
	8 Weeks	0.5188 ± 0.14	0.5031 ± 0.13	0.5625 ± 0.08
	1 Year	0.6254 ± 0.06	1.4339 ± 0.63	4.1117 ± 1.26
	3 Years	1.1064 ± 0.66	0.9670 ± 0.33	1.9193 ± 1.28

Table 6.1. Young's moduli E_{yy} (MPa) values of all respective zones: STZ, MZ and DZ of articular cartilage for all age groups; 4 weeks, 8 weeks, 1 year and 3 years for selected applied strain levels; 2.5%, 5%, 10% and 15% strain. Data shows mean ± SD.

A noticeable reduction in Young's moduli (E_{yy}) of the DZ was observed with increasing level of applied strain (termed strain softening), particularly for skeletally mature tissue. For example, the DZ of the three year old articular cartilage (E_{yy}) was observed to decrease from approximately 10 MPa (at 2.5% applied stain) to 2 MPa (at 15% applied strain). A certain amount of strain softening was also observed in the immature tissue. No significant differences in Poisson's ratio (calculated as the traverse strain (ε_{xx}) divided by the axial strain (ε_{yy}) when loaded in the axial direction) with location (zone) was observed for immature tissue (Figure 6.4). In contrast, at low offset strains the Poisson's ratio of STZ of the one and three year old tissues (0.026 ± 0.014, 0.021 ± 0.014) were significantly smaller than their respective deep (0.25 ± 0.128, 0.27 ± 0.254) zones ($P=0.047$ and $P=0.0034$). Whilst at high strains (15% global applied strain), the Poisson's ratio of STZ of the one year old tissue (0.014 ± 0.007) was significantly smaller than in the DZ (0.15 ± 0.07) of the one year old tissue ($P=0.017$).

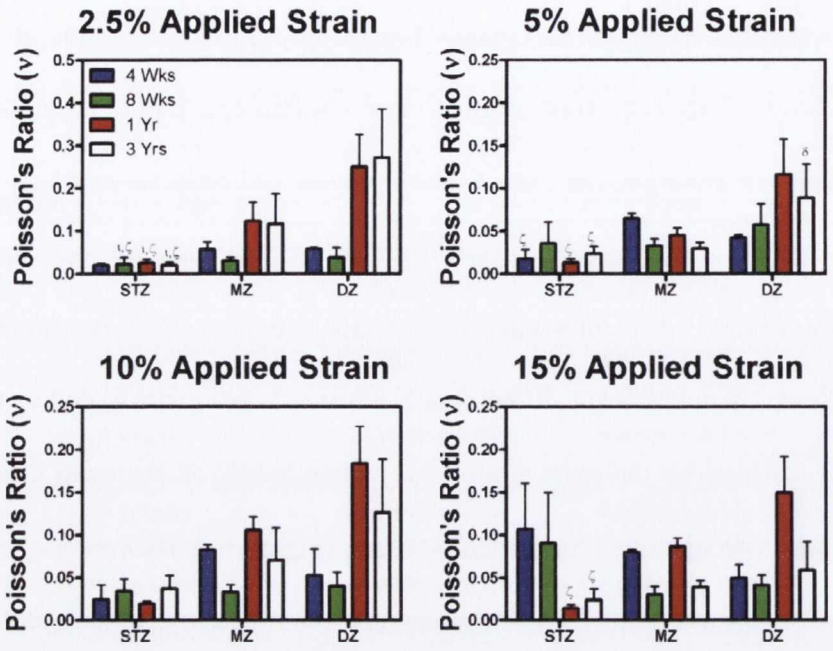

Figure 6.4. Poisson's ratio ν in the zonal direction plotted versus depth from the articular surface divided into three distinct zones-the superficial tangential zone (STZ), the middle zone (MZ) and the deep zone (DZ). In addition the graphs are displayed at increasing global offset strains: 2.5%, 5%, 10% and 15%. Bars show mean with SEM, statistical significance is taken at $p \leq 0.05$. Statistically significant differences are indicated as follows: δ vs. 1Y STZ, ς vs.1Y DZ, θ vs.3Y MZ, ι vs. 3Y DZ.

6.3.2 Increases in tissue compressive properties with age are accompanied by a reduction in the sGAG content and an increase in collagen content

As has been documented previously (Rieppo et al., 2009), the thickness of articular cartilage decreased with age. The mean heights of the tissue with associated standard deviations were 4.4895 ± 0.85484 mm for the 4 week old tissue, reducing significantly ($P<0.0001$) to 2.9863 ± 0.3245 mm in 8 week old immature cartilage tissue. In the one year old tissue, representing the onset of skeletal maturity the cartilage thickness further significantly ($P<0.0001$) decreases to 1.0578±0.1908 mm and in the three year old fully mature tissue the cartilage thickness decreases to 0.8747±0.0613 mm with no significant difference between the mature time points.

It was next determined if the observed increases in tissue mechanical properties with age correlated with changes in the sGAG and collagen content and collagen crosslinking. Biochemical analysis revealed a significant decrease ($P<0.0001$) in sGAG

content with age when normalised to percentage dry weight (Figure 6.5). The one year and three year old mature tissue contained significantly less sGAG than the four week old (P=0.0016 and P=0.0001 respectively) and 8 week old (P=0.0009 and P<0.0001) immature tissue respectively. Overall collagen content significantly increased with age (P<0.0001). The mature three year old tissue contained significantly higher amounts of collagen compared to the 4 (P=0.0016) and 8 week old tissue (P<0.0001) (Figure 6.5). Collagen cross-link analysis revealed a statistically significant decrease in immature cross-links with skeletal development (P=0.001), specifically the one year and three year old tissue contained significantly lower amounts of immature collagen cross-links than the 4 week (P=0.0018 and P=0.0002) and 8 week (P=0.036 and P=0.004) old immature tissue. In addition, there was a significant increase in the ratio of mature to immature cross-links in the mature three year old tissue compared to the 4 week and 8 week old immature tissue (P=0.0036 and P=0.0087) respectively.

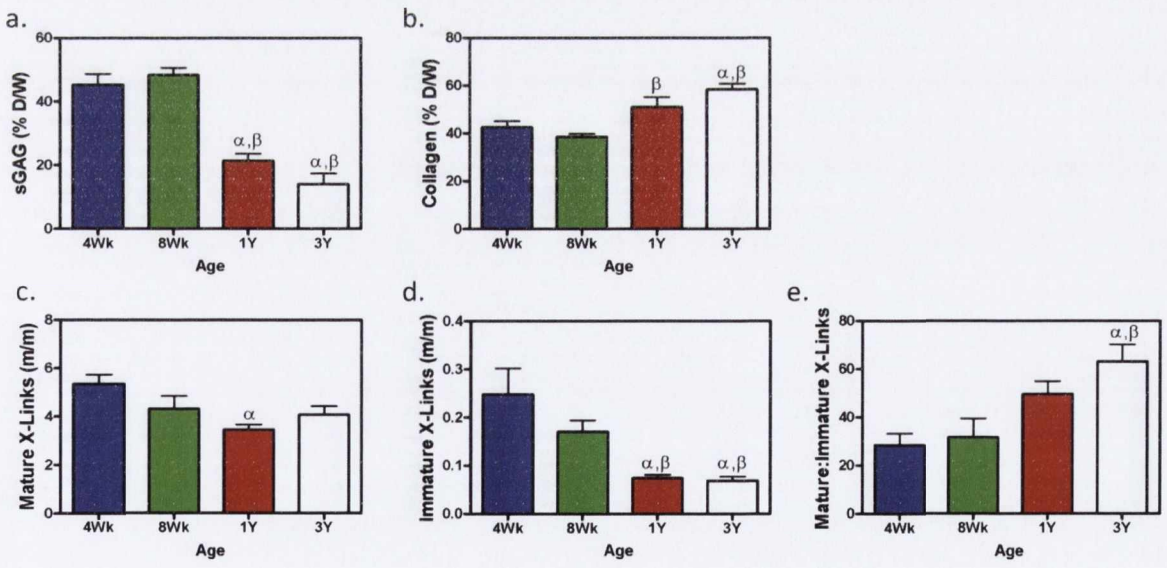

Figure 6.5. (a) Sulphated glycosaminoglycan (sGAG) content expressed per sample dry weight (%), (b) total collagen content expressed per sample dry weight (%), (c) mature collagen cross-links expressed as moles cross-link per mole of collagen (m/m), (d) immature collagen cross-links expressed as moles cross-link per mole of collagen (m/m), (e) the ratio of mature collagen cross-links to immature collagen cross-links. All samples are full thickness articular cartilage cores obtained from developing age groups: 4 weeks old, 8 weeks old, one year old and three years old. Bars show mean with SEM, statistical significance is taken at $p \leq 0.05$. Statistical differences are indicated as follows: α vs. 4 Wks, β vs. 8 Wks.

6.3.3 Increases in the depth dependent mechanical properties of articular cartilage are accompanied by significant changes in the collagen fibril alignment and fibril diameter

Polarised light microscopy (PLM) was first undertaken to help elucidate the time point during skeletal development at which a Benninghoff-like collagen architecture emerges in articular cartilage, see (Figure 6.6). With PLM, large bands of vivid colour known as birefringence indicate extensive degrees of organisation; this can be clearly visualised in the three year old fully mature tissue, which demonstrates clear evidence of such organisation in the superficial tangential zone and in the deep zone of the tissue. In stark contrast very little evidence of organisation can be seen in the immature 4 week old tissue, bar a thin band of highly organised fibrils in the superficial region (Figure 6.6). In the one year old cartilage, where the tissue is beginning to reach skeletal maturity, i.e. closure of the epiphyseal growth plate, the collagen architecture has transitioned from a predominantly isotropic structure observed in the immature cartilage towards an adult phenotype. An extra lamina is also present in the lower part of the deep zone, as evidenced by a region of the tissue displaying a decrease in birefringence (and hence a decrease in the degree of organisation in this region of the tissue). This extra lamina may highlight the process of internal reorganisation of the tissue (Hunziker et al., 2007, Nieminen et al., 2002, Rieppo et al., 2009) from a predominantly isotropic structure in immature articular cartilage to a highly organised Benninghoff architecture present in fully mature tissue.

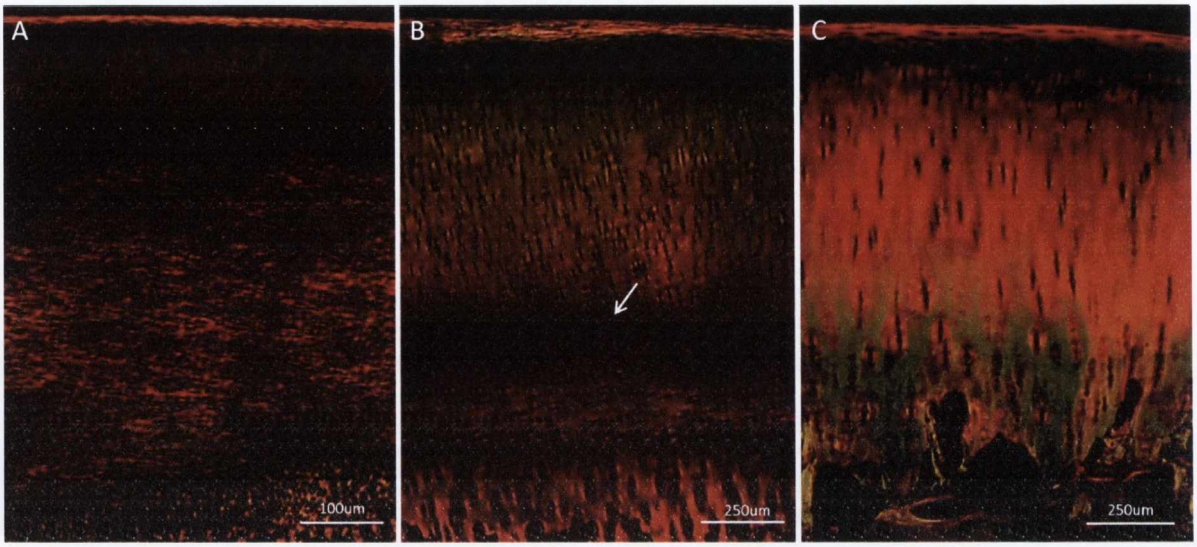

Figure 6.6. Polarised light microscopic images outlining the different stages of development of the collagen architecture; 4 weeks old, one year old and three year old. Arrow indicates an extra lamina or zone within the deep zone of the one year old tissue.

Helium ion microscopy was carried out in order to visualise how the morphology of the collagen network fibrils and fibrillar connections of articular cartilage adapt with age and spatially through the tissue. No clear spatial changes in structural organisation with depth were observed in the immature 4 week old and 8 week old tissue (Figure 6.7). In the superficial tangential zone (100 microns from the articular surface), the collagen fibrils lack any preferential arrangement and are dispersed; it would appear, randomly throughout the region. Similarly, no evidence of collagen fibril alignment can be seen in the middle zone, the upper portion of the deep zone and lower portion of the deep zone at these time points. In addition, fibrils and fibrillar connections are abundant in their numbers throughout the immature tissues. In contrast, in the one year old tissue (Figure 6.8), similar to the polarised light microscopy results, the collagen fibrils appear more structured in their organisation. The collagen fibrils in the superficial tangential zone appear to be arranged into bundles or groups of fibrils. These bundles, in turn, are predominantly aligned parallel to the articular surface. Within these fibril bundles certain

individual collagen fibrils still appear crimped and randomly orientated, particularly in the one year old tissue, which may be due, at least in part, to proteoglycan removal during tissue processing for helium ion microscopy. It is thought that upon sufficient compressive loading these fibrils will be recruited and aligned perpendicular to the direction of loading in their respective fibril bundles. In the middle zone, the collagen fibrils are seen to arcade from the predominantly parallel orientation observed at the articular surface to a perpendicular orientation in the deep zone, thus resulting in a more random organisation. Finally, in the deep zone the collagen fibrils appear predominantly arranged perpendicular to the subchondral bone. In the fully mature three year old articular cartilage (Figure 6.8), the Benninghoff architecture is most apparent. Collagen fibrils are clearly organised parallel to the articular surface in the superficial tangential zone and arcade to a perpendicular arrangement in the deep zone. Fewer fibrils and fibrillar connections can also be seen in both the 1 year old and three year old tissue (Figure 6.9). In addition, an increase in fibril diameter was observed with both age and depth from the surface (Figure 6.9). In the superficial zone average fibril diameter increased significantly from approximately 14 nm in the 4 week old tissue to 76 nm in the three year old tissue ($P<0.0001$). In the middle zone, average fibril diameter increased from approximately 22 nm in the 4 week old tissue to 114 nm in the mature tissue ($P<0.0001$). Finally in the deep zone average fibril diameter increased from approximately 23 nm in the 4 week old tissue to 183 nm in the three year old fully mature tissue ($P<0.0001$). These findings also demonstrate that more dramatic differences in collagen fibril diameter with depth occur in the fully mature tissue.

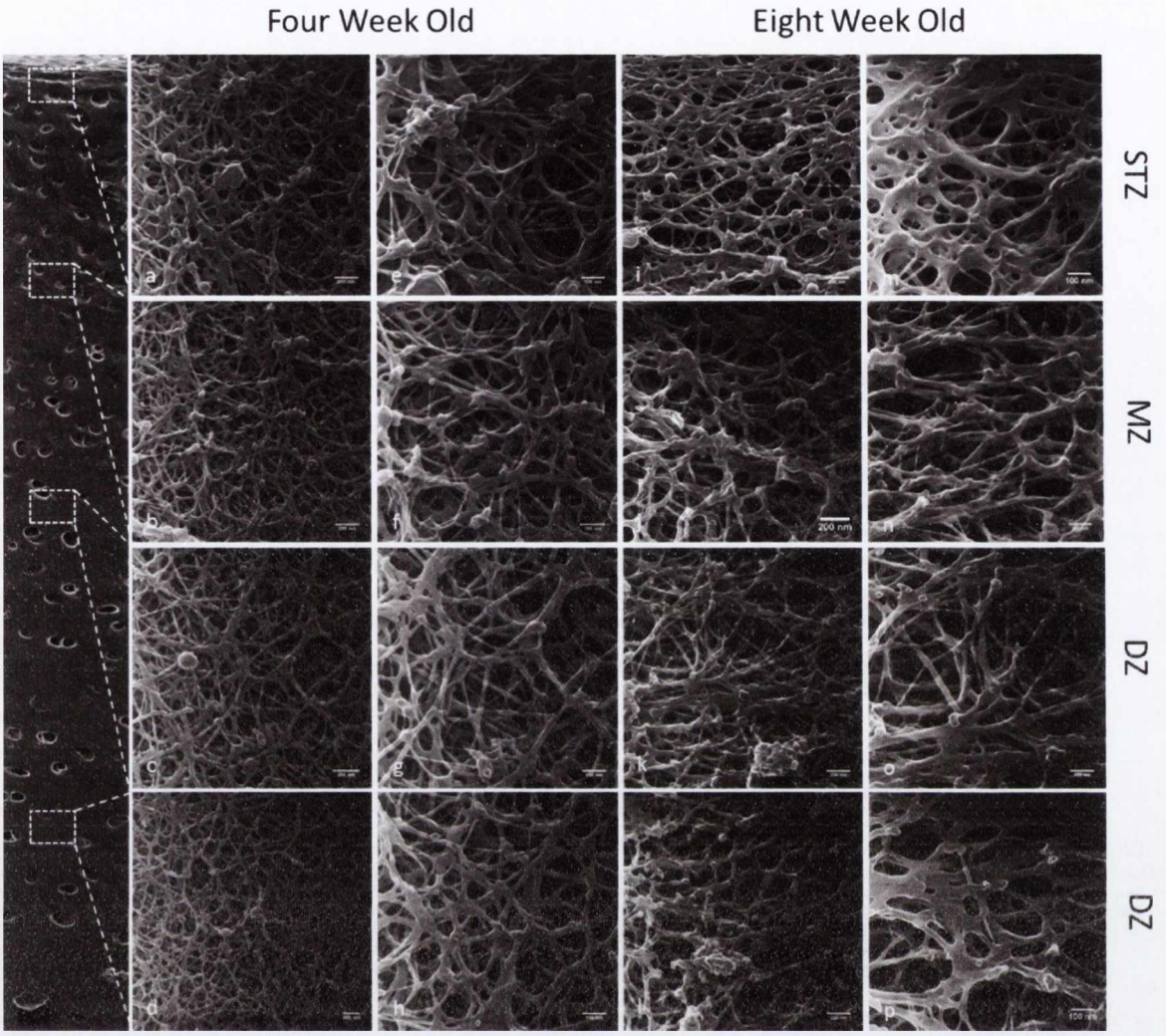

Figure 6.7. Helium ion microscopic images of 4 week old immature collagen architecture (vertically: a-h) and 8 week old immature collagen architecture (vertically: i-p) taken from different zonal depths from the articular surface; the superficial tangential zone (horizontally: a-m), the middle zone (horizontally: b-n), the upper deep zone (horizontally: c-o), and the lower deep zone (horizontally: d-p). Scale bar is 200 nm on images (vertically: a-d, i-l), scale bar is 100 nm on images (vertically: e-h, m-p).

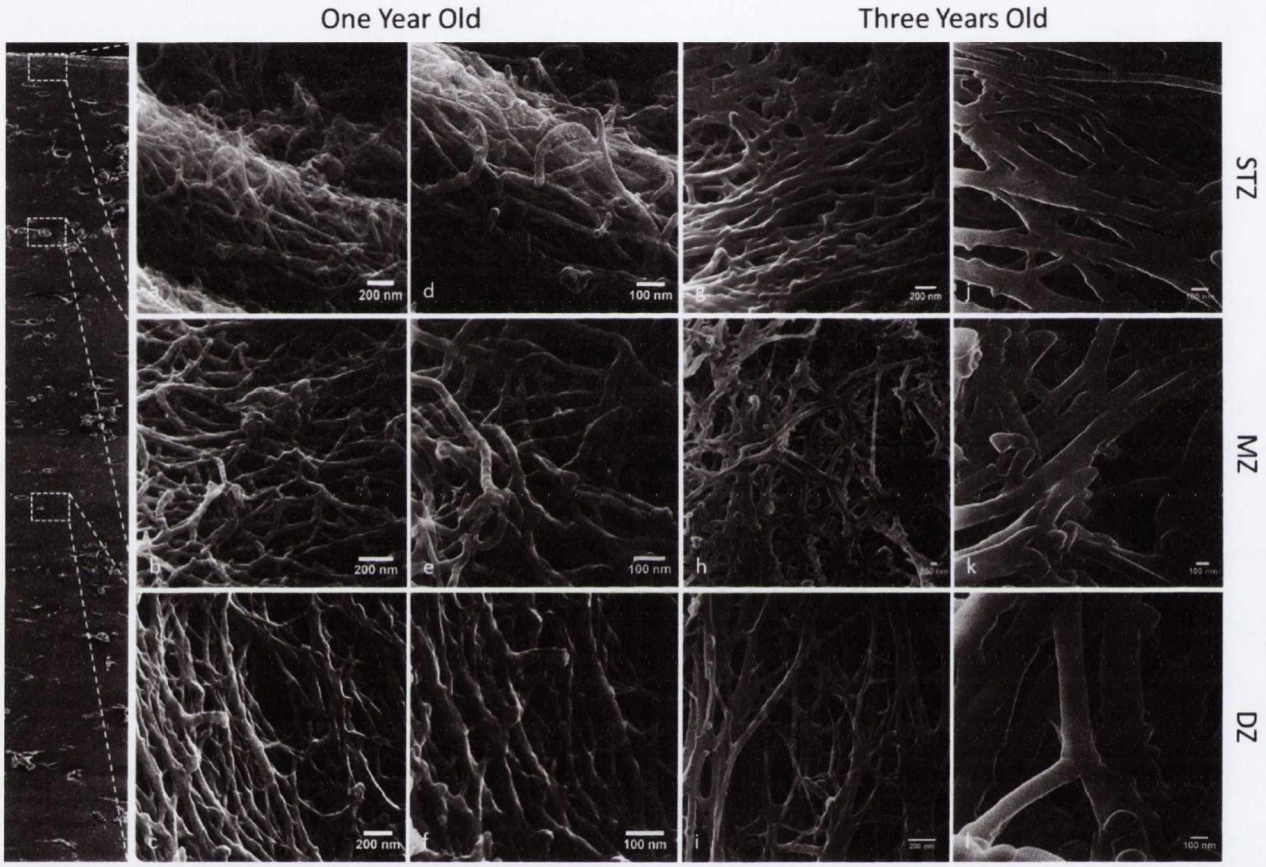

Figure 6.8. Helium ion microscopic images of one year old collagen architecture (vertically: a-f) and three year old mature collagen architecture (vertically: g-l) taken from different zonal depths from the articular surface; the superficial tangential zone (horizontally: a-j), the middle zone (horizontally: b-k), the deep zone (horizontally: c-l). Scale bar is 200 nm on images (vertically: a-c, g-i), scale bar is 100 nm on images (vertically: d-f, j-l).

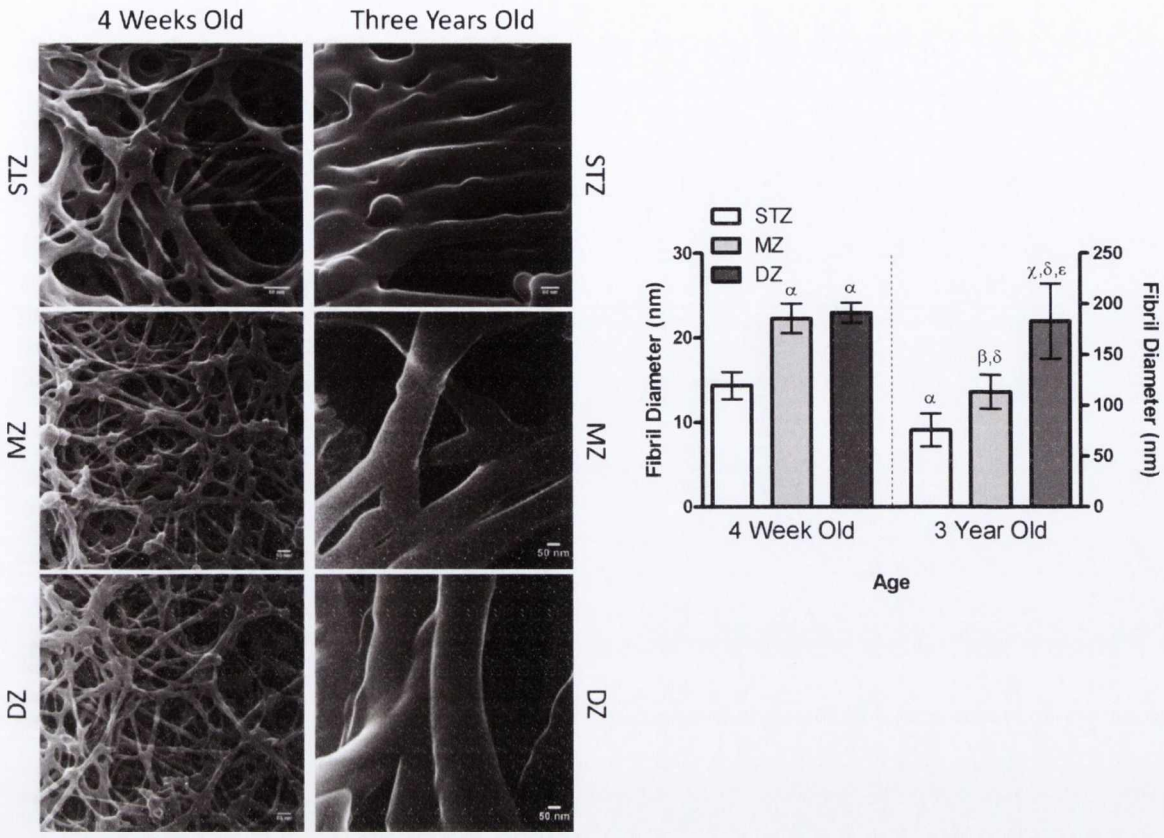

Figure 6.9. Helium ion microscopic images of one month old immature collagen fibrils (A-C) and three year old mature collagen fibrils (D-F) taken from different zonal depths from the articular surface; the superficial tangential zone (A,D), the middle zone (B,E) and the deep zone (C,F). Scale bar is 50 nm. (G) Graph of fibril diameters (nm) across age groups and zones-STZ, MZ and DZ. Bars show mean with SEM, statistical significance is taken at $p \leq 0.05$. Statistical differences are indicated as follows: α vs. 4Wks STZ, β vs.4 Wks MZ, χ vs.4 Wks DZ, δ vs.3Y STZ, ε vs.3Y DZ.

6.3.4 Both collagen network realignment and stiffening with age are predicted to contribute to increases in tissue compressive properties

The above results demonstrate that the alignment of the collagen network of articular cartilage network adapts with skeletal maturation. Furthermore, the inherent stiffness of the collagen network will increase due to increases in the tissue collagen content and increases in the ratio of mature-immature collagen cross-links. In order to investigate the relative impact both of these changes (i.e. collagen 'stiffening' and 'realignment'), in isolation, have on the compressive stiffness of the tissue; a finite strain biphasic material model with a Donnan osmotic swelling pressure was employed. Details on the constitutive model employed for this study can be found in Appendix B; this work was

carried out by Dr. Thomas Nagel. The collagen fibril alignment (either 'isotropic' or 'Benninghoff-like') and collagen fibril stiffness (either 'low' or 'high') were varied while all other material properties in this model were kept constant. Increasing the stiffness of the collagen fibril network, or introducing a Benninghoff-like collagen architecture, was found to have the greatest impact on the model predictions of Young's moduli at low applied strains, see (Figure 6.10). Here increasing the collagen fibril stiffness in isolation was predicted to increase the compressive modulus in the DZ of the tissue by 144% from 2.9 MPa to 7.15 MPa. Introducing a Benninghoff-like architecture whilst maintaining low fibril stiffness was predicted to increase the Young's modulus in the DZ of the tissue by 218% (over the isotropic low fibril stiffness model) to 9.3 MPa at low applied strains. Increasing the collagen fibril stiffness and introducing a Benninghoff-type architecture was predicted to lead to a synergistic increase, with the compressive modulus in the DZ rising by 728% to 24.3 MPa. Dramatic strain softening was predicted in the DZ of the Benninghoff model that incorporated high fibril stiffness, and to a lesser extent in the Benninghoff model that incorporated low fibril stiffness. At high offset strains no dramatic difference in compressive Young's modulus was observed between the four groups. This phenomenon was not observed experimentally. As might be expected, increasing the stiffness of the collagen network in isolation did not lead to a prediction of depth dependent Poisson's ratio. In contrast, an increase in Poisson's ratio with depth was predicted once the Benninghoff collagen architecture was incorporated into the model. Interestingly, this change in architecture predicted a 66% decrease in Poisson's ratio in the STZ of the tissue modelled with a Benninghoff-like architecture and high fibril stiffness compared to a tissue modelled with an isotropic structure and high fibril stiffness at high applied strains; as a result of the parallel fibrils in the STZ of the Benninghoff architecture acting to limit radial expansion (Figure 6.11).

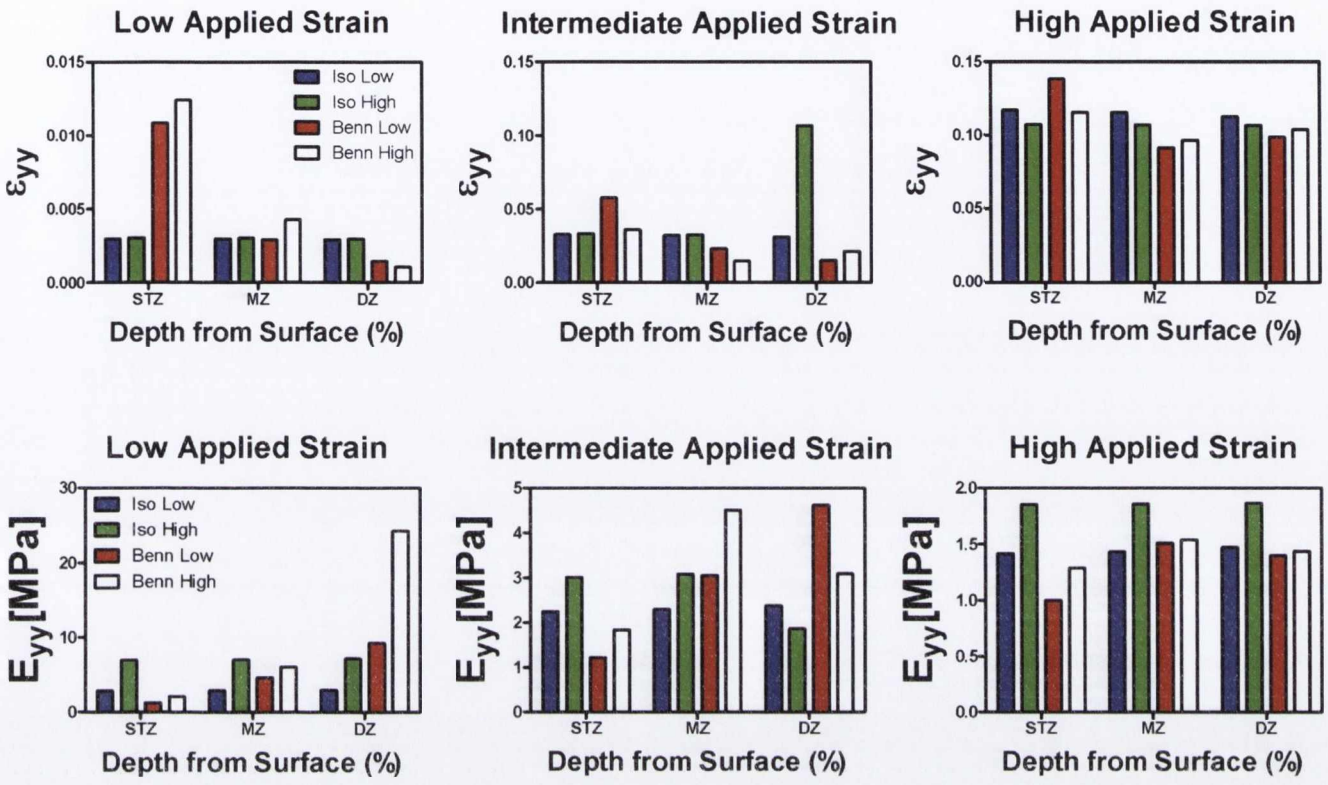

Figure 6.10. Model predications of compressive strain in the zonal direction (ε_{yy}) and incremental Young's modulus E_{yy} (MPa) plotted for specific zones in articular cartilage; STZ, MZ and DZ at increasing levels of applied strain; low, intermediate and high of four different groups: Iso Low, Iso High, Benn Low and Benn High.

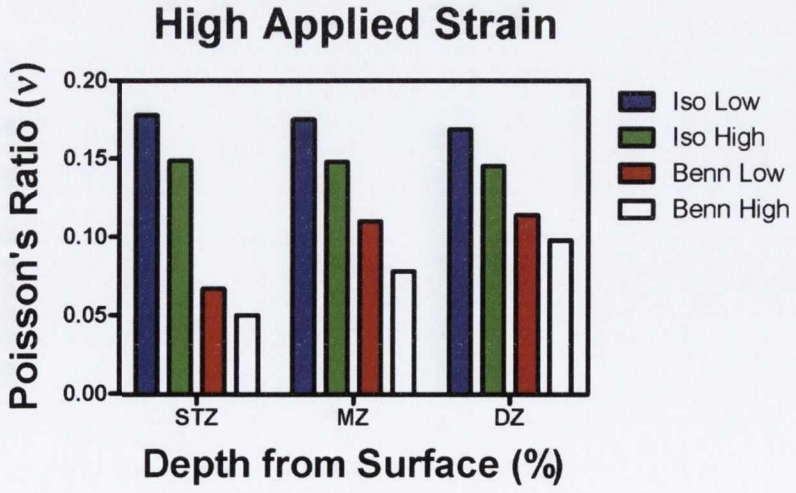

Figure 6.11. Model predications of Poisson's ratio in the zonal direction (ν) plotted for specific zones in articular cartilage; STZ, MZ and DZ at a high level of applied strain four different groups: Iso Low, Iso High, Benn Low and Benn High.

6.4 Discussion

The aim of this study was to investigate how changes to the structure, composition and organisation of articular cartilage from birth to skeletal maturity influence the depth dependent mechanical properties of the tissue. Dramatic increases in Young's modulus with depth from the articular surface were observed in the one year old and three year old mature tissue, whilst less significant changes in Young's modulus with depth were observed in the 4 week and 8 week old tissue. This increase in stiffness with depth is traditionally associated with an increase in sulphated GAG content, resulting in higher fixed charge densities which generate greater Donnan osmotic fluid pressures (Ateshian, 2009). The most dramatic changes that occurred with age were in the deep zone of articular cartilage, where an order of magnitude increase in the compressive properties of the tissue (for low offset strains) was observed from birth to skeletally maturity. Remarkably, this occurred despite the fact that the sGAG content of articular cartilage was observed to decrease with skeletal maturity. Together these finding would suggest that changes to the composition and organisation of the collagen network of articular cartilage with skeletal development play a dominant role in determining the final compressive mechanical properties of the tissue.

To further explore this possibility, a range of biochemical assays and microscopy tools to probe how the collagen network of articular cartilage adapts from birth to skeletal maturity were utilized. Polarised light microscopy revealed substantial reorganisation of the tissue had occurred in both the one year and three year old tissue compared to the 4 week old immature tissue which was primarily isotropic in structure. The collagen architecture of the mature tissue attained what is known as a Benninghoff architecture; where the collagen fibrils are orientated parallel to the articular surface in the superficial tangential zone and perpendicular to the subchondral bone in the deep zone of the tissue.

In addition, helium ion microscopy demonstrated a significant increase in collagen fibril diameter and a decrease in the number of fibril connections as the tissue matured. This decrease in fibrillar connections was accompanied by a significant decrease in immature collagen cross-links with age and an increase in the ratio of mature to immature collagen cross-links. In addition, a significant increase in collagen content with age was observed. Taken together, these results strongly suggest that the collagen network of articular cartilage both stiffens and reorganises with age. The dramatic increase in deep zone compressive modulus with age (9.7 fold increase in the DZ from 4 weeks to 3 years at low offset strains) can be related to these changes to the collagen network. Swelling pressures generated by negatively charged proteoglycans put this collagen network into a state of tension in the absence of external loads (Chahine et al., 2004, Khalsa and Eisenberg, 1997). The stiffer pre-stressed collagen fibrils aligned parallel to the direction of loading in mature tissue will provide greater resistance to axial compressive loading compared to the less stiff unaligned fibrils in immature cartilage, which explains the increased Young's moduli in the deep zone of mature tissue compared to the immature tissue.

In order to elucidate the relative contribution of both collagen network reorganisation and stiffening on the compressive properties of the tissue, a finite strain biphasic material model with a Donnan osmotic swelling pressure was employed. In this framework a model with an isotropic, low stiffness collagen network can be considered similar to the immature tissue, whilst the model with a fully developed Benninghoff architecture and high collagen fibril stiffness can be considered similar to the skeletally mature tissue. These model predictions provide further support for the hypothesis that changes to the collagen network, in isolation, can explain the dramatic increases observed in the compressive properties of articular cartilage during postnatal development. In

particular the dramatic increases in DZ compressive modulus that are observed with age are predicted by a model that includes a Benninghoff architecture and a stiff fibril collagen network (~8 fold increase in stiffness at low offset strains compared to a tissue modelled with an isotropic structure and a low fibril stiffness). A noticeable difference between experimental and model predications was that the model did not predict any differences in the compressive modulus of the tissue in the DZ for tissue for high offset strains. This is not observed experimentally, suggesting certain compositional or organisational changes occurring in articular cartilage with age are not captured by the model and that the simple Neo-Hookean model used for the ground substance is not predictive of the complex behaviour of the tissue at high strains.

Another noticeable difference in the mechanical behaviour of immature and mature tissue was the greater levels of strain softening observed during compressive loading of mature tissue. While such strain softening has been observed previously in AC (Chahine et al., 2004, Schinagl et al., 1997, Wang et al., 2003), it remains to be elucidated if the emergence of such strain softening properties with age are of functional importance to the tissue. These higher levels of strain softening can also be attributed to the vertical arrangement of the collagen fibrils in the deep zone of the mature tissue. Due to pre-existing stresses in the collagen network these fibrils are initially in a tensile state, contributing to tissue compressive properties, however with increasing applied strains these vertical fibrils buckle and will no longer contribute to the load bearing capabilities of the tissue to the same degree. Differences were also observed in the strain-softening behaviour of the one year old and three year old tissue, with the latter undergoing more dramatic softening, which again can be attributed to the younger tissue being less organised and less stiff. Indeed, less dramatic strain softening was also predicted in the finite element model that incorporated a Benninghoff-architecture with low fibril stiffness

compared to the Benninghoff-like model with high fibril stiffness. With higher fibril stiffness, less tensile strains but high stresses will be generated within the collagen network in the free swelling state, meaning that more dramatic strain softening will occur as the tissue is initially compressed under strain control. The fact that such a phenomenon is more pronounced in the three year old tissue compared to the one year old tissue would further suggest that the collagen network of the former is stiffer than the latter.

An additional change associated with postnatal development and maturation of articular cartilage is the significant reduction in thickness of the cartilage tissue ($P<0.0001$) with age. This natural decrease in articular cartilage thickness in conjunction with the reorganisation of the collagen architecture is associated with resorption and neo-formation of the tissue during postnatal development and maturation of all zones except the most superficial one (Hunziker et al., 2007). It is believed that the structural maturation of articular cartilage corresponds to a temporal trend of neo-formation coinciding with cessation of growth activity i.e. closure of the epiphyseal growth plate. This hypothesis can be supported by the dramatic change in organisation and alignment of the collagen architecture between the 4 and 8 week old immature articular cartilage and the one year old tissue which represents the onset of skeletal maturity. In the one year old tissue an extra lamina or zone is visible in the upper portion of the deep zone (Figure 6.6). The lack of birefringence in this zone is indicative of an isotropic layer, one possibly formed through a process of resorption and neo-formation. It is likely that this region gets resorbed as the tissue reaches full skeletal maturity. In addition, even in the immature 4 week old tissue a thin yet highly organised superficial zone is clearly visible. It has been hypothesised (Hunziker et al., 2007) that this region acts to supply the actively dividing, transit amplifying daughter-cell pool that feeds the transitional and upper radial zones during postnatal growth phase of the articular cartilage layer.

Due to articular cartilage's poor capacity to self-repair once damaged, tissue engineering approaches have been pushed to the forefront of new cartilage repair techniques (Kim et al., 2003). Strategies aimed to structurally organise zone-specific cells and encourage heterotypic cell interactions in an effort to improve the functional properties of engineered cartilage are the current focus (Accardi et al., 2013, Klein et al., 2003, Ng et al., 2009, Ng et al., 2005, Sharma et al., 2007, Thorpe et al., 2013). By utilising chondrocytes from different zones and varying the biomaterials in which these cells are encapsulated, biomimetic tissue engineered constructs are aiming to recapitulate the depth-dependent cellular and compressive mechanical inhomogeneity similar to that of native articular cartilage tissue – a feat that has posed a greater challenge than originally appreciated (Ng et al., 2009). Despite expansive efforts to replicate the inhomogeneity of mature articular cartilage, these constructs contain only qualitatively similar zonal biochemical gradients to that of native immature articular cartilage (Klein et al., 2003, Ng et al., 2005, Sharma et al., 2007). In addition, their lack of a developed mature Benninghoff architecture means they possess compressive properties an order of magnitude lower than native articular cartilage tissue. The development of a mechanically competent tissue prior to *in vivo* implantation is clinically relevant, as a soft construct may not be able to preserve the prescribed cell stratification and prevent host cell infiltration (Nagel and Kelly, 2013, Ng et al., 2005). Whilst new techniques such as electro-spinning have recently been developed and employed in order to fabricate fibrous scaffolds upon which cells are seeded (Accardi et al., 2013) the functional mechanical properties of tissue engineering constructs are still lagging behind when compared to native articular cartilage compressive, friction and wear properties; key factors in dictating the evolution of articular surface integrity. The novel findings presented in this study highlight the importance of temporal changes to the collagen network of articular

cartilage for determining its ability to bear compressive loads. Articular cartilage regenerative approaches should focus on engineering its anisotropic collagen architecture and fibril strength in order to recapitulate the mechanical integrity observed in native mature articular cartilage. This study is the first complete quantitative analysis of its kind, and to the best of my knowledge, is the first to describe the dramatic impact that the temporal evolution of the collagen network has on the compressive mechanical properties of articular cartilage during postnatal development and maturation.

Chapter 7 Discussion

"Evolution in mammals has developed extraordinarily efficient musculoskeletal systems for generating and controlling motion...engineers would benefit from an appreciation of nature's design of the extraordinarily efficient and long-lasting animal bearings; conversely, biomedical researchers on arthritis can learn much from engineers with detailed knowledge of the deformational behaviour of nature's bearing materials" (Mow et al., 1992).

As stated in chapter 1, the primary objective of this thesis was to improve our understanding of the evolving nature of articular cartilage mechanics by elucidating the changes to structure and composition of the tissue during postnatal development and maturation and to relate these changes to the depth dependent compressive mechanical properties of the tissue. It was first demonstrated that removal of the superficial region of articular cartilage detrimentally impacts the dynamic compressive properties of the tissue. It is my contention that this occurs because the superficial region of the tissue facilitates the generation of high fluid load support owed to its high collagen fibril density, architectural organisation and low permeability (chapter 4). This was at least partially confirmed by Helium-Ion microscopy of the superficial region in chapter 5 of this thesis. A functional superficial region is not present in skeletally immature articular cartilage, and hence removal of this zone of the tissue only negatively impacts the dynamic modulus of tissue that has attained a skeletally mature architecture (chapter 5). While surface-to-surface measurements provide information on the bulk properties of a tissue, they furnish only indirect insights to the internal behaviour of the tissue and its spatial heterogeneity. Therefore chapter 6 of the thesis used digital image correlation to characterise the depth dependent mechanical properties of the tissue. Here the temporal

evolution of the collagen network was found to have a dramatic impact on the compressive mechanical properties of articular cartilage during postnatal development and maturation. Up to an order of magnitude increase in the compressive properties of the deep zone of articular cartilage was observed from birth to skeletally maturity. Remarkably, this occurred despite the fact that the sGAG content of articular cartilage was observed to decrease with age. Together these finding suggest that changes to the composition and organization of the collagen network of articular cartilage with skeletal development play a dominant role in determining the final compressive mechanical properties of the tissue (chapter 6).

Throughout this thesis many factors relating to the change in compressive modulus of articular cartilage with age have been investigated. In chapter 5, the bulk equilibrium properties and the bulk dynamic modulus of the three year old full thickness tissue were significantly higher than the 4 week old immature tissue in unconfined compression (at 10% applied strain) (Fig. 5.7-5.8). Similarly in chapter 6, all corresponding regions of the three year old tissue were significantly stiffer than the immature 4 week old tissue (at 15% global applied strain). This increase in compressive modulus with age correlated with a decrease in sGAG content (% dry weight) and an increase in collagen content (% dry weight). An increase in compressive stiffness is traditionally solely associated with an increase in sulphated GAG content, resulting in higher fixed charge densities which generate greater Donnan osmotic fluid pressures (Ateshian, 2009). However, more recently, compressive stiffness has also been correlated with an increase in collagen content (Julkunen et al., 2009, Klein et al., 2003, Römgens et al., 2013, Sah et al., 1996, Williamson et al., 2001). It should also be noted that aggrecan, due to its size, is excluded from within the intra-fibrillar space of collagen and is therefore only present in the extra-fibrillar space; the effective fixed charge density (FCD) is thus

higher than that calculated on a total volume basis. Therefore the increase in the content of collagen or molecules associated with the collagen network with skeletal developmental would be predicted to cause a relative increase in the intrafibrillar volume, thereby reducing the extrafibrillar space in which the GAGs reside. Thus the effective FCD, which governs compressive properties, can be increased by changes in the collagen network (Williamson et al., 2001). In addition, the overall increase in fibril diameter, elucidated by helium ion microscopy, within cartilage during development would be expected to provide an increased resistance to fluid flow, which will contribute to increases in the dynamic properties with age. Similarly the observed increase in the ratio of mature to immature collagen cross-links associated with strengthening of the collagen matrix will provide greater compressive and tensile strength to the extracellular matrix.

Previous studies have investigated the bulk compressive modulus of articular during development. The measured mechanical and biochemical properties are reasonably consistent with the data presented in this manuscript, considering the differences in species, developmental ages, testing modalities and location. Williamson et al (2001) characterised the confined compressive modulus of a 1 mm thick layer of femoral articular cartilage from different developmental stages; third trimester bovine foetuses, 1 to 3 week old bovine calf and young adult bovine knees. The mechanical properties were further correlated with tissue components. Their results indicated that the development-associated changes in biomechanical properties (specifically an increase in compressive modulus) were primarily associated with a 2-3 fold increase in collagen content (mg/ml), with no detectible change in GAG (mg/ml) content. The compressive modulus increased from fetus (0.11 ± 0.03 MPa) to calf (0.27 ± 0.02 MPa) to adult (0.31 ± 0.03 MPa) (Williamson et al., 2001). Julkunen et al (2009) investigated the biochemical, biomechanical and structural changes to the articular cartilage of New Zealand white

rabbits from seven age groups; 0 days, 11 days, 4 weeks, 6 weeks, 3 months, 6 months and 18 months. Using creep indentation testing, they demonstrated that the instantaneous modulus increased with age prior to a peak at 4-6 weeks (0-6w: ~5 - 25 MPa, 6w – 18 months; ~25 - 5 MPa). A lower equilibrium modulus was observed before 3-month-age after which the equilibrium modulus continued to increase (0-6w: ~0.5 - 1.5 MPa, 6w – 18 months; 1.5 – 2.5 MPa). Collagen content and cross-linking were positively related to the equilibrium compressive properties of the tissue (Julkunen et al., 2009). Brama et al (2000) investigated the alterations in equine articular cartilage biochemistry that occur up to age one year (neonatal, 5 month old foals and yearlings). Their results indicated that water content (%), DNA (ng/mg dw) content and GAG content (μg/mg dw) decreased significantly during maturation whilst collagen content (mg/mg dw) and hydroxylsylpyridinoline (HP) crosslinks (mol/mol collagen) significantly increased during maturation (Brama et al., 2000). Brommer et al (2005) endeavoured to verify whether the concept of functional adaptation can be confirmed by direct measurement of biomechanical properties of cartilage. Osteochondral plugs of equine articular cartilage from developing age groups; neonatal, 5 months old, 18 months old and mature horses were subjected to indentation testing. Young's modulus increased with age ranging from (1.35 ± 0.39 MPa) in the fetus to (3.19 ± 1.39 MPa) in the mature horse whilst the dynamic modulus at 1 Hz cyclic loading significantly decreased with age ranging from (7.47 ± 1.68 MPa) in the fetus to (5.02 ± 1.24 MPa) in the 5 month old cartilage (Brommer et al., 2005). This is in contrast to the current study where the dynamic modulus was found to increase from (11.28 ± 3.1 MPa) in the 4 week old tissue to (16.26 ± 2.9 MPa) in the 3 year old tissue. Klein et al (2004) investigated the depth dependent compressive properties of bovine articular cartilage from foetal and new-born bovine articular cartilage in confined compression. The results indicated a 4-5 fold increase in

compressive modulus with depth from the articular surface (28 ± 13kPa, 141 ± 10 kPa) and an increase in aggregate modulus with development; ranging from (89 ± 32 kPa) in foetal cartilage to (197 ± 21 kPa) in new-born tissue. Additionally, cartilage matrix constituents; sGAG (g/ml) and collagen content (g/ml), increased with depth from the articular surface whilst cell density (10^6 /ml) decreased. Their results indicate a positive correlation between the compressive modulus of immature bovine cartilage and GAG and collagen content (Klein et al., 2007). The experimental and descriptive findings of all of these studies derive from a wide variety of animal species and contribute to the differences in reported mechanical properties in addition to testing modality and location. In a study comparing the collagen fibril arrangement in the tibial plateau from a range of different species and their relevance to man, Kääb et al. (1998) demonstrated that the porcine collagen structure was the most similar to that of man (Kääb et al., 1998). This justifies the choice of a porcine animal model for addressing the objective of this thesis. Overall these results implicated changes in the collagen component of articular cartilage as having important functional consequences during normal development and growth.

The results in chapter 6 demonstrate that the alignment of the collagen network of articular cartilage network changes with skeletal maturation and that furthermore, the inherent stiffness of the collagen network will increase due to increases in the tissue collagen content and fibril diameter, as well as increases in the ratio of mature-immature collagen cross-links. A finite strain biphasic material model with a Donnan osmotic swelling pressure was employed in order to investigate the relative impact both of these changes (i.e. collagen 'stiffening' and 'realignment'), in isolation, have on the compressive stiffness of the tissue (Simulations undertaken by Dr. Thomas Nagel). Increasing the collagen fibril stiffness in isolation was predicted to lead to a 2.4 fold increase in the compressive modulus of the DZ of the tissue from 2.9 MPa to 7.15 MPa,

whilst introducing a Benninghoff-like architecture and maintaining low fibril stiffness was predicted to lead to a 3.2 fold increase (over the isotropic low fibril stiffness model) in the Young's modulus of the DZ of the tissue to 9.3 MPa at low applied strains. Increasing the collagen fibril stiffness and introducing a Benninghoff-type architecture was predicted to lead to a dramatic synergistic increase, with the compressive modulus in the DZ rising 8.3 fold to 24.3 MPa, and furthermore led to a 66% decrease in Poisson's ratio in the STZ. These findings illustrate the significant importance of reorganisation of the collagen network during development and skeletal maturity. The biomechanical explanations behind these increases are speculated upon in the subsequent paragraphs.

The imbalance of ions between the interstitial and extra-tissue fluid volumes in articular cartilage gives rise to an osmotic pressure that is balanced by tension in the collagen fibrils (Setton et al., 1993). This swelling pressure, induces a tensile state of stress (and strain) in the absence of external loading, known as pre-stress (and associated swelling strain) in the collagen network (Chahine et al., 2004). When the applied compressive strain is smaller than the swelling strain, the solid matrix remains in a state of tension and the slope of the stress-strain response is reflective of the tensile modulus of the collagen network (Ateshian et al., 2009, Chahine et al., 2004). With increasing applied strains, the vertical fibrils in the DZ of the tissue buckle and will no longer contribute to the load bearing capabilities of the tissue to the same degree. This is known as strain softening (Bursac et al., 2000, Chahine et al., 2004) and was observed in chapter 4 and 6 of this thesis. Whilst they do not contribute to the compressive properties of the tissue to the same degree as in their pre-stressed or tensile state, the buckled deep zone collagen fibrils still appear to contribute to the compressive resistance of the tissue and further continue to modulate the FCD of the tissue. Furthermore, beyond ~ 20% strain, it has been demonstrated that cartilage exhibits nonlinear strain-stiffening (Ateshian et al.,

1997, Chahine et al., 2004, Schinagl et al., 1997). It has recently been shown that collagen fibrils significantly contribute to the compressive properties of cartilaginous tissues even at high strain magnitudes and that the effect depends on fibril orientation (Römgens et al., 2013); whereby higher recorded stiffness correlated with higher collagen content and lower GAG and initial water content. Higher osmotic pressure was also considered as a contribution to the non-linear increase in compressive stiffness; at high strains the repelling force between negative charges of the proteoglycans may become more pronounced and contribute to increases in the osmotic pressure. This could be a partial possible explanation for why even at higher offset strains the compressive modulus of the mature three year old tissue is significantly stiffer then the immature 4 week old tissue (chapter 6). Investigating this further would involve observing the variation in stress-strain and modulus-strain responses under various bathing salt concentrations, where a hypotonic salt solution is known to increase the osmotic pressure in articular cartilage whereas a hypertonic solution decreases it (Basser et al., 1998, Chahine et al., 2004, Maroudas, 1979, Canal Guterl et al., 2010, Wang et al., 2002b).

The superficial tangential zone of articular cartilage is essential to the tissue's load-distributing function (Hosseini et al., 2013). While the compressive modulus of this superficial region is lower than the rest of the tissue (Bevill et al., 2010, Glaser and Putz, 2002, Torzilli, 1993, Torzilli et al., 1983), it has been demonstrated that upon removal of this layer the tissue is more susceptible to damage from impact loading (Rolauffs et al., 2010). Furthermore, through indentation testing, it has been shown that removal of the STZ impairs the load-bearing properties of the tissue (Glaser and Putz, 2002), which may be due to fact that the STZ is able to recruit a larger area of deep zone cartilage to carry compressive loads (Hosseini et al., 2013). In chapter 4, it was demonstrated that although this layer is less stiff than the remainder of the tissue in axial compression, it plays a key

role in elevating the dynamic material properties of the tissue. It was speculated this was due to the superficial region facilitating the generation of higher fluid load support during dynamic loading, due to its dense collagen fibril network and organisation. Furthermore, as the parallel collagen fibrils in this region are compressed they further act to decrease the hydraulic permeability of the tissue. In chapter 5, it was demonstrated that the superficial region of articular cartilage develops into a functionally important region of the tissue during postnatal development, and hence removal of this region only led to a reduction in the dynamic modulus of the tissue when it has reached a certain level of skeletal maturity. This is due to the development of a Benninghoff-type architecture in the tissue, highlighting again the importance of a fully developed collagen architecture to the dynamic compressive properties of articular cartilage.

There are potential limitations associated with this thesis. In chapters 4 and 5, slicing the cartilage into layers may have an impact on the functional properties of the tissue by affecting the intrinsic continuity of the tissue and possibly damaging the tissue structure. Although scanning electron microscopy has previously demonstrated that the surface of both cut and intact articular cartilage display similar collagen fibril architecture (Torzilli, 1993), artefacts due to cutting cannot be ruled out and the isolation of specific zones may have compound effects on their functional properties. The porcine tissue tested, in chapter 4, was not skeletally mature and therefore its collagen architecture does not equate that of fully mature samples, although analysis confirmed a tissue organisation that mimics certain aspects of the architecture of adult cartilage. In preliminary studies whereby only the top 10% of the total cartilage thickness was removed (data not shown), no statistically significant decrease in the dynamic modulus was observed, which may be due to the lack of a fully developed Benninghoff architecture. In addition in chapter 5, whilst classifying the superficial region as the top 15% of the tissue is within traditional

definitions, age related changes in the tissue structure could mean that some of the transitional zone may also have been removed. However, for the purpose of investigating what role the presence of the superficial region plays in determining the dynamic properties of the tissue, it's of higher importance that the entire superficial tangential zone be removed.

The biomechanical functionality of articular cartilage is derived from both its biochemical composition and the architecture of the collagen network. Due to articular cartilage's poor capacity to self-repair once damaged, tissue engineering approaches have been pushed to the forefront of new cartilage repair techniques (Kim et al., 2003). In tissue engineering terms, the development of a mechanically competent tissue prior to *in vivo* implantation is clinically relevant, as a soft construct may not be able to support physiological loads (Ng et al., 2009). Consequently articular cartilage regenerative approaches should focus on engineering the anisotropic collagen architecture and fibril strength of mature tissue in order to recapitulate the mechanical integrity observed in native articular cartilage which is vital for its long term ability to bear compressive loads. Therefore it is essential to improve our understanding of the evolving nature of articular cartilage mechanics and tissue function during development and maturation by elucidating the changes to structure and composition of the tissue, as attempted in this thesis.

Chapter 8 Conclusions

8.1 Main results

The overall objective of this thesis was to improve our understanding of the evolving nature of articular cartilage mechanics by elucidating the changes in structure and composition of the tissue during postnatal development and maturation and to relate these changes to the depth dependent compressive mechanical properties of the tissue. The main conclusions of this thesis are as follows:

- The superficial region plays a key role in determining the dynamic properties of the tissue. This is likely due to the fact that it facilitates the generation of higher fluid load support owed to its high collagen fibril density, architectural organisation and low permeability.
- This functional superficial region is not present in skeletally immature articular cartilage, and hence removal of this zone of the tissue only negatively impacts the dynamic modulus of tissue that has attained a skeletally mature architecture.
- An order of magnitude increase in the compressive properties of the deep zone of articular cartilage (for low offset strains) was observed from birth to skeletally maturity. This occurred despite the fact that the sGAG content of articular cartilage was observed to decrease with skeletal maturity.
- The inherent stiffness of the collagen network increased due to increases in the tissue collagen content and increases in the ratio of mature-immature collagen cross-links.

This thesis demonstrates that the Benninghoff-type organisation of the collagen network of skeletally mature articular cartilage and the inherent stiffness of this collagen matrix; due to mature collagen cross-links and increased fibril diameter, play a dominant role in determining the final compressive mechanical properties of articular cartilage.

8.2 Future Directions

This thesis has provided a contribution towards our understanding of the evolving mechanical properties of articular cartilage during postnatal development and maturation and the important role that the collagen network plays in the tissues flow dependent and flow independent compressive properties. However, many questions remain to be answered in this vast and exciting field of cartilage mechanics and age. The following recommendations are made for future work in this area.

- The specific composition of the articular cartilage matrix changes with development; chondroitin-4 sulphate is reported to be the predominant glycosaminoglycan (GAG) in immature cartilage, while chondroitin-6 sulphate is predominant in mature tissue (Torzilli et al., 1998). Whilst it was shown that GAG content decreased during postnatal development and age, further quantification of the type of PG's present in articular cartilage with age may help to elucidate how specific PG's contribute to the mechanical properties of the tissue.
- Immunohistochemical analysis on immature and mature cartilage samples in order to investigate the change in collagen type. Additionally, further biochemical analysis investigating more cross-link types. For example pyrrole analysis as an alternative mature cross-link and glycation products with cross-links.
- A repetition of the study in chapter 6 under various bathing salt concentrations in order to observe the variation in stress-strain and modulus-strain responses during

postnatal development and age under various osmotic pressures. This may help further elucidate why even at higher offset strains the compressive modulus of the mature three year old tissue is significantly stiffer then the immature 4 week old tissue (chapter 6).

- Utilisation of the insights made from this study into the importance of a fully developed Benninghoff-like collagen architecture to the compressive response of articular cartilage to the creation of biomimetic tissue engineered contructs. Ultimately aiming to recapitulate the depth-dependent cellular and compressive mechanical inhomogeneity similar to that of native articular cartilage tissue, this could consist of using state of the art electo-spinning techniques and a combination of chondrocytes from different zonal regions.
- It is known that some small leucine-rich proteoglycans (SLRPs), including decorin and fibromodulin, can interact with and regulate collagen fibrillogenesis (Scott, 1988). Through these interactions, fibril assembly and diameter can be influenced (Mow and Huiskes, 2005, Scott, 1988). Further investigation into SLRPs and their effect on collagen fibril assembly and diamter in order to elucidate if these same effects could be recapituated *in vitro* in tissue engineered constructs.

Bibliography

References

ACCARDI, M. A., MCCULLEN, S. D., CALLANAN, A., CHUNG, S., CANN, P. M., STEVENS, M. M. & DINI, D. 2013. Effects of fiber orientation on the frictional properties and damage of regenerative articular cartilage surfaces. *Tissue Engineering - Part A,* 19**,** 2300-2310.

AKIZUKI, S., MOW, V. C., MULLER, F., PITA, J. C., HOWELL, D. S. & MANICOURT, D. H. 1986. Tensile properties of human knee joint cartilage: I. Influence of ionic conditions, weight bearing, and fibrillation on the tensile modulus. *Journal of Orthopaedic Research,* 4**,** 379-392.

ANDRIACCHI, T. P., KOO, S. & SCANLAN, S. F. 2009. Gait mechanics influence healthy cartilage morphology and osteoarthritis of the knee. *Journal of Bone and Joint Surgery - Series A,* 91**,** 95-101.

ARMSTRONG, C. G. & MOW, V. C. 1982. Variations in the intrinsic mechanical properties of human articular cartilage with age, degeneration, and water content. *Journal of Bone and Joint Surgery - Series A,* 64**,** 88-94.

ATESHIAN, G. A. 2009. The role of interstitial fluid pressurization in articular cartilage lubrication. *Journal of Biomechanics,* 42**,** 1163-1176.

ATESHIAN, G. A., CHAHINE, N. O., BASALO, I. M. & HUNG, C. T. 2004. The correspondence between equilibrium biphasic and triphasic material properties in mixture models of articular cartilage. *Journal of Biomechanics,* 37**,** 391-400.

ATESHIAN, G. A. & HUNG, C. T. 2006. The natural synovial joint: Properties of cartilage. *Proceedings of the Institution of Mechanical Engineers, Part J: Journal of Engineering Tribology,* 220**,** 657-670.

ATESHIAN, G. A. & MOW, V. C. 2005. Friction, Lubrication, and Wear of Articular Cartilage and Diarthroidal Joints. *In:* MOW, V. C. & HUISKES, R. (eds.) *Basic Orthopaedic Biomechanics and Mechano-Biology.* Philadelphia: Lippincott Williams & Wilkins.

ATESHIAN, G. A., RAJAN, V., CHAHINE, N. O., CANAL, C. E. & HUNG, C. T. 2009. Modeling the matrix of articular cartilage using a continuous fiber angular distribution predicts many observed phenomena. *Journal of Biomechanical Engineering,* 131.

ATESHIAN, G. A., WARDEN, W. H., KIM, J. J., GRELSAMER, R. P. & MOW, V. C. 1997. Finite deformation biphasic material properties of bovine articular cartilage from confined compression experiments. *Journal of Biomechanics,* 30**,** 1157-1164.

ATHANASIOU, K. A., ROSENWASSER, M. P., BUCKWALTER, J. A., MALININ, T. I. & MOW, V. C. 1991. Interspecies comparisons of in situ intrinsic mechanical properties of distal femoral cartilage. *Journal of Orthopaedic Research,* 9**,** 330-340.

AVERY, N. C., SIMS, T. J. & BAILEY, A. J. 2009. Quantitative determination of collagen cross-links. *Methods in molecular biology,* 522**,** 103-121.

BANK, R. A., BAYLISS, M. T., LAFEBER, F. P. J. G., MAROUDAS, A. & TEKOPPELE, J. M. 1998. Ageing and zonal variation in post-translational modification of collagen in normal human articular cartilage: The age-related increase in Non-Enzymatic Glycation affects biomechanical properties of cartilage. *Biochemical Journal,* 330**,** 345-351.

BANNISTER, D. W. & BURNS, A. B. 1970. Adaptation of the Bergman and Loxley Technique for Hydroxyproline Determination to the AutoAnalyser and its Use in Determining Plasma Hydroxyproline in the Domestic Fowl. *Analyst,* 95**,** 596-600.

BASSER, P. J., SCHNEIDERMAN, R., BANK, R. A., WACHTEL, E. & MAROUDAS, A. 1998. Mechanical properties of the collagen network in human articular cartilage as measured by osmotic stress technique. *Archives of Biochemistry and Biophysics,* 351**,** 207-219.

BENNINGHOFF, A. 1925. Form und Bau der Gelenkknorpel in ihren Beziehungen zur Funktion - Zweiter Teil: Der Aufbau des Gelenkknorpels in seinen Beziehungen zur Funktion. *Zeitschrift fur Zellforschung und Mikroskopische Anatomie,* 2**,** 783-862.

BERGMAN, I. & LOXLEY, R. 1963. Two improved and simplified methods for the spectrophotometric determination of hydroxyproline. *Analytical Chemistry,* 35, 1961-1965.

BEVILL, S. L., THAMBYAH, A. & BROOM, N. D. 2010. New insights into the role of the superficial tangential zone in influencing the microstructural response of articular cartilage to compression. *Osteoarthritis and Cartilage,* 18, 1310-1318.

BRAMA, P. A. J., TEKOPPELE, J. M., BANK, R. A., BARNEVELD, A. & VAN WEEREN, P. R. 2000. Functional adaptation of equine articular cartilage: The formation of regional biochemical characteristics up to age one year. *Equine Veterinary Journal,* 32, 217-221.

BROMMER, H., BRAMA, P. A. J., LAASANEN, M. S., HELMINEN, H. J., VAN WEEREN, P. R. & JURVELIN, J. S. 2005. Functional adaptation of articular cartilage from birth to maturity under the influence of loading: a biomechanical analysis. *Equine Veterinary Journal,* 37, 148-154.

BROOM, N. D. 1984. Further insights into the structural principles governing the function of articular cartilage. *Journal of Anatomy,* 139, 275-294.

BROOM, N. D. & MARRA, D. L. 1986. Ultrastructural evidence for fibril-to-fibril associations in articular cartilage and their functional implication. *J Anat,* 146, 185-200.

BROOM, N. D. & SILYN-ROBERTS, H. 1990. Collagen-collagen versus collagen-proteoglycan interactions in the determination of cartilage strength. *Arthritis and Rheumatism,* 33, 1512-1517.

BUCKWALTER, J. A., MANKIN, H. J. & GRODZINSKY, A. J. 2005. Articular cartilage and osteoarthritis. *Instructional course lectures,* 54, 465-480.

BURSAC, P., MCGRATH, C. V., EISENBERG, S. R. & STAMENOVIC, D. 2000. A microstructural model of elastostatic properties of articular cartilage in confined compression. *Journal of Biomechanical Engineering,* 122, 347-353.

BURSAC, P. M., OBITZ, T. W., EISENBERG, S. R. & STAMENOVIC, D. 1999. Confined and unconfined stress relaxation of cartilage: Appropriateness of a transversely isotropic analysis. *Journal of Biomechanics,* 32, 1125-1130.

BUSCHMANN, M. D. & GRODZINSKY, A. J. 1995. A molecular model of proteoglycan-associated electrostatic forces in cartilage mechanics. *Journal of Biomechanical Engineering,* 117, 179-192.

BUSCHMANN, M. D., KIM, Y. J., WONG, M., FRANK, E., HUNZIKER, E. B. & GRODZINSKY, A. J. 1999. Stimulation of aggrecan synthesis in cartilage explants by cyclic loading is localized to regions of high interstitial fluid flow. *Archives of Biochemistry and Biophysics,* 366, 1-7.

BUTLER, D. L., GOLDSTEIN, S. A., GULDBERG, R. E., GUO, X. E., KAMM, R., LAURENCIN, C. T., MCINTIRE, L. V., MOW, V. C., NEREM, R. M., SAH, R. L., SOSLOWSKY, L. J., SPILKER, R. L. & TRANQUILLO, R. T. 2009. The Impact of Biomechanics in tissue engineering and Regenerative medicine. *Tissue Engineering - Part B: Reviews,* 15, 477-484.

CANAL, C. E., HUNG, C. T. & ATESHIAN, G. A. 2008. Two-dimensional strain fields on the cross-section of the bovine humeral head under contact loading. *Journal of Biomechanics,* 41, 3145-3151.

CANAL GUTERL, C., HUNG, C. T. & ATESHIAN, G. A. 2010. Electrostatic and non-electrostatic contributions of proteoglycans to the compressive equilibrium modulus of bovine articular cartilage. *Journal of Biomechanics,* 43, 1343-1350.

CHAHINE, N. O., HUNG, C. T. & ATESHIAN, G. A. 2007. In-situ measurements of chondrocyte deformation under transient loading. *European Cells and Materials,* 13, 110-111.

CHAHINE, N. O., WANG, C. C. B., HUNG, C. T. & ATESHIAN, G. A. 2004. Anisotropic strain-dependent material properties of bovine articular cartilage in the transitional range from tension to compression. *Journal of Biomechanics,* 37, 1251-1261.

CHANGOOR, A., TRAN-KHANH, N., MÉTHOT, S., GARON, M., HURTIG, M. B., SHIVE, M. S. & BUSCHMANN, M. D. 2011. A polarized light microscopy method for accurate and reliable grading of collagen organization in cartilage repair. *Osteoarthritis and Cartilage,* 19**,** 126-135.

CHEN, S. S., FALCOVITZ, Y. H., SCHNEIDERMAN, R., MAROUDAS, A. & SAH, R. L. 2001. Depth-dependent compressive properties of normal aged human femoral head articular cartilage: Relationship to fixed charge density. *Osteoarthritis and Cartilage,* 9**,** 561-569.

COHEN, N. P., FOSTER, R. J. & MOW, V. C. 1998. Composition and dynamics of articular cartilage: Structure, function, and maintaining healthy state. *Journal of Orthopaedic and Sports Physical Therapy,* 28**,** 203-215.

COHEN, Z. A., MCCARTHY, D. M., KWAK, S. D., LEGRAND, P., FOGARASI, F., CIACCIO, E. J. & ATESHIAN, G. A. 1999. Knee cartilage topography, thickness, and contact areas from MRI: In- vitro calibration and in-vivo measurements. *Osteoarthritis and Cartilage,* 7**,** 95-109.

DILLMAN, C. J. 1975. Kinematic analyses of running. *Exercise and Sport Sciences Reviews,* 3**,** 193-218.

DONNAN, F. G. 1995. Theory of membrane equilibria and membrane potentials in the presence of non-dialysing electrolytes. A contribution to physical-chemical physiology. *Journal of Membrane Science,* 100**,** 45-55.

ERNE, O. K., REID, J. B., EHMKE, L. W., SOMMERS, M. B., MADEY, S. M. & BOTTLANG, M. 2005. Depth-dependent strain of patellofemoral articular cartilage in unconfined compression. *Journal of Biomechanics,* 38**,** 667-672.

ETHERINGTON, D., J. & SIMS, T., J. 1981. Detection and estimation of collagen. *Journal of the Science of Food and Agriculture,* 32**,** 539-546.

EYRE, D. 2002. Collagen of articular cartilage. *Arthritis Research,* 4**,** 30-35.

EYRE, D. R. 1980. Collagen: Molecular diversity in the body's protein scaffold. *Science,* 207**,** 1315-1322.

EYRE, D. R., WEIS, M. A. & WU, J. J. 2006. Articular cartilage collagen: An irreplaceable framework? *European Cells and Materials,* 12**,** 57-63.

FRANK, E. H., GRODZINSKY, A. J., PHILIPS, S. L. & GRIMSHAW, P. E. 1990. Physicochemical and Bioelectrical Determinants of Cartilage Material Properties. *In:* RATCLIFFE, A., WOO, S. L. Y. & MOW, V. C. (eds.) *Biomechanics of Diarthrodial Joints.* New York: Springer.

FREEMAN, M. A. R. 1973. *Adult Articular Cartilage,* Great Britain, Sir Issac Pitman and Sons LTD.

GANNON, A. R., NAGEL, T. & KELLY, D. J. 2012. The role of the superficial region in determining the dynamic properties of articular cartilage. *Osteoarthritis and Cartilage,* 20**,** 1417-1425.

GARDNER, D. L. 1992. *Pathological Basis of the Connective Tissue Disease* London, Edward Arnold.

GE, Z., LI, C., HENG, B. C., CAO, G. & YANG, Z. 2012. Functional biomaterials for cartilage regeneration. *Journal of Biomedical Materials Research - Part A,* 100 A**,** 2526-2536.

GLASER, C. & PUTZ, R. 2002. Functional anatomy of articular cartilage under compressive loading quantitative aspects of global, local and zonal reactions of the collagenous network with respect to the surface integrity. *Osteoarthritis and Cartilage,* 10**,** 83-99.

GÖRKE, U. J., GÜNTHER, H., NAGEL, T. & WIMMER, M. A. 2010. A large strain material model for soft tissues with functionally graded properties. *Journal of Biomechanical Engineering,* 132.

GRUSHKO, G., SCHNEIDERMAN, R. & MAROUDAS, A. 1989. Some biochemical and biophysical parameters for the study of the pathogenesis of osteoarthritis: a comparison between the processes of ageing and degeneration in human hip cartilage. *Connective Tissue Research,* 19**,** 149-176.

GU, W. Y., LAI, W. M. & MOW, V. C. 1993. Transport of fluid and ions through a porous-permeable charged-hydrated tissue, and streaming potential data on normal bovine articular cartilage. *Journal of Biomechanics,* 26, 709-723.

GU, W. Y., LAI, W. M. & MOW, V. C. 1997. A triphasic analysis of negative osmotic flows through charged hydrated soft tissues. *Journal of Biomechanics,* 30, 71-78.

GU, W. Y., LAI, W. M. & MOW, V. C. 1998. A mixture theory for charged-hydrated soft tissues containing multi- electrolytes: Passive transport and swelling behaviors. *Journal of Biomechanical Engineering,* 120, 169-180.

GUILAK, F., JONES, W. R., TING-BEALL, H. P. & LEE, G. M. 1999. The deformation behavior and mechanical properties of chondrocytes in articular cartilage. *Osteoarthritis and Cartilage,* 7, 59-70.

GUILAK, F., RATCLIFFE, A. & MOW, V. C. 1995. Chondrocyte deformation and local tissue strain in articular cartilage: A confocal microscopy study. *Journal of Orthopaedic Research,* 13, 410-421.

HAGG, R., BRUCKNER, P. & HEDBOM, E. 1998. Cartilage fibrils of mammals are biochemically heterogeneous: Differential distribution of decorin and collagen IX. *Journal of Cell Biology,* 142, 285-294.

HAN, E., CHEN, S. S., KLISCH, S. M. & SAH, R. L. 2011. Contribution of proteoglycan osmotic swelling pressure to the compressive properties of articular cartilage. *Biophysical Journal,* 101, 916-924.

HARDINGHAM, T. 1981. Proteoglycans: their structure, interactions and molecular organization in cartilage. *Biochem Soc Trans,* 9, 489-97.

HARDINGHAM, T. E. 1979. The role of link-protein in the structure of cartilage proteoglycan aggregates. *Biochemical Journal,* 177, 237-247.

HARDINGHAM, T. E., MUIR, H., KWAN, M. K., LAI, W. M. & MOW, V. C. 1987. Viscoelastic properties of proteoglycan solutions with varying proportions present as aggregates. *Journal of Orthopaedic Research,* 5, 36-46.

HOLZAPFEL, G. A., GASSER, T. C. & OGDEN, R. W. 2000. A new constitutive framework for arterial wall mechanics and a comparative study of material models. *Journal of Elasticity,* 61, 1-48.

HONNER, R. & THOMPSON, R. C. 1971. The nutritional pathways of articular cartilage. An autoradiographic study in rabbits using 35S injected intravenously. *Journal of Bone and Joint Surgery - Series A,* 53, 742-748.

HOSSEINI, S. M., WU, Y., ITO, K. & VAN DONKELAAR, C. C. 2013. The importance of superficial collagen fibrils for the function of articular cartilage. *Biomechanics and Modeling in Mechanobiology,* 1-11.

HUANG, C. Y., MOW, V. C. & ATESHIAN, G. A. 2001. The role of flow-independent viscoelasticity in the biphasic tensile and compressive responses of articular cartilage. *Journal of Biomechanical Engineering,* 123, 410-417.

HUNZIKER, E. B., KAPFINGER, E. & GEISS, J. 2007. The structural architecture of adult mammalian articular cartilage evolves by a synchronized process of tissue resorption and neoformation during postnatal development. *Osteoarthritis and Cartilage,* 15, 403-413.

HWANG, W. S., LI, B., JIN, L. H., NGO, K., SCHACHAR, N. S. & HUGHES, G. N. F. 1992. Collagen fibril structure of normal, aging, and osteoarthritic cartilage. *Journal of Pathology,* 167, 425-433.

HWANG, W. S., NGO, K. & SAITO, K. 1990. Silver staining of collagen fibrils in cartilage. *Histochemical Journal,* 22, 487-490.

HYTTINEN, M. M., HOLOPAINEN, J., VAN WEEREN, P. R., FIRTH, E. C., HELMINEN, H. J. & BRAMA, P. A. J. 2009. Changes in collagen fibril network organization and proteoglycan distribution in equine articular cartilage during maturation and growth. *Journal of Anatomy,* 215, 584-591.

IGNAT'EVA, N. Y., DANILOV, N. A., AVERKIEV, S. V., OBREZKOVA, M. V., LUNIN, V. V. & SOBOL, E. N. 2007. Determination of hydroxyproline in tissues and the evaluation of the collagen content of the tissues. *Journal of Analytical Chemistry,* 62, 51-57.

JOY, D. C. 2012. Multi-Beam Ion Microscopy. *Microscopy Today,* 20, 10-15.

JULKUNEN, P., HARJULA, T., IIVARINEN, J., MARJANEN, J., SEPPANEN, K., NARHI, T., AROKOSKI, J., LAMMI, M. J., BRAMA, P. A., JURVELIN, J. S. & HELMINEN, H. J. 2009. Biomechanical, biochemical and structural correlations in immature and mature rabbit articular cartilage. *Osteoarthritis and Cartilage,* 17, 1628-1638.

JULKUNEN, P., IIVARINEN, J., BRAMA, P. A., AROKOSKI, J., JURVELIN, J. S. & HELMINEN, H. J. 2010. Maturation of collagen fibril network structure in tibial and femoral cartilage of rabbits. *Osteoarthritis and Cartilage,* 18, 406-415.

JULKUNEN, P., KORHONEN, R. K., NISSI, M. J. & JURVELIN, J. S. 2008. Mechanical characterization of articular cartilage by combining magnetic resonance imaging and finite-element analysis - A potential functional imaging technique. *Physics in Medicine and Biology,* 53, 2425-2438.

JULKUNEN, P., WILSON, W., JURVELIN, J. S., RIEPPO, J., QU, C. J., LAMMI, M. J. & KORHONEN, R. K. 2008b. Stress-relaxation of human patellar articular cartilage in unconfined compression: Prediction of mechanical response by tissue composition and structure. *Journal of Biomechanics,* 41, 1978-1986.

JURVELIN, J. S., BUSCHMANN, M. D. & HUNZIKER, E. B. 1996. Optical and mechanical determination of Poisson's ratio of adult bovine humeral articular cartilage. *Journal of Biomechanics,* 30, 235-241.

KÄÄB, M. J., GWYNN, I. A. & NÖTZLI, H. P. 1998. Collagen fibre arrangement in the tibial plateau articular cartilage of man and other mammalian species. *Journal of Anatomy,* 193, 23-34.

KATZ, E. P., WACHTEL, E. J. & MAROUDAS, A. 1986. Extrafibrillar proteoglycans osmotically regulate the molecular packing of collagen in cartilage. *Biochimica et Biophysica Acta - General Subjects,* 882, 136-139.

KEMPSON, G. E., FREEMAN, M. A. R. & SWANSON, S. A. V. 1968. Tensile properties of articular cartilage [16]. *Nature,* 220, 1127-1128.

KHALSA, P. S. & EISENBERG, S. R. 1997. Compressive behavior of articular cartilage is not completely explained by proteoglycan osmotic pressure. *Journal of Biomechanics,* 30, 589-594.

KIM, T. K., SHARMA, B., WILLIAMS, C. G., RUFFNER, M. A., MALIK, A., MCFARLAND, E. G. & ELISSEEFF, J. H. 2003. Experimental model for cartilage tissue engineering to regenerate the zonal organization of articular cartilage. *Osteoarthritis and Cartilage,* 11, 653-664.

KIM, Y. J., BONASSAR, L. J. & GRODZINSKY, A. J. 1995. The role of cartilage streaming potential, fluid flow and pressure in the stimulation of chondrocyte biosynthesis during dynamic compression. *Journal of Biomechanics,* 28, 1055-1066.

KIRÁLY, K., HYTTINEN, M. M., LAPVETELÄINEN, T., ELO, M., KIVIRANTA, I., DOBAI, J., MÓDIS, L., HELMINEN, H. J. & AROKOSKI, J. P. A. 1997. Specimen preparation and quantification of collagen birefringence in unstained sections of articular cartilage using image analysis and polarizing light microscopy. *Histochemical Journal,* 29, 317-327.

KIVIRANTA, P., RIEPPO, J., KORHONEN, R. K., JULKUNEN, P., TOYRAS, J. & JURVELIN, J. S. 2006. Collagen network primarily controls poisson's ratio of bovine articular cartilage in compression. *Journal of Orthopaedic Research,* 24, 690-699.

KLEIN, T. J., CHAUDHRY, M., BAE, W. C. & SAH, R. L. 2007. Depth-dependent biomechanical and biochemical properties of fetal, newborn, and tissue-engineered articular cartilage. *Journal of Biomechanics,* 40, 182-190.

KLEIN, T. J., SCHUMACHER, B. L., SCHMIDT, T. A., LI, K. W., VOEGTLINE, M. S., MASUDA, K., THONAR, E. J. M. A. & SAH, R. L. 2003. Tissue engineering of stratified articular cartilage from chondrocyte subpopulations. *Osteoarthritis and Cartilage,* 11, 595-602.

KORHONEN, R. K., LAASANEN, M. S., TOYRAS, J., RIEPPO, J., HIRVONEN, J., HELMINEN, H. J. & JURVELIN, J. S. 2002. Comparison of the equilibrium response of articular cartilage in unconfined compression, confined compression and indentation. *Journal of Biomechanics,* 35, 903-909.

LAASANEN, M. S., TOYRAS, J., KORHONEN, R. K., RIEPPO, J., SAARAKKALA, S., NIEMINEN, M. T., HIRVONEN, J. & JURVELIN, J. S. 2002. Biomechanical properties of knee articular cartilage. *Biorheology,* 40, 133-140.

LECOCQ, M., GIRARD, C. A., FOGARTY, U., BEAUCHAMP, G., RICHARD, H. & LAVERTY, S. 2008. Cartilage matrix changes in the developing epiphysis: Early events on the pathway to equine osteochondrosis? *Equine Veterinary Journal,* 40, 442-454.

LEE, R. C., FRANK, E. H., GRODZINSKY, A. J. & ROYLANCE, D. K. 1981. Oscillatory compressional behavior of articular cartilage and its associated electromechanical properties. *Journal of Biomechanical Engineering,* 103, 280-292.

LEVIN, A. S., CHEN, C. T. C. & TORZILLI, P. A. 2005. Effect of tissue maturity on cell viability in load-injured articular cartilage explants. *Osteoarthritis and Cartilage,* 13, 488-496.

LIPSHITZ, H., ETHEREDGE, R., 3RD & GLIMCHER, M. J. 1976. Changes in the hexosamine content and swelling ratio of articular cartilage as functions of depth from the surface. *J Bone Joint Surg Am,* 58, 1149-53.

LU, X. L. & MOW, V. C. 2008. Biomechanics of articular cartilage and determination of material properties. *Medicine and Science in Sports and Exercise,* 40, 193-199.

LU, X. L., MOW, V. C. & GUO, X. E. 2009. Proteoglycans and mechanical behavior of condylar cartilage. *Journal of Dental Research,* 88, 244-248.

MAAS, S. A., ELLIS, B. J., ATESHIAN, G. A. & WEISS, J. A. 2012. FEBio: Finite elements for biomechanics. *Journal of Biomechanical Engineering,* 134.

MANSOUR, J. M. 2003. Biomechanics of Cartilage. *In:* OATIS, C. A. (ed.) *Kinesiology: the Mechanics and Pathomechanics of Human Movement.* Lippincott Willaims and Wilkins.

MANSOUR, J. M. & MOW, V. C. 1976. The permeability of Articular Cartilage under Compressive Strain and at High Pressures. *Journal of Bone and Joint Surgery,* 58-A, 509-516.

MAROUDAS, A. 1976. Balance between swelling pressure and collagen tension in normal and degenerate cartilage. *Nature,* 260, 808-809.

MAROUDAS, A. 1979. Physio-chemical properties of articular cartilage. *In:* FREEMAN, M. A. R. (ed.) *Adult Articular Cartilage.* 2nd ed. Tunbridge Wells, England: Pitman.

MAROUDAS, A. & BANNON, C. 1981. Measurement of swelling pressure in cartilage and comparison with osmotic pressure of constituent proteoglycans. *Biorheology,* 18, 619-632.

MAROUDAS, A. & BULLOUGH, P. 1968. Permeability of articular cartilage. *Nature,* 219, 1260-1261.

MAROUDAS, A., MUIR, H. & WINGHAM, J. 1969. The correlation of fixed negative charge with glycosaminoglycan content of human articular cartilage. *BBA - General Subjects,* 177, 492-500.

MAROUDAS, A., WACHTEL, E., GRUSHKO, G., KATZ, E. P. & WEINBERG, P. 1991. The effect of osmotic and mechanical pressures on water partitioning in articular cartilage. *Biochimica et Biophysica Acta - General Subjects,* 1073, 285-294.

MENDLER, M., EICH-BENDER, S. G., VAUGHAN, L., WINTERHALTER, K. H. & BRUCKNER, P. 1989. Cartilage contains mixed fibrils of collagen types II, IX, and XI. *Journal of Cell Biology,* 108, 191-197.

MOREL, V. & QUINN, T. M. 2004. Cartilage injury by ramp compression near the gel diffusion rate. *Journal of Orthopaedic Research,* 22, 145-151.

MOW, V. C., ATESHIAN, G. A., LAI, W. M. & GU, W. Y. 1998. Effects of fixed charges on the stress-relaxation behavior of hydrated soft tissues in a confined compression problem. *International Journal of Solids and Structures,* 35, 4945-4962.

MOW, V. C. & GUO, X. E. 2002. Mechano-electrochemical properties of articular cartilage: Their inhomogeneities and anisotropies. *Annual Review of Biomedical Engineering.*

MOW, V. C. & HUISKES, R. 2005. *Basic Orthopaedic Biomechanics and Mechano-Biology,* Philadelphia, Lippincott Williams & Wilkins.

MOW, V. C., KUEI, S. C., LAI, W. M. & ARMSTRONG, C. G. 1980. Biphasic creep and stress relaxation of articular cartilage in compression: Theory and experiments. *Journal of Biomechanical Engineering,* 102, 73-84.

MOW, V. C., RATCLIFFE, A. & ROBIN POOLE, A. 1992. Cartilage and diarthrodial joints as paradigms for hierarchical materials and structures. *Biomaterials,* 13, 67-97.

MUIR, H. 1980. The chemistry of the ground substance of joint cartilage. *In:* SOKOLOFF, L. (ed.) *The Joints and Synovial Fluid.* New York: Academic Press.

MUIR, H. 1983. Proteoglycans as organizers of the intercellular matrix. *Biochemical Society Transactions,* 11, 613-622.

NAGEL, T. & KELLY, D. J. 2010. The influence of fiber orientation on the equilibrium properties of neutral and charged biphasic tissues. *Journal of Biomechanical Engineering,* 132, 114506.

NAGEL, T. & KELLY, D. J. 2013. The composition of engineered cartilage at the time of implantation determines the likelihood of regenerating tissue with a normal collagen architecture. *Tissue Engineering - Part A,* 19, 824-833.

NARMONEVA, D. A., WANG, J. Y. & SETTON, L. A. 1999. Nonuniform swelling-induced residual strains in articular cartilage. *Journal of Biomechanics,* 32, 401-408.

NG, K. W., ATESHIAN, G. A. & HUNG, C. T. 2009. Zonal chondrocytes seeded in a layered agarose hydrogel create engineered cartilage with depth-dependent cellular and mechanical inhomogeneity. *Tissue engineering. Part A,* 15, 2315-2324.

NG, K. W., WANG, C. C. B., MAUCK, R. L., KELLY, T. A. N., CHAHINE, N. O., COSTA, K. D., ATESHIAN, G. A. & HUNG, C. T. 2005. A layered agarose approach to fabricate depth-dependent inhomogeneity in chondrocyte-seeded constructs. *Journal of Orthopaedic Research,* 23, 134-141.

NIEMINEN, M. T., RIEPPO, J., SILVENNOINEN, J., TÖYRÄS, J., HAKUMÄKI, J. M., HYTTINEN, M. M., HELMINEN, H. J. & JURVELIN, J. S. 2002. Spatial assessment of articular cartilage proteoglycans with Gd-DTPA-enhanced T1 imaging. *Magnetic Resonance in Medicine,* 48, 640-648.

O'HARA, B. P., URBAN, J. P. G. & MAROUDAS, A. 1990. Influence of cyclic loading on the nutrition of articular cartilage. *Annals of the Rheumatic Diseases,* 49, 536-539.

OWEN, J. R. & WAYNE, J. S. 2006. Influence of a superficial tangential zone over repairing cartilage defects: Implications for tissue engineering. *Biomechanics and Modeling in Mechanobiology,* 5, 102-110.

OWEN, J. R. & WAYNE, J. S. 2010. Contact models of repaired articular surfaces: Influence of loading conditions and the superficial tangential zone. *Biomechanics and Modeling in Mechanobiology,* 10, 461-471.

PARK, S., HUNG, C. T. & ATESHIAN, G. A. 2004. Mechanical response of bovine articular cartilage under dynamic unconfined compression loading at physiological stress levels. *Osteoarthritis and Cartilage,* 12, 65-73.

PARK, S., KRISHNAN, R., NICOLL, S. B. & ATESHIAN, G. A. 2003. Cartilage interstitial fluid load support in unconfined compression. *Journal of Biomechanics,* 36, 1785-1796.

PERERA, J. R., GIKAS, P. D. & BENTLEY, G. 2012. The present state of treatments for articular cartilage defects in the knee. *Annals of the Royal College of Surgeons of England,* 94, 381-387.

POOLE, C. A., FLINT, M. H. & BEAUMONT, B. W. 1987. Chondrons in cartilage: Ultrastructural analysis of the pericellular microenvironment in adult human articular cartilages. *Journal of Orthopaedic Research,* 5, 509-522.

PROVENZANO, P. P. & VANDERBY JR, R. 2006. Collagen fibril morphology and organization: Implications for force transmission in ligament and tendon. *Matrix Biology,* 25, 71-84.

REDLER, I., MOW, V. C., ZIMNY, M. L. & MANSELL, J. 1975. The ultrastructure and biomechanical significance of the tidemark of articular cartilage. *Clinical Orthopaedics and Related Research,* no.112, 357-362.

RIEPPO, J., HALLIKAINEN, J., JURVELIN, J. S., KIVIRANTA, I., HELMINEN, H. J. & HYTTINEN, M. M. 2008. Practical considerations in the use of polarized light microscopy in the analysis of the collagen network in articular cartilage. *Microscopy Research and Technique,* 71, 279-287.

RIEPPO, J., HALMESMAKI, E., SITTONEN, U., LAASANEN, M. S., TOYRAS, J., KIVIRANTA, I., HYTTINEN, M. M., JURVELIN, J. S. & HELMINEN, H. J. Histological Differences of Human, Bovine, and Porcine Cartilage. 49th Annual Meeting of the Orthopaedic Research Society (poster), 2003 New Orleans, Louisiana.

RIEPPO, J., HYTTINEN, M. M., HALMESMAKI, E., RUOTSALAINEN, H., VASARA, A., KIVIRANTA, I., JURVELIN, J. S. & HELMINEN, H. J. 2009. Changes in spatial collagen content and collagen network architecture in porcine articular cartilage during growth and maturation. *Osteoarthritis and Cartilage,* 17, 448-455.

ROLAUFFS, B., MUEHLEMAN, C., LI, J., KURZ, B., KUETTNER, K. E., FRANK, E. & GRODZINSKY, A. J. 2010. Vulnerability of the superficial zone of immature articular cartilage to compressive injury. *Arthritis & Rheumatism,* 62, 3016-3027.

RÖMGENS, A. M., VAN DONKELAAR, C. C. & ITO, K. 2013. Contribution of collagen fibers to the compressive stiffness of cartilaginous tissues. *Biomechanics and Modeling in Mechanobiology,* 1-11.

ROTH, V. & MOW, V. C. 1980. The intrinsic tensile behavior of the matrix of bovine articular cartilage and its variation with age. *Journal of Bone and Joint Surgery - Series A,* 62, 1102-1117.

ROUGHLEY, P. J. & LEE, E. R. 1994. Cartilage proteoglycans: Structure and potential functions. *Microscopy Research and Technique,* 28, 385-397.

SAARAKKALA, S., JULKUNEN, P., KIVIRANTA, P., MÄKITALO, J., JURVELIN, J. S. & KORHONEN, R. K. 2010. Depth-wise progression of osteoarthritis in human articular cartilage: investigation of composition, structure and biomechanics. *Osteoarthritis and Cartilage,* 18, 73-81.

SAH, R. L., TRIPPEL, S. B. & GRODZINSKY, A. J. 1996. Differential effects of serum, insulin-like growth factor-I, and fibroblast growth factor-2 on the maintenance of cartilage physical properties during long-term culture. *Journal of Orthopaedic Research,* 14, 44-52.

SAH, R. L. Y., KIM, Y. J., DOONG, J. Y. H., GRODZINSKY, A. J., PLAAS, A. H. K. & SANDY, J. D. 1989. Biosynthetic response of cartilage explants to dynamic compression. *Journal of Orthopaedic Research,* 7, 619-636.

SCHINAGL, R. M., GURSKIS, D., CHEN, A. C. & SAH, R. L. 1997. Depth-dependent confined compression modulus of full-thickness bovine articular cartilage. *Journal of Orthopaedic Research,* 15, 499-506.

SCHINAGL, R. M., TING, M. K., PRICE, J. H. & SAH, R. L. 1996. Video microscopy to quantitate the inhomogeneous equilibrium strain within articular cartilage during confined compression. *Annals of Biomedical Engineering,* 24, 500-512.

SCHMIDT, M. B., MOW, V. C., CHUN, L. E. & EYRE, D. R. 1990. Effects of proteoglycan extraction on the tensile behavior of articular cartilage. *Journal of Orthopaedic Research,* 8, 353-363.

SCHNEIDER, C. A., RASBAND, W. S. & ELICEIRI, K. W. 2012. NIH Image to ImageJ: 25 years of image analysis. *Nature Methods,* 9, 671-675.

SCOTT, J. E. 1988. Proteoglycan-fibrillar collagen interactions. *Biochemical Journal,* 252, 313-323.

SETTON, L. A., TOHYAMA, H. & MOW, V. C. 1998. Swelling and curling behaviors of articular cartilage. *Journal of Biomechanical Engineering,* 120, 355-361.

SETTON, L. A., ZHU, W. & MOW, V. C. 1993. The biphasic poroviscoelastic behavior of articular cartilage: Role of the surface zone in governing the compressive behavior. *Journal of Biomechanics,* 26, 581-592.

SHARMA, B., WILLIAMS, C. G., KIM, T. K., SUN, D., MALIK, A., KHAN, M., LEONG, K. & ELISSEEFF, J. H. 2007. Designing zonal organization into tissue-engineered cartilage. *Tissue Engineering,* 13, 405-414.

SHIRAZI, R. & SHIRAZI-ADL, A. 2008. Deep vertical collagen fibrils play a significant role in mechanics of articular cartilage. *Journal of Orthopaedic Research,* 26, 608-615.

SOLTZ, M. A. & ATESHIAN, G. A. 1998. Experimental verification and theoretical prediction of cartilage interstitial fluid pressurization at an impermeable contact interface in confined compression. *Journal of Biomechanics,* 31, 927-934.

SOLTZ, M. A. & ATESHIAN, G. A. 2000. Interstitial Fluid Pressurization during Confined Compression Cyclical Loading of Articular Cartilage. *Annals of Biomedical Engineering,* 28, 150-159.

SOULHAT, J., BUSCHMANN, M. D. & SHIRAZI-ADL, A. 1999. A fibril-network-reinforced biphasic model of cartilage in unconfined compression. *Journal of Biomechanical Engineering,* 121, 340-347.

STOCKWELL, R. A. 1970. Changes in the acid glycosaminoglycan content of the matrix of ageing human articular cartilage. *Annals of the Rheumatic Diseases,* 29, 509-515.

SUH, J. K., LI, Z. & WOO, S. L. Y. 1995. Dynamic behavior of a biphasic cartilage model under cyclic compressive loading. *Journal of Biomechanics,* 28, 357-364.

SUTTON, M. A., ORTEU, J.-J. & SCHREIER, H. W. 2009. Digital Image Correlation (DIC). *In:* SUTTON, M. A., ORTEU, J.-J. & SCHREIER, H. W. (eds.) *Image Correlation for Shape, Motion and Deformation Measurements.* NY: Springer.

SWINDLE, M. M. & SMITH, A. C. 1998. Comparative anatomy and physiology of the pig. *Scandinavian Journal of Laboratory Animal Science,* 25, 11-21.

TANAKA, E., YAMANO, E., DALLA-BONA, D. A., WATANABE, M., INUBUSHI, T., SHIRAKURA, M., SANO, R., TAKAHASHI, K., VAN EIJDEN, T. & TANNE, K. 2006. Dynamic compressive properties of the mandibular condylar cartilage. *Journal of Dental Research,* 85, 571-575.

THORPE, S. D., NAGEL, T., CARROLL, S. F. & KELLY, D. J. 2013. Modulating Gradients in Regulatory Signals within Mesenchymal Stem Cell Seeded Hydrogels: A Novel Strategy to Engineer Zonal Articular Cartilage. *PLoS ONE,* 8.

TORZILLI, P. A. 1984. Mechanical response of articular cartilage to an oscillating load. *Mechanics Research Communications,* 11, 75-82.

TORZILLI, P. A. 1993. Effects of temperature, concentration and articular surface removal on transient solute diffusion in articular cartilage. *Medical and Biological Engineering and Computing,* 31, S93-S98.

TORZILLI, P. A., DETHMERS, D. A., ROSE, D. E. & SCHRYUER, H. F. 1983. Movement of interstitial water through loaded articular cartilage. *Journal of Biomechanics,* 16, 169-179.

TORZILLI, P. A., GRANDE, D. A. & ARDUINO, J. M. 1998. Diffusive properties of immature articular cartilage. *Journal of Biomedical Materials Research,* 40, 132-138.

TREPPO, S., KOEPP, H., QUAN, E. C., COLE, A. A., KUETTNER, K. E. & GRODZINSKY, A. J. 2000. Comparison of biomechanical and biochemical properties of cartilage from human knee and ankle pairs. *Journal of Orthopaedic Research,* 18, 739-748.

VAN TURNHOUT, M. C., KRANENBARG, S. & VAN LEEUWEN, J. L. 2010a. Contribution of postnatal collagen reorientation to depth-dependent mechanical properties of articular cartilage. *Biomechanics and Modeling in Mechanobiology,* 1-11.

VAN TURNHOUT, M. C., SCHIPPER, H., ENGEL, B., BUIST, W., KRANENBARG, S. & VAN LEEUWEN, J. L. 2010b. Postnatal development of collagen structure in ovine articular cartilage. *BMC Developmental Biology,* 10.

VANDEN BERG-FOELS, W. S., SCIPIONI, L., HUYNH, C. & WEN, X. 2012. Helium ion microscopy for high-resolution visualization of the articular cartilage collagen network. *Journal of Microscopy,* 246, 168-176.

VENN, M. F. 1978. Variation of chemical composition with age in human femoral head cartilage. *Annals of the Rheumatic Diseases,* 37, 168-174.

WACHTEL, E., MAROUDAS, A. & SCHNEIDERMAN, R. 1995. Age-related changes in collagen packing of human articular cartilage. *Biochimica et Biophysica Acta - General Subjects,* 1243, 239-243.

WANG, C. C., DENG, J. M., ATESHIAN, G. A. & HUNG, C. T. 2002a. An automated approach for direct measurement of two-dimensional strain distributions within articular cartilage under unconfined compression. *J Biomech Eng,* 124, 557-67.

WANG, C. C. B., CHAHINE, N. O., HUNG, C. T. & ATESHIAN, G. A. 2003. Optical determination of anisotropic material properties of bovine articular cartilage in compression. *Journal of Biomechanics,* 36, 339-353.

WANG, C. C. B., GUO, X. E., SUN, D., MOW, V. C., ATESHIAN, G. A. & HUNG, C. T. 2002b. The functional environment of chondrocytes within cartilage subjected to compressive loading: A theoretical and experimental approach. *Biorheology,* 39, 11-25.

WANG, C. C. B., HUNG, C. T. & MOW, V. C. 2001. An analysis of the effects of depth-dependent aggregate modulus on articular cartilage stress-relaxation behavior in compression. *Journal of Biomechanics,* 34, 75-84.

WATANABE, H., YAMADA, Y. & KIMATA, K. 1998. Roles of aggrecan, a large chondroitin sulfate proteoglycan, in cartilage structure and function. *Journal of Biochemistry,* 124, 687-693.

WAYNE, J. S. 1995. Load partitioning influences the mechanical response of articular cartilage. *Annals of Biomedical Engineering,* 23, 40-47.

WEISS, C., ROSENBERG, L. & HELFET, A. J. 1968. An ultrastructural study of normal young adult human articular cartilage. *Journal of Bone and Joint Surgery - Series A,* 50, 663-674.

WILLIAMSON, A. K., CHEN, A. C., MASUDA, K., THONAR, E. J. M. A. & SAH, R. L. 2003. Tensile mechanical properties of bovine articular cartilage: Variations with growth and relationships to collagen network components. *Journal of Orthopaedic Research,* 21, 872-880.

WILLIAMSON, A. K., CHEN, A. C. & SAH, R. L. 2001. Compressive properties and function-composition relationships of developing bovine articular cartilage. *Journal of Orthopaedic Research,* 19, 1113-1121.

WILSON, W., HUYGHE, J. M. & VAN DONKELAAR, C. C. 2007. Depth-dependent compressive equilibrium properties of articular cartilage explained by its composition. *Biomechanics and Modeling in Mechanobiology,* 6, 43-53.

WILSON, W., VAN DONKELAAR, C. C., VAN RIETBERGEN, B. & HUISKES, R. 2005. A fibril-reinforced poroviscoelastic swelling model for articular cartilage. *Journal of Biomechanics,* 38, 1195-1204.

WONG, M., PONTICIELLO, M., KOVANEN, V. & JURVELIN, J. S. 2000. Volumetric changes of articular cartilage during stress relaxation in unconfined compression. *Journal of Biomechanics,* 33, 1049-1054.

WOO, S. L. Y., AKESON, W. H. & JEMMOTT, G. F. 1976. Measurements of nonhomogeneous, directional mechanical properties of articular cartilage in tension. *Journal of Biomechanics,* 9, 785-791.

XIA, Y. 2008. Averaged and Depth-Dependent Anisotropy of Articular Cartilage by Microscopic Imaging. *Seminars in Arthritis and Rheumatism,* 37, 317-327.

ZEHBE, R., RIESEMEIER, H., KIRKPATRICK, C. J. & BROCHHAUSEN, C. 2012. Imaging of articular cartilage - Data matching using X-ray tomography, SEM, FIB slicing and conventional histology. *Micron,* 43, 1060-1067.

ZHU, W., IATRIDIS, J. C., HLIBCZUK, V., RATCLIFFE, A. & MOW, V. C. 1996. Determination of collagen-proteoglycan interactions in vitro. *Journal of Biomechanics,* 29**,** 773-783.

ZHU, W., LAI, W. M. & MOW, V. C. 1991. The density and strength of proteoglycan-proteoglycan interaction sites in concentrated solutions. *Journal of Biomechanics,* 24**,** 1007-1018.

ZHU, W., MOW, V. C., KOOB, T. J. & EYRE, D. R. 1993. Viscoelastic shear properties of articular cartilage and the effects of glycosidase treatments. *J Orthop Res,* 11**,** 771-81.

Appendix A

Least squared fit method in order to determine the permeability of articular cartilage during confined compression stress-relaxation tests.

```
%clear all; clc; close all;
%this m-file determines permeability at a specific strain, strain after
the first compression

%Ensures that the time and stress vectors are the same length,
concatenates the longer
%vector to the length of the shorter
if length(t)>length(mowstress)
    t = t(1:length(mowstress));
elseif length(t)<length(mowstress)
    mowstress = mowstress(1:length(t));
elseif length(t) == length(mowstress)
    t = t;
    mowstress = mowstress;
end


a = input('Please enter the thickness of the sample (m): ');
strainrate = input('Please enter the applied strain rate (m/min): ');
edotomin = strainrate/a;     %determines strain rate in percent per min;
edoto = edotomin/60;         %determines strain rate in percent per
second;
[tnotstress, I] = max(mowstress);   %determines the index time tnot
(time when relaxation begins)by picking the maximum stress value
tnot = t(I);  %returns the time tnot, not in indicial form

%the following four lines determine the compressive modulus
automatically
%lastfour = mowstress((length(mowstress)-4):length(mowstress));
%lastfoursum = sum(lastfour);
%lastfouravg = sum(lastfour)/6;
%Ha = lastfouravg/(edoto*tnot)
Ha = input('Please enter the compressive modulus (Pa): ');

%plot the raw data
plot(t, mowstress, 'go')
title('Raw Data')
xlabel('Time (sec)')
ylabel('Stress (N/m^2)')

newsum = 0;
i = 1;
z = 1;
c = 1;
n = 1;

%create two time vectors, one for compression and one for relaxation
for z = 1:length(t)
    if t(z) <= tnot
        tnew(z) = t(z);   %tnew is time vector consisting of points in
stress
    end
```

```
    if (t(z) >= tnot) && (c<11)
        tnewg(c) = t(z);  %tnewg is time vector consisting of points in
relaxation
        c = c+1;
    end
end



%determine stress at all values of permeability
y = 1;
x = 1;
%runs through all the below values of permeability and does least-square
fit
perm = [1e-18:1e-16:9e-14];
for x = 1:length(perm)
tau(x) = (a^2)/((pi^2)*Ha*perm(x));   %creates a vector tau at all
values of permeability
    for i = 1:length(tnewg) %runs through points from tnot to
equilibrium (relaxation)
    for n = 1:25
       %this loop calculates the inner sum in Mow's equation, n from 1
to 25, and at all values of tau and time
        innersumg(n) = (exp((-(n^2)*tnewg(i))/tau(x))-exp((-
(n^2)*(tnewg(i)-tnot))/tau(x)))/(n^2);
   end
newsumg(i) = sum(innersumg);
%creates a matrix of stresses at all times after tnot, each row is a
permeability, each column is for a time data point
stressg(x,i) = (Ha*edoto)*tnot -
(2*edoto*(a^2))/((pi^2)*perm(x))*newsumg(i);
end
end

q = length(tnew);

%creates a vector newmowstress which is the stress data points from tnot
until equilibrium
newmowstress = mowstress(q:length(mowstress));

%creates error vector at each value of permeability
for y = 1:length(perm)
   for j = 1:length(tnewg)
    error1(y,j) = (stressg(y,j) - newmowstress(j))^2;  %takes difference
between equation point and data point
    mysum = sum(error1,2);
    end
end

[smallest, I] = min(mysum);  %returns index of permeability that gives
least error
bestfit = perm(I) %returns value of permeability that gives least error

besttau = (a^2)/((pi^2)*Ha*bestfit); %computes tau at bestfit value of
permeability

%determine stress at each value of time (in relaxation) with the bestfit
permeability
```

```
for i = 1:length(tnewg)
    for n = 1:25
       innersumg(n) = (exp((-(n^2)*tnewg(i))/besttau)-exp((-
(n^2)*(tnewg(i)-tnot))/besttau))/(n^2);
   end
newsumg(i) = sum(innersumg);
newstressg(i) = (Ha*edoto)*tnot -
(2*edoto*(a^2))/((pi^2)*bestfit)*newsumg(i);
end

%determine stress at each value of time (in compression) with the
bestfit permeability
newsum = 0;
i = 1;
z = 1;
c = 1;
n = 1;


for i = 1:length(tnew)
    for n = 1:25
       innersum(n) = exp((-(n^2)*tnew(i))/besttau)/(n^2);
   end
newsum(i) = sum(innersum);
newstress(i) = (Ha*edoto)*t(i) + (edoto*(a^2))/(3*bestfit) -
(2*edoto*(a^2))/((pi^2)*bestfit)*newsum(i);
end


%plot raw data with bestfit line using linear model
figure
plot(tnew, mowstress(1:length(tnew)), '-go', tnewg, newmowstress(1:10),
'-go')
title('Linear Biphasic Model')
xlabel('Time (sec)')
ylabel('Stress(N/m^2)')
hold on

%Plots entire curve together instead of two separate parts
%for i=1:227
    %if i <= 54
%         newstresstotal(i) = newstress(i);
%     else newstresstotal(i) = newstressg(i-54);
%     end
% end

%plot(t, newstresstotal)
 plot(tnew, newstress)
 plot(tnewg, newstressg)



hold on

%the following two lines return the time and stress vectors for the
bestfit equation, if desired
lineartime = [tnew tnewg]';
linearstress = [newstress newstressg]';
```

Appendix B

This work was performed and written by Dr. Thomas Nagel

B.1 Constitutive Model

A finite strain biphasic material model with a Donnan osmotic swelling pressure was implemented, where the solid matrix was modelled as an overlay of a Neo-Hookean component and several families of fibrils (Görke et al., 2010). To capture both isotropic and anisotropic fibril distributions, the fibril network was modelled as consisting of a quasi-isotropic network of 7 secondary and, in the case of anisotropy, 2 primary families of fibrils (Wilson et al., 2005). In models with an isotropic fibril arrangement, the overall collagen network stiffness was equally distributed among the 7 secondary fibrils, while in simulations with anisotropic fibril architectures the primary and secondary fibrils were assigned weights according to (Wilson et al., 2005) such that the primary fibrils forming the characteristic Benninghoff architecture were significantly stiffer than the secondary isotropic network. Independent of the architecture, the overall fibril stiffness (sum over all families) was kept constant. As was performed previously (Nagel and Kelly, 2010), a Holzapfel-type free energy functional (Holzapfel et al., 2000) was used as a constitutive model for the individual fibrils. The fibril stiffness values were determined as described in (Nagel and Kelly, 2010).

The described model was implemented into the source code of FEBio (version 1.6.1, (Maas et al., 2012)). After a free swelling step, steady state unconfined compression tests were simulated by lowering a frictionless contact platen onto the surface of the cartilage plug. To mimic the presence of the bone, displacements at the cartilage-bone interface were constrained in all directions. Lateral surfaces were traction-free and were assigned homogeneous Dirichlet boundary conditions for the pore pressure.

Samples were compared in terms of their global nominal equilibrium Young's moduli (Nagel and Kelly, 2010) to represent the overall sample stiffness. Local Young's moduli were calculated where depth-dependent properties were of interest.

B.1.1 Sensitivity to a variation of collagen network properties (in isolation)

To investigate the relative influence of the collagen fibril stiffness and the network architecture, a second set of simulations were run. Average homogeneous material properties for the porosity (80%) and the fixed charge density (0.0002 mEq/mm^3) were used for all models. The geometry of the mature samples was used exclusively. Isotropic and Benninghoff fibril architectures were investigated each with the baseline fibril stiffness values used so far and with a ten-fold increased fibril stiffness to account for possible variations due to a higher collagen and cross-linking content.